Model Predictive Control of Modular Multilevel Converters

by

Andrés Mauricio López Cañón M.Sc.

UNIVERSITÄT PADERBORN
Die Universität der Informationsgesellschaft

FAKULTÄT FÜR
ELEKTROTECHNIK,
INFORMATIK UND
MATHEMATIK

Model Predictive Control of Modular Multilevel Converters

Von der Fakultät für Elektrotechnik, Informatik und Mathematik
der Universität Paderborn

zur Erlangung des akademischen Grades

Doktor der Ingenieurwissenschaften (Dr.-Ing.)

genehmigte Dissertation

von

Andrés Mauricio López Cañón M.Sc.

Erster Gutachter:	Prof. Daniel Quevedo
Zweiter Gutachter:	Prof. Toit Mouton

Tag der mündlichen Prüfung: 04.09.2018

Paderborn 2018

Diss. EIM-E/343

Declaration

I hereby declare that I prepared this thesis entirely on my own and have not used outside sources without declaration in the text. Any concepts or quotations applicable to these sources are clearly attributed to them. This thesis has not been submitted in the same or substantially similar version, not even in part, to any other authority for grading and has not been published elsewhere.

Erklärung

Ich versichere, dass ich die Arbeit ohne fremde Hilfe und ohne Benutzung anderer als der angegebenen Quellen angefertigt habe und dass die Arbeit in gleicher oder ähnlicher Form noch keiner anderen Prüfungsbehörde vorgelegen hat und von dieser als Teil einer Prüfungsleistung angenommen worden ist. Alle Ausführungen, die wörtlich oder sinngemäß übernommen worden sind, sind als solche gekennzeichnet.

City, Date

Signature

Kurzfassung

Die vorliegende Arbeit befasst sich mit der Anwendung modellprädiktiver Regelungen (englisch: *Model Predictive Control* (MPC)) auf modulare Mehrpunktstromrichter (englisch: *Modular Multilevel Converter* (MMC)). Das zentrale Ziel ist dabei, den Aufwand zur Lösung des zugrundeliegenden Optimierungsproblems zu reduzieren und gleichzeitig die geforderten Konverterzustände einzuhalten.

Typische Modelle für MMCs zeichnen sich durch eine Vielzahl an Zuständen und wertdiskreten Eingangsgrößen aus. Derartige Modelle führen in Kombination mit MPC insbesondere dann auf komplexe Optimierungsprobleme, wenn lange Prädiktionshorizonte erforderlich sind. Um dieses Problem zu umgehen, wird im Rahmen der Arbeit ein vereinfachtes Modell vorgestellt, welches sowohl die Systemordnung reduziert als auch Diskontinuitäten resultierend aus wertdiskreten Schaltvorgängen eliminiert. Die Genauigkeit und Grenzen des neuartigen Modellierungsansatzes werden ausgiebig diskutiert, um eine verlässliche Anwendung zu ermöglichen. Das reduzierte Modell wir anschließend eingesetzt, um geeignete Referenzwerte für die Regelung des MMCs zu bestimmen. Insbesondere wird für das Anwendungsbeispiel in der Arbeit aufgezeigt, wie Referenzwerte so gewählt werden können, dass die Restwelligkeit in den einzelnen Modulen des Stromrichters reduziert werden.

Die Komplexität des MPC-Optimierungsproblems wird unter Verwendung des vereinfachten Modells weiter reduziert, indem nur je ein wertkontinuierlicher Reglereingriff pro Konverterarm betrachtet wird. Darüber hinaus wird untersucht, unter welchen Bedingungen sich ein konvexes Optimierungsproblem ergibt. Diese Bedingungen sind für viele Anwendungsfälle erfüllt, so dass etablierte und effiziente Algorithmen zur Lösung des Optimierungsproblems eingesetzt werden können. Dies ist insbesondere für die oben angesprochenen, langen Prädiktionshorizonte gewinnbringend. Die entwickelten, maßgeschneiderten MPC Schemata für MMC werden abschließend in einer realitätsnahen Simulationsumgebung erprobt.

Abstract

This work addresses problems that arise with the application of Model Predictive Control (MPC) to Modular Multilevel Converters (MMCs), by aiming to reduce the complexity of the optimization problem associated with the controller while properly tracking the converter states.

Due to the complexity of the MMC, principally attributed to the high dimension of its state space model along with the high number of discontinuous switching variables available, solving the optimization problem associated with the MPC can be challenging. This becomes more significant when long prediction horizons are required. In order to address this problem, this work presents a reduced order model that aims to reduce the complexity of the state space model of the MMC and to eliminate the discontinuities associated with the converter switches. In order to validate this approach, the accuracy and limitations of this model are analyzed and identified in detail. Moreover, with the help of the reduced order model, detailed references for the MMC are carefully designed and, for the case presented in this work, reference parameters are selected optimally in order to reduce the voltage ripple in the converter modules.

The complexity of the optimization problem associated with the MPC is also reduced with the help of the reduced order model by considering just one continuous control signal per converter arm. To further aid the optimization, a method to derive conditions that guarantee its convexity is presented. By guaranteeing convexity, it is possible to use very well studied and efficient optimization algorithms, easing the application of MPC on MMC, especially in the case where long prediction horizons are required. In order to illustrate the proposed procedure, numerical examples are presented in a simulation environment.

Contents

1. Introduction

Power converters play an essential role in energy distribution systems, allowing the control of the energy flow and enabling the incorporation of different kinds of energy sources [Erl14]. The manipulable control inputs in these converters are typically discrete-valued switching signals. This makes the development of high-performance control laws inherently difficult. Modular Multilevel Converters (MMCs) are an increasingly popular class of converters that use a series connection of several basic modules and provide significant advantages in high power and high voltage applications in comparison with other power converter topologies [LM03]. The main advantages of the MMC come from its modularity and easy scalability, giving one the possibility to work with high voltages and high power using relatively low voltage components and low switching frequencies. It has been shown that this improves efficiency and reduces harmonic distortion [XZZ16, DQB+15, IAH+11, PPC+13, RGM15, PRFK12, AI15, LZW+15]. All these characteristics make the MMC a very important topology for industry. Some of its applications include: wind energy conversion, HVDC grids, and medium voltage drives [LM03, MGRP10, PBR+15]. Due to the relevance of this topology, several studies have proposed different techniques to improve performance and address important issues. These include: modulation techniques [IANN12a, HZM16, LYLZ16], voltage balancing techniques [FZXX15], optimal capacitor ripple reduction [IAH+11, PPC+13], several control approaches [QS12, RGM15, PRFK12, GDY+16] and energy quality and reliability [XZZ16, WP16]. All of these works also aim to understand operation principles of MMCs.

An MMC usually has tens or even hundreds of switches that can be driven independently. Classical control approaches using linear controllers, can become very complex when the number of control variables increases, often leading to poor performance. This motivates the use of Model Predictive Control (MPC) for governing MMCs. An MPC can deal easily with system constraints and system failures; it also has the potential to reduce switching losses and harmonic distortion when compared to classical linear techniques [Gey11, BB12, LHWB06]. Another advantage of the MPC framework is the possibility to explicitly consider the future behavior of the system and take that into account in the current control action [BVP+12, QAG14, AMM14, dOKM00, CWR13].

This work addresses the problem of MPC for MMCs by dividing it into three main parts. First, a modelling technique that reduces the analytical complexity of the MMC is introduced and validated. The second part consists in using this model to elucidate analytically the relationship between the MMC variables, and then to design optimal references for control purposes. Finally, the last part uses the model with reduced complexity and the optimal references, and analyzes in detail the problem of the application of MPC to MMCs. The remainder of the present chapter discusses the motivation behind this work and gives an overview of the proposed solutions.

1.1. System modeling

In the first part of this work the efforts are focused on analysing the problem of obtaining a simple mathematical model of the MMC. The goal of the model is to be able to obtain relatively simple mathematical expressions that, not only describe the converter accurately, but also allow one to obtain insight into the behaviour of the system. This insight can be used as a guideline for different design purposes such as: selection of references for control, injection of current harmonics for voltage ripple reduction, or selection of control laws for different applications [SHN+16].

The following sections describe the classical modeling approach of MMCs, mention its drawbacks and discuss new approaches to MMC's modeling. This also opens the path to discuss the motivation and procedures that constitute the first part of the current work

1.1.1. Modular Multilevel Converter

The MMC is a power converter topology which transforms the waveform of an electrical variable from DC to AC, or vice versa (see fig. 1.1) [LM03, Mar10].

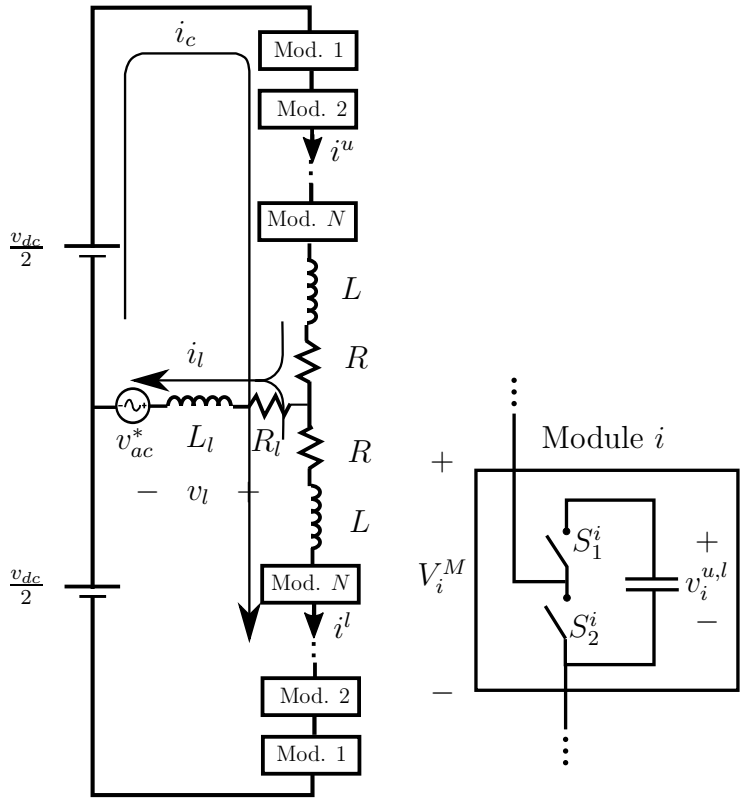

Figure 1.1.: MMC with N modules per arm. Here, v_l denotes the output voltage of the converter, i_l stands for the load current, i_c for the circulating current and, i^u and i^l for the current in the upper and lower arm respectively. S_1^i and S_2^i represent the switches and, $v_i^{u,l}$ and V_i^M describe the voltage of the capacitors and the modules, respectively.

In order to control the MMC, the switch positions of each module shown in fig. 1.1 can

be chosen independently to be one of two possible values: "inserted" or "not-inserted". A module is considered "inserted" when its voltage (V_i^M) is equal to the voltage of its respective capacitor. Conversely, a module is considered "not-inserted" when its voltage (V_i^M) is equal to 0.

The desired waveforms of output currents and voltages of the MMC are sinusoidal and can be defined as

$$i_l(t) = \hat{i}_l \cos(\omega t + \phi), \tag{1.1}$$

$$v_l(t) = \hat{v}_l \cos(\omega t), \tag{1.2}$$

where $\hat{i}_l$ is the amplitude of the output current and ω represents the angular frequency. The phase angle ϕ and the voltage amplitude $\hat{v}_l$ can be calculated depending on $v_{ac}^*(t)$, R_l and L_l. $v_{ac}^*(t)$ is also a sinusoidal voltage that ideally shares the same phase angle as i_l (for unitary power factor) and can be defined as follows

$$v_{ac}^*(t) = \hat{v}_{ac} \cos(\omega t + \phi), \tag{1.3}$$

where $\hat{v}_{ac}$ represents the amplitude.

Using electrical circuit analysis methods, an MMC with N submodules per arm can be described by the following state space model

$$\dot{x}(t) = \mathcal{A}\left(\vec{\mu}^u(t), \vec{\mu}^l(t)\right) x(t) + \mathcal{B}[v_{dc} \quad v_{ac}^*(t)]^T, \tag{1.4}$$

where

$$x(t) \triangleq \begin{bmatrix} i_c(t) & i_l(t) & v_1^u(t) & \cdots & v_N^u(t) & v_1^l(t) & \cdots & v_N^l(t) \end{bmatrix}^T, \tag{1.5}$$

is the system state. In eq. (1.5), i_c is the circulating current, whereas v_i^u and v_i^l represent the capacitor voltages of the ith module of the upper (u) and lower (l) arms respectively.

In eq. (1.4), $\vec{\mu}^u(t)$ and $\vec{\mu}^l(t)$ represent the control signals for the modules in the upper and lower arms. Each individual component of these control signals can take the value of 1 (module inserted) or 0 (module not inserted):

$$\vec{\mu}^u(t) \triangleq \begin{bmatrix} \mu_1^u(t) & \cdots & \mu_N^u(t) \end{bmatrix}^T,\ \mu_i^u(t) \in \{0, 1\}, \tag{1.6}$$

$$\vec{\mu}^l(t) \triangleq \begin{bmatrix} \mu_1^l(t) & \cdots & \mu_N^l(t) \end{bmatrix}^T,\ \mu_i^l(t) \in \{0, 1\}. \tag{1.7}$$

The matrix $\mathcal{A}\left(\vec{\mu}^u(t), \vec{\mu}^l(t)\right)$ is defined as

$$\mathcal{A}\left(\vec{\mu}^u(t), \vec{\mu}^l(t)\right) \triangleq \begin{bmatrix} \mathcal{A}_{1,1} & \mathcal{A}_{1,2}\left(\vec{\mu}^u(t), \vec{\mu}^l(t)\right) \\ \mathcal{A}_{2,1}\left(\vec{\mu}^u(t), \vec{\mu}^l(t)\right) & 0 \end{bmatrix}, \tag{1.8}$$

with

$$\begin{aligned}
\mathcal{A}_{1,1} &= \begin{bmatrix} -\frac{R}{L} & 0 \\ 0 & -\frac{R+2R_l}{L+2L_l} \end{bmatrix}, \\
\mathcal{A}_{1,2}\left(\vec{\mu}^u(t), \vec{\mu}^l(t)\right) &= \begin{bmatrix} -\frac{1}{2L}\vec{\mu}^u(t)^T & -\frac{1}{2L}\vec{\mu}^l(t)^T \\ -\frac{1}{L+2L_l}\vec{\mu}^u(t)^T & \frac{1}{L+2L_l}\vec{\mu}^l(t)^T \end{bmatrix}, \\
\mathcal{A}_{2,1}\left(\vec{\mu}^u(t), \vec{\mu}^l(t)\right) &= \begin{bmatrix} \frac{1}{C}\vec{\mu}^u(t) & \frac{1}{2C}\vec{\mu}^u(t) \\ \frac{1}{C}\vec{\mu}^l(t) & -\frac{1}{2C}\vec{\mu}^l(t) \end{bmatrix}.
\end{aligned} \tag{1.9}$$

Finally, $\mathcal{B}$ is given by:

$$\mathcal{B} \triangleq \begin{bmatrix} \frac{1}{2L} & 0 & \cdots & 0 \\ 0 & -\frac{2}{L+2L_l} & \cdots & 0 \end{bmatrix}^T. \tag{1.10}$$

As it is possible to see in eq. (1.4), MMCs are complex power converters that exhibit a non-linear and discontinuous behaviour, partially due to the binary nature of all the control inputs in eqs. (1.6) and (1.7). It is also possible to see that the size of the state space vector in eq. (1.5), and the number of control inputs, grow proportionally with the number of modules used. All this makes it considerably difficult to analyze more in detail the behavior of the MMC, motivating the study of a simpler but accurate modelling technique.

1.1.2. Current approaches and proposed methodology

In order to be able to obtain useful information about the MMC behavior, the model presented in section 1.1.1 needs to be refined and simplified. Several modeling approaches for the MMC have been presented in the literature. Some of these approaches are designed for simulation purposes with various levels of complexity [PSD+12, XGZ15, GGJ11]. The simpler models often neglect some of the dynamics of the converter and do not consider power losses, opening the path for more accurate methods to be proposed [BSBG16]. For a more detailed analysis of the converter, a more complex model is required. In [RPK+16, SLL+13], models that aim to obtain detailed information about the converter losses and behaviour in steady state are proposed. However, important information about the dynamics of the MMC cannot be obtained. In other works [RWB11, AÄN+14, YDLH16, HAN+13], more detailed continuous dynamical models of the MMC are presented. These models exhibit a reduced number of state space and control variables while maintaining the nonlinearities of the MMC. In [ÄAS+11, AÄH+14], these kind of models have been used to determine open-loop control strategies that use calculated steady state values and estimated voltage ripple values to achieve energy control with asymptotic stability. In general, all these models are represented in the *abc* frame, complicating the analysis of the converter due to the multiplication of two time varying signals. In [JJ16], a more convenient representation in the *dq* frame is presented. However, the analysis is carried out for a small signal application ignoring, in most cases, the dynamics of the second order harmonic.

The first part of the current thesis presents and analyses a reduced order model for MMCs, which reduces the number of state variables and control inputs. Here, its accuracy is verified while identifying its limitations. This is done by analyzing the frequency response of the converter in the case where the control signals present discontinuities

associated with quantization and also in cases where these discontinuities are neglected. This is particularly useful in the case where the number of modules is low and the control signals are considered continuous in order to obtain a continuous system representation. An interesting phenomenon is that the accuracy of the reduced order model is greatly affected when the operating frequency of the converter matches some specific frequencies. Following an analytical procedure, expressions for some of the frequencies where the error of the reduced order model is more significant, are presented, constituting the main contribution of the first part of this work. These frequencies are poorly damped resonant modes that depend on the converter parameters and the harmonic content of the inputs. In [LGZ16, LCM16], it is shown that these poorly damped modes can generate instability in a closed loop control strategy. The method presented in this work is a straightforward alternative to identify such frequencies and therefore, it has also potential use for stability analysis [COY16].

1.2. References for controlling MMCs

A closed-loop control law is often required to drive the outputs of a physical system to a desired value. The main advantage of the closed loop structure is that it constantly monitors the output $y(t)$ and, by comparison with a desired reference value $r(t)$, determines the control action $u(t)$ [GGS01]. A basic closed-loop control structure is shown in fig. 1.2.

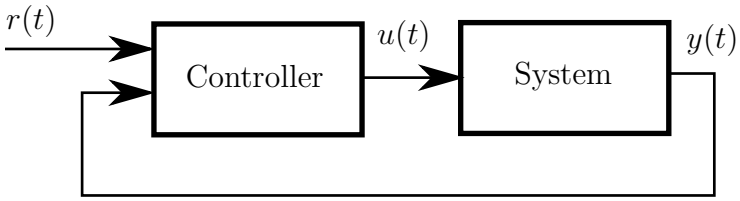

Figure 1.2.: Basic closed-loop control structure. Here $y(t)$ stands for the controlled variables in the system, $u(t)$ for the control action and $r(t)$ for the controller references.

In most applications, it is desired that the system output $y(t)$ follows the reference $r(t)$. Thus references must be properly selected in order to achieve good controlled system performance.

The second part of this work focuses on designing detailed references for MMCs, optimized to reduce capacitor voltage ripple. This is done by using the model presented in the first part of this work. The results of these first two parts will be employed to design an MPC law in later parts. Note that adequate references are required independently of the control technique used.

There are three important variables to control in an MMC: the output current i_l, the capacitor voltage of each module $v_i^{u,l}$, and the circulating current i_c (see fig. 1.1). The output current is the current delivered to the load and its desired waveform is purely sinusoidal. The capacitor voltages are desired to be the same for all modules in the same arm, distributing the voltage stress evenly in all the modules. The role of the circulating current is to transfer the power from the input voltage source to the rest of the circuit. In

some works with MMCs, the references given to their controllers are simplified DC versions of the actual waveforms. These assume an ideal case of infinite capacitances [QS12, PRFK12]. In a realistic case, with finite value capacitances, several AC components appear in the circulating current and the capacitor voltages. With existing methods, these AC components are left uncontrolled if the simplified DC references are used. To improve control loop performance, it is important that the references are designed adequately, this requires the knowledge of the possibilities and limitations of the system, cf. [QAP+12].

Some of the MMC's internal variables, specifically the circulating current and common mode voltage, can be controlled in order to improve the converter performance [LWY+15, MB15, DC15, JJF15, HZXF15, DQS15]. This is achieved by adding or removing harmonic components in a controlled manner, aiming to manipulate aspects such as voltage ripple in the capacitors or losses in the converter. In [PCK+15], a useful method to generate references for circulating current injection based on present measurements is proposed. This method facilitates the online calculation of the injected currents; however, the analysis is done based on power flow and with a limited number of harmonics. This analysis is extended in [WHMB18], where the effects of the semiconductor devices are also considered in the circulating current generation method. In [YLL+17], the circulating current is used to reduce power losses, but it does not directly consider the capacitor voltage ripple. Similarly, [PCP+15] introduces a discontinuous modulation technique that reduces power losses and capacitor voltage ripple. However, due to the introduction of such discontinuities, obtaining an analytical expression that guarantees optimality is very complex. Approaches in [SKF17, LLH+17, HZM17] address the problem of reducing the capacitor voltage ripple by using additional hardware. In some cases, however, hardware modifications are not possible. In [APE17], a different perspective of the problem is presented by analyzing the power transfer between modules. With this, circulating current and common model voltages can be properly selected. However, the analysis is limited only to minimize the previously mentioned power transfer. In [DWYZ17, TAA+16, DS13], common voltage injection and circulating current injection are applied to the MMC using control strategies, including Model Predictive Control (MPC), showing how these techniques can be used in conjunction with a controller. In [DS13], the controller is in charge of generating indirectly circulating current harmonic components based on approximate model of the capacitor voltage. However, the approximation does not consider all the harmonic components, limiting its potential. All the previously mentioned works limit their analysis to a second order harmonic in the circulating current and, in most cases, optimality is not guaranteed. In [TMG17], the analysis is extended to higher number of harmonic components. Moreover, the authors point out the high complexity of using nonlinear optimization techniques to find these optimal harmonic components on-line, and propose a method that reduces the problem to a linear program. They inject current harmonic and zero sequence voltage harmonics to reduce the energy fluctuations in the circuit, as consequence, the capacitor voltage ripple is reduced. Here, we focus on the injection of circulating current harmonic components analysing directly the capacitor voltage waveform. Although non-linear optimizations are required, it is shown that, with the method presented here, different figures of merit can be easily considered in the optimization. Moreover, we will show that the results can be approximated with relatively high accuracy by a linear function. This can potentially eliminate the requirement of on-line

optimizations or look-up tables. One of the objectives of the current thesis is to extend the approach of [PCK+15, VCR14] by analyzing directly the impact of the injection of several harmonic components in the converter currents (up to 8^{th} order) on the capacitor voltage ripple. This is done based on well-defined analytical expressions that allow one to describe completely the relationship between circulating current and capacitor voltages. The analytical expressions also allow one to consider any figure of merit as objective in the optimization, and to freely manipulate the phase and amplitude of the harmonics to guarantee the optimality of the results.

The reduced order model, which is presented in the first part of this work, is employed to reduce the analytical complexity of the converter [KHL14, AÄN09]. This model simplifies the analysis by removing the discontinuities produced by the switches, and reducing the number of state space variables and control inputs. This allows one to obtain continuous analytical expressions that relate different variables in the converter. In particular, it is possible to relate the voltage ripple in the capacitors with the harmonic components in the circulating current through a continuous analytical expression, allowing one to easily perform fast numerical optimization methods with the possibility to include any number of harmonic components in the analysis. Moreover, our results show that close to optimal values of the circulating current harmonic components can be obtained by a linear function that uses the phase and amplitude of the load current as independent variables. The accuracy of this method is evaluated showing good results for a wide range of cases. This method significantly reduces the computational effort needed to calculate the circulating current harmonic components in comparison with other methods [GGJ11, EDD11]. This, and the analysis using detailed analytical expressions, represent the main contribution of the second part of this thesis.

1.3. Control approach

The third and last part of this work addresses the problem related with the analysis of control laws for MMCs. Due to its flexibility, ability to easily deal with system constraints, and the fact that control actions can be taken considering predictions of the response of the system in the future, MPC is the technique of choice in this work [GPM89, BBM17, May14].

The types of systems where MPC has been used are diverse, including chemical, biological, mechanical and electrical systems among others [CB12]. Particularly, in electrical applications, some of the most popular systems where MPC has been applied to, are switching power converters [KCV+09, RKE+13, VLF+14, QAG14, GQ14b]. Most of these converters are bilinear systems, thus the need to investigate finite horizon optimal control of bilinear systems arises [BvdBV04, MLDD07, FDG08].

Bilinear systems usually appear in many control problems. This has motivated the study of properties, techniques an algorithms to solve these problems more efficiently [PY10, Ell09, Ekm05, Bro75, Top03b, Top03a]. In particular, in applications with MPC, robustness and stability of these bilinear systems have been the focus of analyses [BCK03, FDG08, KNM95]. Moreover, transforming complex non-linear systems into bilinear ones, to simplify their analysis and application of MPC, has also been employed [YLL11]. Along with the MPC framework, a numerical optimization procedure is required. Algorithms for

non-linear optimization, such as Sequential Quadratic Programming, are often used to deal with the bilinearity of the problem [KB11, NW06]. The complexity of such optimization grows significantly with the prediction horizon of the MPC, motivating the study of methods for its simplification.

In the following sections, details about discrete time modeling of bilinear systems and the basics behind the MPC are mentioned. Moreover, a discussion about some of the MPC properties, principally the convexity of the associated optimization, is presented. This opens the path to present the motivations behind the last part of this work, and to show how the results derived in the first two parts become crucial for the proper application of the MPC.

1.3.1. Discrete time modeling of bilinear systems

Discrete time modeling is necessary for MPC applications since, as it is shown later in section 1.3.2, it requires the prediction of the future behavior of the system which is divided into discrete time steps. Here, a generalized bilinear discrete time system is presented. This model is then transformed into an equivalent one with the purpose of simplifying the analysis later presented in chapter 4. Moreover, the model is going to be employed as a template for the analysis, and later is going to be replaced with the MMC's model.

Let us consider the following discrete time system:[1]

$$z(k+1) = \left(\mathcal{A}(k) + \sum_{i \in \mathbb{I}} \mathcal{B}_i(k) \upsilon_i(k) \right) z(k) + \mathcal{C}(k), \tag{1.11}$$

where $z(k)$ represents the state space vector, $\mathbb{I} = \{1, 2, ..., \mathfrak{I}\}$ contains the indices of all available inputs, $\mathcal{A}(k), \mathcal{B}_i(k) \in \mathbb{R}^{n \times n}$, $\mathcal{C}(k) \in \mathbb{R}^{n \times 1}$ and $\upsilon_i(k)$ represent the constrained control inputs.

The model presented here represents a generic bilinear system. In chapter 4 it is shown that the MMC using the model presented in chapter 2, can be described in discrete time with a structure as in eq. (1.11).

1.3.2. Principles of Model Predictive Control

The MPC technique consists in deciding the control action based on current state measurements of the system (say, $x(0)$), a mathematical model of the system (i.e. eq. (4.2)), and the prediction of the following $\mathcal{H}$ future values of the variable of interest (prediction horizon). In order to decide the control action, a cost function J is minimized. Then, only the most immediate control action is applied and the optimization of the cost function is run again in the next time step (see fig. 1.3).

A cost function used as standard practice in the application of the MPC technique can

[1] The discrete time variable k can be defined $t = T_s k$, where T_s represents the sampling time of the MPC and t represents the time.

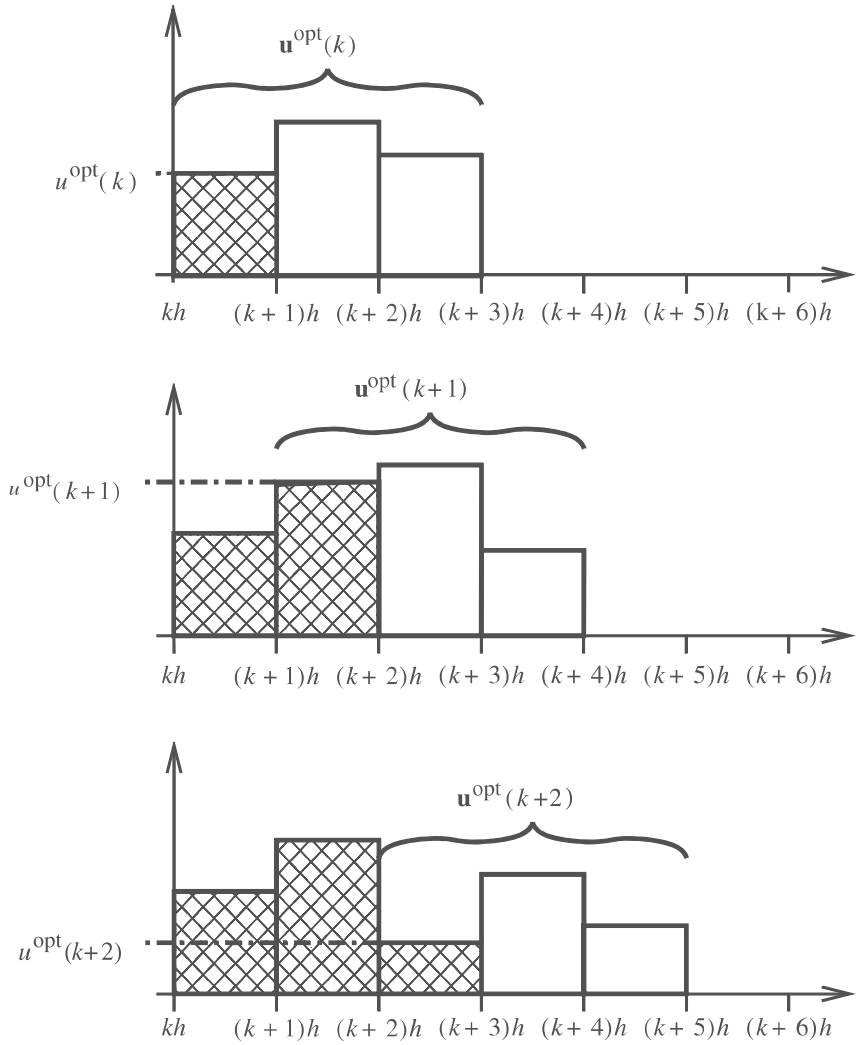

Figure 1.3.: Example of an MPC with prediction horizon 3 [QAG14]. Here $u^{\mathrm{opt}}(k)$ represents the optimal control action.

be defined as follows:

$$J(x(0),...,x(\mathcal{H}),u_i(0),..,u_i(\mathcal{H}-1)) = \sum_{h=1}^{\mathcal{H}} J_h^{\dagger}(x(h),u_i(h-1)), \quad \forall i \in \mathbb{I}, \tag{1.12}$$

where the stage cost $J_h^{\dagger}(x(h),u_i(h-1))$ is written as

$$J_h^{\dagger}(x(h),u_i(h-1)) = \|x(h)-\bar{x}(h)\|_M^2 + \frac{\lambda_h^{\dagger}}{2}\sum_{i\in\mathbb{I}}(u_i(h-1)-\bar{u_i}(h-1))^2, \quad \forall i \in \mathbb{I}. \tag{1.13}$$

Let us consider the case where the whole state vector $x(k)$ is controlled. Then, in eqs. (1.12) and (1.13), $x(k)$ represent the state and $u_i(k)$ the constrained control inputs, where $u_i(k) \in \mathbb{U}$, $\mathbb{U}$ being a set of all the possible values of $u_i(k)$. In eq. (1.13), $\|v\|_M^2 = v^T M v$ represents the square of the weighted Euclidean norm with M being a

diagonal matrix with positive entries, $\lambda_h^\dagger$ is a non-negative weighting parameter and $\bar{x}(h)$ and $\bar{u}_i(h)$ represent the state and input references, respectively.

It is possible to write the goal of the MPC as an optimization problem subject to constraints as follows:

$$\begin{aligned} \min_{\mathbf{u}_i(\mathcal{H}-1),\forall i\in\mathbb{I}} \quad & J^\dagger(x(0),...,x(\mathcal{H}),u_i(0),..,u_i(\mathcal{H}-1)) \\ \text{s.t.} \quad & h(\mathbf{u}_i(\mathcal{H}-1))=0 \\ & g(\mathbf{u}_i(\mathcal{H}-1))\leq 0, \qquad \forall i\in\mathbb{I} \\ & u_i(k)\in\mathbb{U} \end{aligned} \tag{1.14}$$

The last part of this work, presented in chapter 4, will focus on analyzing the cost function J and properly selecting the design parameter $\lambda_h^\dagger$ that guarantee its convexity. More on the importance of this will be addressed in the following sections

1.3.3. Finite control set MPC and MPC with PWM

MPC provides the flexibility to deal with the control of power electronics in two different ways [QAG14]. One of them is to allow the MPC to drive the switches in the converter directly (Finite Control Set (FCS)) [GQ14b, RKE+13, VBSH15]. This implies that the control variables only take finite (e.g. binary) values. The main advantages of this approach is that it delivers better performance during transients and allows one the freedom to manipulate switching instants. However, it requires more elaborate optimization algorithms due to the binary nature of the control variables, and it is also necessary to execute the control algorithm often to ensure the switching is produced with a high enough frequency (see fig. 1.4 (a)). The second option is to make use of a Pulse With Modulator (PWM) which transforms the binary control signal into a continuous one. Some of its disadvantages include a decrease in performance during transients due to the impossibility to manipulate the switching instants freely (see fig. 1.4 (b)). However, performance in steady state is often improved [ALQ13], this also extends to the frequency spectrum of the voltages and currents, that can be controlled easily due to the predictable spectrum of the PWM. Due to the continuous nature of the control variables, a numerical optimization algorithm that finds the optimal control action is required. In comparison with the FCS problem, the complexity of the optimization problem is significantly reduced due to the continuous nature of the control variables and the possibility to use convex constraints. These last points motivate our choice of using a PWM and work towards a simpler and faster optimization procedure.

1.3.4. Numerical optimization

Numerical optimization has been widely used and studied for many different applications. In general, optimization problems can be categorized as convex and non-convex [BV04, MS13, HU89, Yak92]. Non-convex problems can have several local minimum points. Moreover, convergence of numerical algorithms to one of these local minima can be a challenge in some cases. Once a local minimum is found, it is not easy to guarantee that such point also corresponds to the global minimum, possibly leading to suboptimal results. Algorithms designed for non-convex optimization problems tend

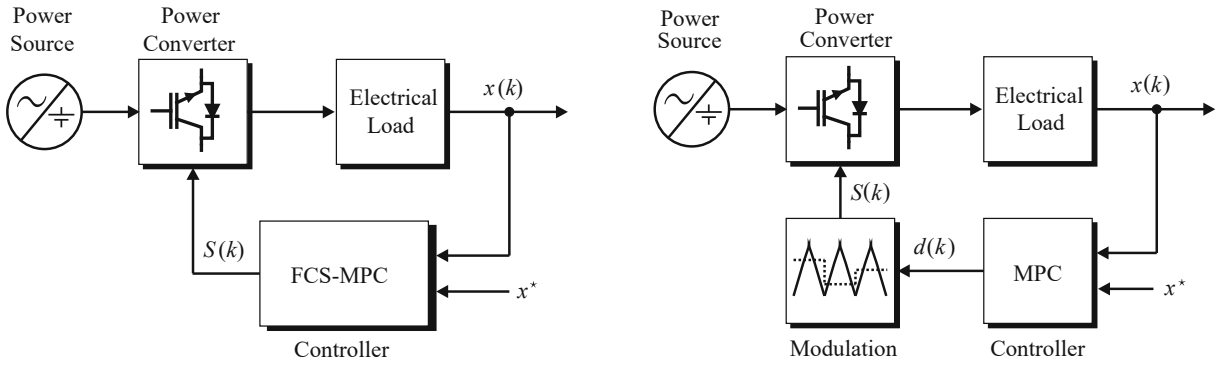

(a) Finite Control Set MPC

(b) MPC with PWM

Figure 1.4.: Types of MPC in applications for power electronics [QAG14].

to be more resource consuming when compared with algorithms for convex problems [Aus87, Nes13, PH02, HL04, Can04, BLO05, BX09, TS02]. On the other hand, convex optimization problems are simpler and have been widely studied. For these type of problems only one minimum exists, which also corresponds to the global minimum. This eases significantly the procedure of achieving an optimal result. Thus, simpler, faster and less computationally intensive optimization algorithms are required.

Industrial optimization problems often involve complex system models that usually result in non-convex optimization problems. Several attempts to reduce the complexity of non-convex problems by associating them to a convex equivalent have been reported. In [CMC+14], the convexity of a special class of bilinear systems is studied. However, the results are limited to a particular case of positive switched systems. In [ST95], an approximate convex envelope of the objective function is used along with modified constraints to ensure convexity on a determined region. However, the accuracy of these results can be compromised due to the use of an approximation. The work in [GF08] gives an overview of a transformation that is able to make positive polynomials convex, which is the base of geometric programming. This, however, cannot be extended to other types of polynomials, restricting its application. In [HA14], the problems are limited to such where only the control constraints are non-convex. In [REFA06], the sum of squares convexification technique is used along with polynomial optimization to find the solution to MPC problems. The drawback of this technique lies on its high computational complexity and its exponential increase with the prediction horizon. In [PHW99, HCVH17], convexification techniques with applicability to power electronics are presented. However, these are restricted to mixed-integer problems.

The last part of this work focuses on analyzing the optimization problem that arises when quadratic cost functions are used in MPC with PWM for power converters, which can be typically modeled as bilinear systems (see fig. 1.4 (b)). The goal is to find conditions that allow one to exploit the useful properties of convex optimization on MPC for power electronics, which is typically a non-convex problem. The development of these conditions are the main contribution of this part of the work and, along with the results of the first two parts, they are used to present an MPC strategy with reduced complexity for MMCs.

1.4. Outline

This section describes the outline of this work and mentions the contributions and related publications associated with each chapter

Chapter 2

This chapter analyses the mathematical modeling of the MMC, elucidating an explicit analytical relationship between all its state variables. A reduced order model is presented as a way of simplifying the analysis and modeling of the converter. Moreover, a detailed analysis and validation of this model is carried out explaining its limitations. Frequencies where its accuracy is compromised are properly identified as a function of the converter parameters. Here it is concluded that, as long as one stays sufficiently far from these frequencies, the accuracy of the reduced order model is sufficiently good.

Most of the contributions presented in this chapter can be found in [LQA+18b, LQA+14].

Chapter 3

In this chapter, the reduced order model of chapter 2 is used to propose a method of selecting optimal harmonic components. The analysis shows the impact of up to an 8th harmonic in the circulating current and additional harmonic components in the load current. The method is shown to provide accurate results by using analytical expressions obtained with the reduced order model or linear approximations to obtain the optimal harmonic components. Moreover, the impact of the harmonic components in the circulating current over the power transfer between the converter arms is also analyzed.

Most of the contributions presented in this chapter can be found in [LQA+15, LQA+18a].

Chapter 4

This last part of the work applies the results obtained in the previous chapters to MPC for MMCs. First, the problem of FCS MPC is addressed, mentioning its drawbacks and motivations behind the use of PWM. Under this motivation, the optimization problem associated with the MPC is analyzed and conditions to guarantee its convexity are derived. Analytical methods are provided to estimate these conditions and its effectiveness is verified. The results here allows one to use simple and fast optimization algorithms for convex problems in the application of MPC for MMCs.

Most of the contributions presented in this chapter can be found in [LQA+14, LQAG18].

Chapter 5

Finally, general conclusions are presented along with a discussion about future work.

2. Reduced order model of MMCs: validation and limitations

This chapter presents a reduced order model that allows one to eliminate the discontinuities of the MMC produced by the switching elements, and to reduce the number of control and state space variables. This model also allows one to obtain explicit analytical expressions that describe the behavior of the converter variables, and gives the possibility to approximate the control function (number of modules inserted) by a continuous value. This chapter extends the concept in [IANN12b] further, and analyzes the effects of this approximation on the accuracy of the model by estimating the frequency response in different situations. In order to estimate this response, several approaches are used; these include numerical solutions and also derivation of analytical expressions based on Fourier expansion and linearized models. The subsequent analysis shows that the accuracy of the reduced order model is low when close to the resonant frequencies of the converter, due to the additional frequency components introduced by quantization effects. This produces a modulation effect that displaces the resonant frequencies of the reduced order model (when continuous signals are used) in comparison with those of the full order MMC (with quantization). This generates differences in where the amplitude peak related to the resonance is located, producing inaccuracies. The results presented show that, given sufficient knowledge about the resonant frequencies, it is possible to determine beforehand if the response of the reduced order model is accurate enough. This information can be helpful when designing an MMC based on this model.

In the following sections, a reduced order model is introduced and the implications of its application are discussed. This is followed by a frequency response analysis where the limitations of this model are identified. Later, the model introduced here is going to be used in chapter 3 to design optimized references for MMCs for control purposes, and in chapter 4 to help the MPC to predict the future behavior of the MMC.

2.1. Reduced order model

The MMC is a highly nonlinear, discontinuous system with multiple inputs as is shown in section 1.1.1 on page 2. The discontinuities make the system harder to analyze. In order to simplify the analysis of the system and obtain analytical expressions for the variables of interest, this section proposes an approximation method to reduce the order of the model, the number of inputs, and remove the discontinuities.

Lemma 1. *Consider the MMC model described in eq.* (1.4)*, and assume that the capacitor*

voltages are balanced[1]*:*

$$v_i^u(t) = v_j^u(t) = v^u(t), \quad \forall i, j \in \{1, 2, \ldots, N\} \tag{2.1}$$

and

$$v_i^l(t) = v_j^l(t) = v^l(t), \quad \forall i, j \in \{1, 2, \ldots, N\} \tag{2.2}$$

Then the MMC model in eq. (1.4) *reduces to:*

$$\dot{x}(t) = A\left(\breve{\mu}^u(t), \breve{\mu}^l(t)\right) x(t) + B[v_{dc} \quad v_{ac}^*(t)]^T, \tag{2.3}$$

where

$$A\left(\breve{\mu}^u(t), \breve{\mu}^l(t)\right) \triangleq \begin{bmatrix} -\frac{R}{L} & 0 & -\frac{1}{2L}\breve{\mu}^u(t) & -\frac{1}{2L}\breve{\mu}^l(t) \\ 0 & -\frac{R+2R_l}{L+2L_l} & -\frac{1}{L+2L_l}\breve{\mu}^u(t) & \frac{1}{L+2L_l}\breve{\mu}^l(t) \\ \frac{1}{NC}\breve{\mu}^u(t) & \frac{1}{2NC}\breve{\mu}^u(t) & 0 & 0 \\ \frac{1}{NC}\breve{\mu}^l(t) & -\frac{1}{2NC}\breve{\mu}^l(t) & 0 & 0 \end{bmatrix}, \tag{2.4}$$

$$B \triangleq \begin{bmatrix} \frac{1}{2L} & 0 & 0 & 0 \\ 0 & -\frac{2}{L+2L_l} & 0 & 0 \end{bmatrix}^T, \tag{2.5}$$

and the system state is now given by

$$x(t) \triangleq \begin{bmatrix} i_c(t) & i_l(t) & v^u(t) & v^l(t) \end{bmatrix}^T. \tag{2.6}$$

In this model, the modulation functions are

$$\breve{\mu}^u(t) \triangleq \sum_{j=1}^{N} \mu_j^u(t), \quad \breve{\mu}^u(t) \in \{0, \ldots, N\}, \tag{2.7}$$

and

$$\breve{\mu}^l(t) \triangleq \sum_{j=1}^{N} \mu_j^l(t), \quad \breve{\mu}^l(t) \in \{0, \ldots, N\}. \tag{2.8}$$

These functions represent the number of modules inserted in the upper and lower arms respectively, and depend on the control law adopted.

Proof. Note that in the equation related to the derivative of i_c in eq. (1.4), using eq. (2.1) gives the following :

$$-\frac{v_1^u(t)}{2L}\mu_1^u(t) - \cdots - \frac{v_N^u(t)}{2L}\mu_N^u(t) = -\frac{v^u(t)}{2L}\sum_{j=1}^{N}\mu_j^u(t). \tag{2.9}$$

Let $\breve{\mu}^u(t)$ be the modulation function defined in eq. (2.7). Therefore, it can be concluded that

$$-\frac{v_1^u(t)}{2L}\mu_1^u(t) - \cdots - \frac{v_N^u(t)}{2L}\mu_N^u(t) = -\frac{v^u(t)}{2L}\breve{\mu}^u(t). \tag{2.10}$$

[1]Note that $v^u = v^l$ is not imposed.

An analogous procedure can be carried out for the remaining terms in the equations of the derivatives of i_c and i_l for the lower arm of the converter

Since the capacitor voltages on each arm are assumed equal, only two state space variables are now required to represent the voltages of all the modules. Adding all the capacitor voltages of the upper arm yields

$$\sum_{j=1}^{N} v_j^u(t) = \sum_{j=1}^{N} \left(\frac{i_c(t)}{C} \mu_j^u(t) + \frac{i_l(t)}{2C} \mu_j^u(t) \right). \tag{2.11}$$

Using eqs. (2.1) and (2.7), the previous expression can be simplified as follows:

$$N v^u(t) = \frac{i_c(t)}{C} \check{\mu}^u(t) + \frac{i_l(t)}{2C} \check{\mu}^u(t). \tag{2.12}$$

An analogous procedure can be followed for the voltages in the lower arm, leading to eqs. (2.3) to (2.5)

□

It is important to note that when the reduced order model is used, it is implicitly assumed that the voltages in all the capacitors are balanced according to eqs. (2.1) and (2.2). Note that when this condition is fulfilled, it is possible to represent the capacitor voltages of all modules with one voltage per arm and use aggregated control signals as in eqs. (2.7) and (2.8) without using any approximation. All the information about any modulation technique used, or about the control inputs $\mu_j^{u,l}$ in general, is now contained in $\check{\mu}^{u,l}$. Thus, if the voltages of the capacitors are balanced (see eqs. (2.1) and (2.2)), then the full order model and the reduced order model using eqs. (2.7) and (2.8) provide the same result.

The reduced order model facilitates the derivation of analytical solutions by reducing the number of input variables and the size of the state vector. This can be used for a more detailed analysis of the converter such will be shown throughout this work.

2.1.1. Implications of using continuous control signals

In some cases, it may be convenient to express the aggregated control signals in eqs. (2.7) and (2.8) as the sum of an equivalent continuous valued signal $\mu^{u,l}(t)$ and a quantization effect $Q_n(t)$, produced by having only a finite number of modules in the converter, as follows:

$$\check{\mu}^{u,l}(t) = \mu^{u,l}(t) + Q_n(t). \tag{2.13}$$

If desired, $Q_n(t)$ can be neglected using only the continuous part $\mu^{u,l}(t)$. In particular, if $\mu^{u,l}(t)$ are smooth, then only differentiable functions need to be taken into account, easing the analysis. Note that this step implies an approximation and it is especially important when a low number of modules are available (i.e. $Q_n(t)$ comparable with $\mu^{u,l}(t)$). It is because of this approximation that the results of the reduced order model may differ from the ones of the full order MMC.

Neglecting the quantization allows one to obtain analytical expressions of variables such as the capacitor voltages. These expressions can then be used for optimization and

reference design as shown in chapter 3. However, the quantization affects the frequency response of the circuit, leading to inaccuracies when this is neglected.

Due to the non-linearity in the model, there is a modulation effect that comes from the multiplication of the control signal with the capacitor voltages, see eq. (2.3). This effect moves the resonant frequencies (i.e. peaks of amplitude in i_c) of the converter when additional frequency components are considered in the control signals. As shown next, this accentuates the error of the reduced order model at some specific frequencies.

To illustrate the effect of the quantization at different frequencies, let us consider numerical values of the parameters of the converter as in table 2.1. Moreover, let us define the following control inputs:

- smooth control inputs:

$$\mu^u(t) = N\frac{1+\cos(\omega t)}{2}, \quad \mu^l(t) = N\frac{1-\cos(\omega t)}{2}. \tag{2.14}$$

- quantized control inputs:

$$\breve{\mu}^u(t) = \text{ni}\left(N\frac{1+\cos(\omega t)}{2}\right), \; \breve{\mu}^l(t) = \text{ni}\left(N\frac{1-\cos(\omega t)}{2}\right), \tag{2.15}$$

  where the operation ni(•) approximates the argument to the nearest integer.

Figure 2.1 shows the response of an open loop MMC to the control inputs in eqs. (2.14) and (2.15) with fundamental frequency $\omega = 2\pi 60$. A clear difference between the two cases (with and without quantization) can be observed. Interestingly, the situation changes when the frequency of the sinusoidal input is changed to $\omega = 2\pi 50$, see fig. 2.2. The simulation shows that the difference between the response of the model without the quantization and the model with the quantization is minimal for this frequency. In fig. 2.3, a simulation with the error produced by neglecting the quantization effect for MMCs with different numbers of modules is shown. The error is calculated as the Root Mean Square of the difference of the simulated waveforms over one period in steady state. The simulation shows that a larger error is presented for some specific frequencies. This error tends to be larger the lower the number of levels. However, sufficiently far from the aforementioned frequencies, the error for $N = 4$, $N = 8$ and $N = 12$ becomes low and very similar. This also holds true for a higher number of levels, which implies that the reduced order model represents a good approximation of the MMC even with a low number of levels as long as the operation is sufficiently far from these critical frequencies. In the following sections, the reasons behind these differences are going to be analyzed in more detail.

In fig. 2.3 several peaks in the error plots can be noticed. In general, it is possible to group these peaks into two different cases: the high frequency peak (around 60Hz) and its duplicates due to the nonlinearities in the system (i.e modulation due to the multiplication of the control signal and the module voltages), and the low frequency peak (around 15Hz) and its duplicates. In fig. 2.3 this grouping is shown for the case with $N = 8$. These error peaks are directly related with the resonant frequencies of the converter. We shall give special attention to the peak with the highest frequency since it may be located close to the typical operating frequencies of the converter (50Hz or 60Hz). This observation

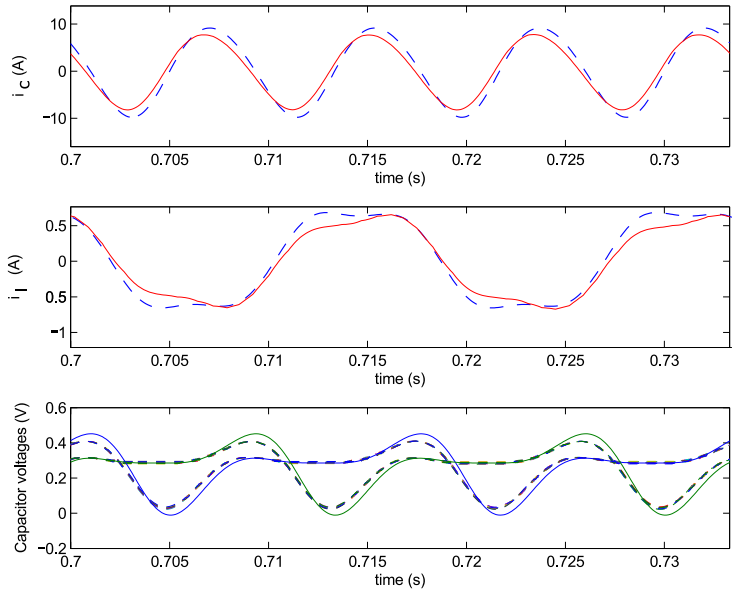

Figure 2.1.: Effects of the quantization at 60Hz (Solid lines: without quantization, dashed lines: with quantization).

Table 2.1.: Parameter values in p.u. at $\omega = 2\pi 50$ for an MMC (The p.u. (per unit) values are normalized with respect to the grid voltage (3800 V) and the nominal current (650 A)). P.F. stands for power factor.

Variable	R	X_L (ωL)	X_C $(\frac{1}{\omega C})$	R_l	X_{L_l} (ωL_l)	v_{dc}	$\hat{v}^*_{ac}$	$P.F.$
Value	0.004	0.075	0.089	0.01	0.15	2.19	1	1

shows that the quality of the model is frequency dependent and motivates our subsequent analysis.

Let us first define what we shall refer to as the "frequency response of the MMC". Due to the non-linear nature of the system, frequency multiples of the input frequency are likely to appear in the converter currents and voltages. This motivates us to define the frequency response of the MMC as the amplitude of the second harmonic of the circulating current i_c as a function of the frequency in the control signals ω (see eqs. (2.14) and (2.15)). The reason why the second harmonic of i_c is chosen for the analysis is mainly due to the following facts: (i) this is the lowest order harmonic in the circulating current, (ii) its amplitude is significantly higher than the amplitude of the other harmonics, (iii) as shown in fig. 2.3, the resonance of this second order harmonic is more likely to match the operating frequency of the converter[2]. In the following sections we are going to focus our efforts into determining the relation of these resonant frequencies with the converter parameters.

[2]Note that the resonant frequencies are independent of our choice of considering the second order harmonic of i_c as variable for the analysis.

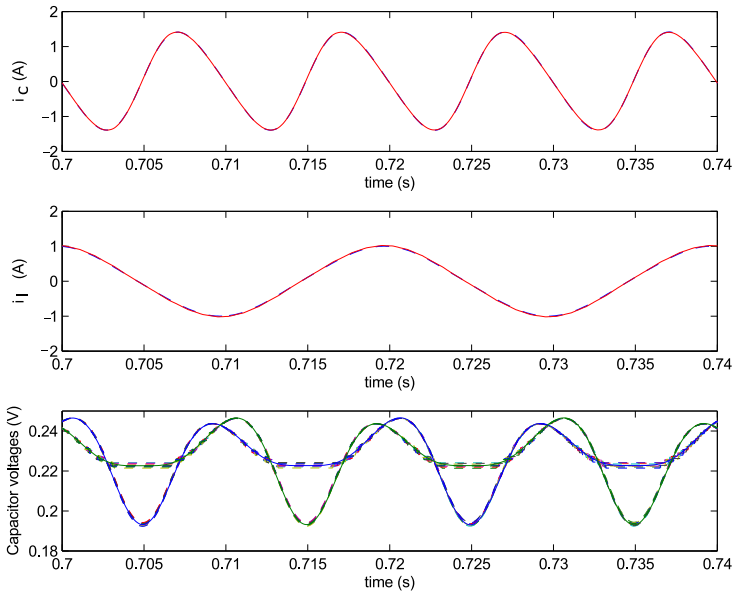

Figure 2.2.: Effects of the quantization at 50Hz (Solid lines: without quantization, dashed lines: with quantization).

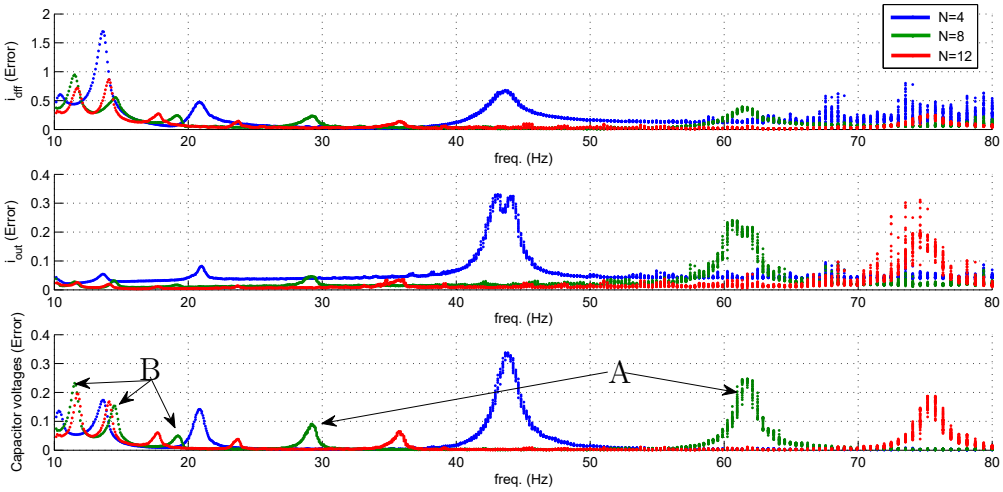

Figure 2.3.: Error produced by the quantization effect using 4, 8 and 12 modules for different frequency values. (A) High frequency peaks. (B) Low frequency peaks.

2.1.2. Effects of capacitor voltage imbalances in the reduced order model

The reduced order model assumes that the capacitor voltages in all the modules are properly balanced. If this holds true, the prediction of the reduced order model can closely match its full order counterpart as seen in fig. 2.2. However, good voltage balancing is not always possible.

This subsection aims to evaluate the effects of module voltage imbalances in the ac-

curacy of the reduced order model. This analysis is done by setting a voltage balancing control algorithm in the full order MMC that allows a specific maximum voltage difference between the modules of the same arm, also known as voltage imbalance ($\delta v^{u,l}_{max}$). This result is then compared with the prediction of the reduced order model for several values of $\delta v^{u,l}_{max}$.

In fig. 2.4, the increment of the RMS error of the reduced order model as a function of the relation between the maximum allowed voltage imbalance $\delta v^{u,l}_{max}$ and the module voltage ripple $\Delta v^{u,l}$ is shown. For this test, a frequency of 50Hz is used and the reference RMS error values are taken from fig. 2.3 ($N = 8$). As expected, the error presented in the module voltages is increased significantly due to the allowed imbalance. However, for the rest of the variables, an increment of less than 10%, with an allowed voltage imbalance of up to 35% of the module voltage ripple, is shown. It is worth noticing that the circulating current is more affected by the voltage imbalances due to the low arm impedance.

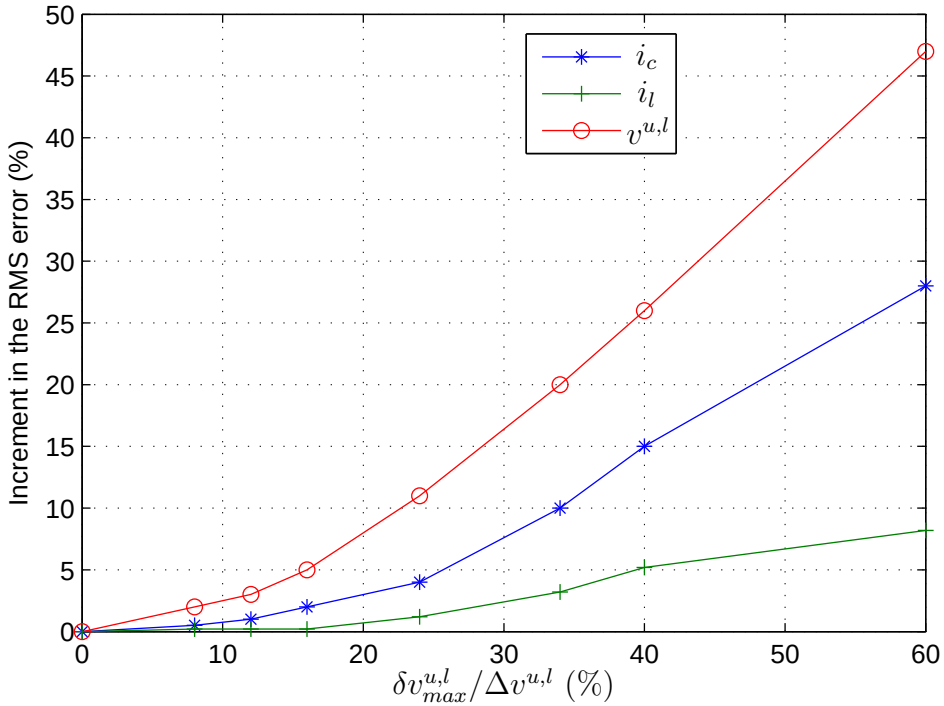

Figure 2.4.: Increment in the RMS error of the prediction of the reduced order model introduced by voltage imbalances in the capacitors as a function of the relation between the maximum voltage difference between capacitors of the same arm (voltage imbalance $\delta v^{u,l}_{max}$) and the voltage ripple $\Delta v^{u,l}$. Reference values: $i_c(error) = 8.3 \cdot 10^{-3}$, $i_l(error) = 17.7 \cdot 10^{-3}$, $i_c(error) = 4 \cdot 10^{-3}$, $\Delta v^{u,l} = 0.05$ p.u..

2.1.3. Blocking and de-blocking modes

As protective measure, the blocking mode is commonly used in unbalanced grid conditions. This mode consists in switching off all the switches in the modules on either of the arms

of the converter, forcing the current to flow through the parallel diode associated to the semiconductor devices. In order to include the blocking mode in the simplified model of the MMC, the equivalent configuration shown in fig. 2.5 can be used. More details of this configuration and blocking and de-blocking modes can be found in [AÄNN12, AÄN13] where the configuration in fig. 2.5 was originally proposed.

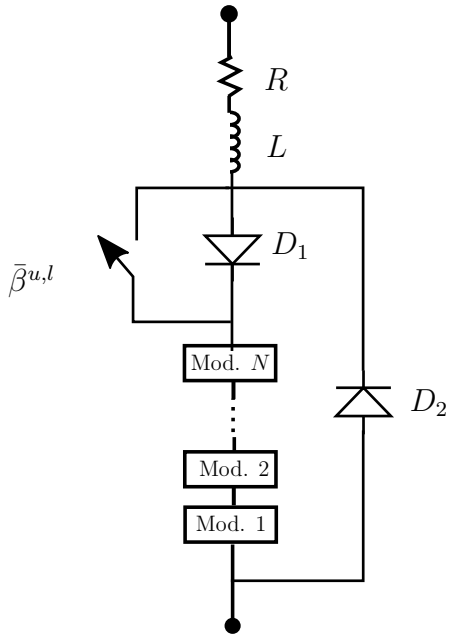

Figure 2.5.: MMC arm including blocking and de-blocking modes. In blocking mode ($\beta^{u,l} = 1$ switch open), D_1 blocks partially the current that goes through the modules. In this case, the current flows through D_2 instead. In blocking mode $\mu^{u,l}$ are set to N.

The original MMC equations in eq. (2.3) can be modified to include the blocking modes as follows:

$$\begin{aligned}\dot{i_c}(t) = &-\frac{R}{L}i_c(t) - \frac{1}{2L}\left(1-\beta^u \mathrm{u}\left(-i_c-\frac{i_l}{2}\right)\right)\left(N\beta^u + \breve{\mu}^u(t)\left(1-\beta^u\right)\right)v^u - \\ &\frac{1}{2L}\left(1-\beta^l \mathrm{u}\left(-i_c+\frac{i_l}{2}\right)\right)\left(N\beta^l + \breve{\mu}^u(t)\left(1-\beta^l\right)\right)v^l + \frac{1}{2L}v_{dc}\end{aligned} \tag{2.16}$$

$$\begin{aligned}\dot{i_l}(t) = &-\frac{R+2R_l}{L+2L_l}i_l(t) - \frac{1}{L+2L_l}\left(1-\beta^u \mathrm{u}\left(-i_c-\frac{i_l}{2}\right)\right)\left(N\beta^u + \breve{\mu}^u(t)\left(1-\beta^u\right)\right)v^u + \\ &\frac{1}{L+2L_l}\left(1-\beta^l \mathrm{u}\left(-i_c+\frac{i_l}{2}\right)\right)\left(N\beta^l + \breve{\mu}^u(t)\left(1-\beta^l\right)\right)v^l - \frac{2}{L+2L_l}v^*_{ac}\end{aligned} \tag{2.17}$$

$$\dot{v}^u(t) = \left(\frac{1}{NC}i_c + \frac{1}{2NC}i_l\right)\left(N\beta^u + \breve{\mu}^u(t)\left(1-\beta^u\right)\right)\left(1-\beta^u \mathrm{u}\left(-i_c-\frac{i_l}{2}\right)\right) \tag{2.18}$$

$$\dot{v}^l(t) = \left(\frac{1}{NC}i_c - \frac{1}{2NC}i_l\right)\left(N\beta^l + \breve{\mu}^l(t)\left(1-\beta^l\right)\right)\left(1-\beta^l \mathrm{u}\left(-i_c + \frac{i_l}{2}\right)\right) \tag{2.19}$$

where u(∗) represents the step function, β^u and β^l represent the blocking signals of the upper and lower arm respectively ($\beta^{u,l} = 1$ represents a blocked arm). In the blocking state, the control signals $\mu^{u,l}$ are forced to N and the arm voltage depends on the direction of the current (see fig. 2.5).

In the following sections, the frequency response of the MMC will be analyzed. However, due to the mathematical complexity that arises when the blocking mode is included (see eqs. (2.16) to (2.19)), the method presented in section 2.3, used to analyze the frequency response and for the accuracy assessment, cannot be applied due to the impossibility of transforming the system into a component wise linear system as we will see in eq. (2.27). For this reason, the subsequent analyses are going to be performed without including the blocking mode.

2.2. Estimation of the MMC frequency response (Linearization approach)

This section presents a preliminary approach to obtain information about the frequency response of the MMC that uses a linearized version of the reduced order model around an operation point. The linearization technique is widely used in many applications. One of them is design of control laws for power converters, where it is important that the information provided by the linearized model matches as close as possible the original model to guarantee proper performance and good stability properties. This approach aims to derive simple analytical expressions for the resonant frequencies based on linear differential equations that later will be used for comparison with more elaborate approaches. This will also serve as a criteria to determine the accuracy of the linearized model of the MMC.

The linear model can be written based on eq. (2.3), as follows:

$$\dot{\tilde{x}}(t) = A\left(\bar{\mu}^u, \bar{\mu}^l\right)\tilde{x}(t) + B(x(0))[v_{dc} \quad v_{ac}^*(t) \quad \tilde{\mu}^{u,l}(t)]^T, \tag{2.20}$$

where $\bar{\mu}^{u,l}$ represent the control signals in the operational point, $\tilde{\mu}^{u,l}(t)$ and $\tilde{x}(t) = [\tilde{i}_c \quad \tilde{i}_l \quad \tilde{v}^u \quad \tilde{v}^l]$ the incremental variables associated with the control signals and the state space vector respectively, and $B(x(0))$ a constant matrix that depends on the initial conditions $x(0)$. Since the matrix $A\left(\bar{\mu}^u, \bar{\mu}^l\right)$ is in charge of determining the placement of the poles and resonant frequencies of the system, we focus our analysis in this term of the equation.

To simplify the calculations, let us assume that $\|R + j\omega L\| \ll \|R_l + j\omega L_l\|$. Therefore, the resonant frequencies can be analyzed by considering two different equivalent circuits; a circuit for the higher frequencies and an additional circuit for the lower frequencies, as shown in fig. 2.6. The following analysis uses this assumption and the linearized model in eq. (2.20) to derive analytical expressions of the resonant frequencies of the MMC. In section 2.3, the results of the resonant frequencies obtained with the linearized model will be compared with results obtained with more accurate methods, which can be very useful

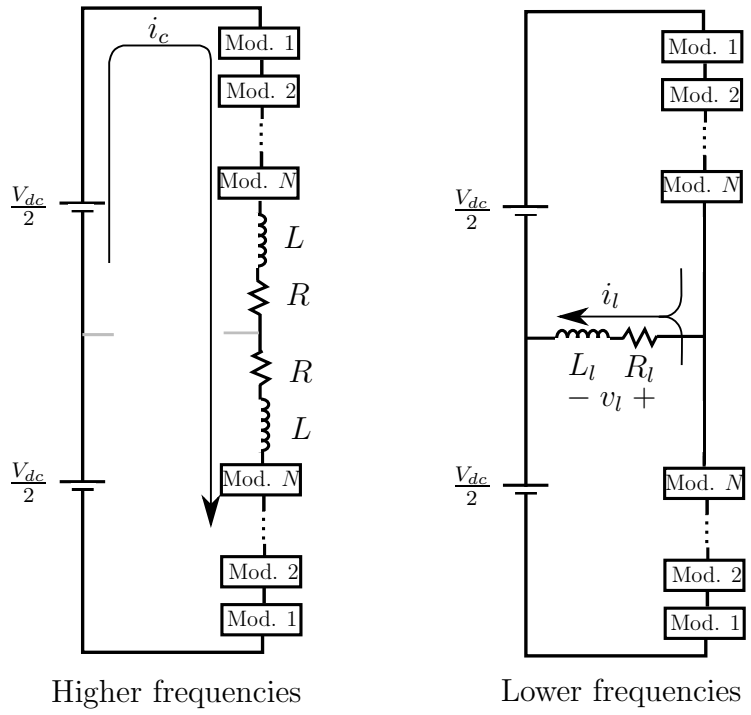

Figure 2.6.: Approximate circuits of the MMC to compute its resonant frequencies.

when one wishes to evaluate the accuracy of the linearized model specially in the case of stability of control loops. Moreover, it will provide more insight into the problem of explaining the results in fig. 2.3.

2.2.1. High Frequencies

Under the assumption $\|R + j\omega L\| \ll \|R_l + j\omega L_l\|$, it is possible to rewrite the differential equations of the linear system in eq. (2.20) and, taking into account that the operation lies in the high frequency range as shown in fig. 2.6 (i.e. $\|R_l + j\omega L_l\| \to \infty$ or $i_l = 0$), develop analytical expressions for the resonant frequencies of the converter. According to eq. (2.20), the following holds:

$$\begin{aligned} \dot{\tilde{i}}_c &= -\frac{R}{L}\tilde{i}_c - \frac{1}{2L}\bar{\mu}^u\tilde{v}^u - \frac{1}{2L}\bar{\mu}^l\tilde{v}^l + \dots, \\ \dot{\tilde{v}}^u &= \frac{1}{NC}\bar{\mu}^u\tilde{i}_c + \dots, \qquad \dot{\tilde{v}}^l = \frac{1}{NC}\bar{\mu}^l\tilde{i}_c + \dots. \end{aligned} \tag{2.21}$$

For the sake of simplicity, some terms are omitted in eq. (2.21) since they have no effect over the value of the resonant frequencies.

By obtaining the second derivative of $\tilde{i}_c$ using eq. (2.21), and substituting $\dot{\tilde{v}}^u$ and $\dot{\tilde{v}}^l$, the following is obtained:

$$\begin{aligned}\ddot{\tilde{i}}_c =& -\frac{R}{L}\dot{\tilde{i}}_c - \frac{1}{2L}\bar{\mu}^u\left(\frac{1}{CN}\bar{\mu}^u\right)\tilde{i}_c - \frac{1}{2L}\bar{\mu}^l\left(\frac{1}{CN}\bar{\mu}^l\right)\tilde{i}_c + \dots \\ =& -\frac{R}{L}\dot{\tilde{i}}_c - \frac{1}{2LCN}\left(\left(\bar{\mu}^u\right)^2 + \left(\bar{\mu}^l\right)^2\right)\tilde{i}_c + \dots .\end{aligned} \tag{2.22}$$

It is assumed that $\bar{\mu}^u + \bar{\mu}^l = N$ and $\bar{\mu}^u = \alpha N$, where $0 < \alpha < 1$. α is a constant value that depends on the linearization point. Using the second order differential equation in eq. (2.22), a value for the resonant frequency can be obtained as:

$$f_1 = \frac{1}{\sqrt{\frac{2LC}{N}\frac{1}{\alpha^2+(1-\alpha)^2}}}, \quad \frac{\sqrt{2}}{2}\frac{1}{\sqrt{\frac{2LC}{N}}} \leq f_1 < \frac{1}{\sqrt{\frac{2LC}{N}}} \tag{2.23}$$

Due to the fact that i_c contains mainly second order harmonics, an interesting phenomenon occurs. This consists in the resonance being produced when the input frequency is equal to $\frac{f_1}{2}$. Due to the system non-linearities, this input frequency produces an i_c with frequency f_1, matching the resonance frequency. Note that this phenomenon is not captured by the linear model analyzed in this section. This will be corroborated and analyzed further with the method presented in section 2.3.

2.2.2. Low Frequencies

For the low frequency case, as presented in fig. 2.6, R and L are considered as 0. eq. (2.20) can be used under this consideration to write the following set of differential equations

$$\begin{aligned} 0 &= -\bar{\mu}^u\tilde{v}^u - \bar{\mu}^l\tilde{v}^l + \dots, & \dot{\tilde{i}}_l &= -\frac{R_l}{L_l}\tilde{i}_l - \frac{1}{2L_l}\bar{\mu}^u\tilde{v}^u + \frac{1}{2L_l}\bar{\mu}^l\tilde{v}^l + \dots, \\ \dot{\tilde{v}}^u &= \frac{1}{NC}\bar{\mu}^u\left(\tilde{i}_c + \frac{\tilde{i}_l}{2}\right) + \dots, & \dot{\tilde{v}}^l &= \frac{1}{NC}\bar{\mu}^l\left(\tilde{i}_c - \frac{\tilde{i}_l}{2}\right) + \dots . \end{aligned} \tag{2.24}$$

In an analogous procedure as for the high frequency case, the second derivative of $\tilde{i}_l$ is obtained and $\dot{\tilde{v}}^u$ and $\dot{\tilde{v}}^l$ are substituted, leading to:

$$\begin{aligned}\ddot{\tilde{i}}_l =& -\frac{R_l}{L_l}\dot{\tilde{i}}_l + \frac{1}{L_l}\bar{\mu}^l\dot{\tilde{v}}^l \\ =& -\frac{R_l}{L_l}\dot{\tilde{i}}_l - \frac{1}{NL_lC}\frac{1}{\left(\frac{1}{\bar{\mu}^u}\right)^2 + \left(\frac{1}{\bar{\mu}^l}\right)^2}\tilde{i}_l + \dots .\end{aligned} \tag{2.25}$$

Considering again that $\bar{\mu}^u + \bar{\mu}^l = N$ and $\bar{\mu}^u = \alpha N$, where $0 < \alpha < 1$, and using the second order differential equation in eq. (2.25), a value for the resonant frequency can be obtained as:

$$f_2 = \frac{1}{\sqrt{\frac{L_lC}{N}\left(\frac{\alpha^2+(1-\alpha)^2}{\alpha^2(1-\alpha)^2}\right)}}, \quad 0 < f_2 \leq \frac{\sqrt{2}}{4}\frac{1}{\sqrt{\frac{L_lC}{N}}} \tag{2.26}$$

2.3. Estimation of the frequency response of the MMC (Fourier approach)

In order to address the problem of obtaining information about the frequency response of the MMC in more detail, an approach using Fourier series approximation that analyzes each frequency component separately is applied. For detailed information of such techniques please refer to [TSC14, NÄI+12a]. In [JJF15, RF16], this Fourier method is applied to an MMC under nominal operating conditions and validated against a fully detailed electromagnetic transient model in PSCAD/EMTDC (see fig. 2.7). Here, each of the semiconductor switches used in the converter modules are modeled using an ideal switch S, diodes D_1 and D_2 in series and antiparallel configurations, which are modelled using the classical diode exponential function, and a snubber circuit. This model has been used successfully in studies for large scale implementations showing a good representation of its real life counter part. More details on this model and its application can be found in [PSD+12].

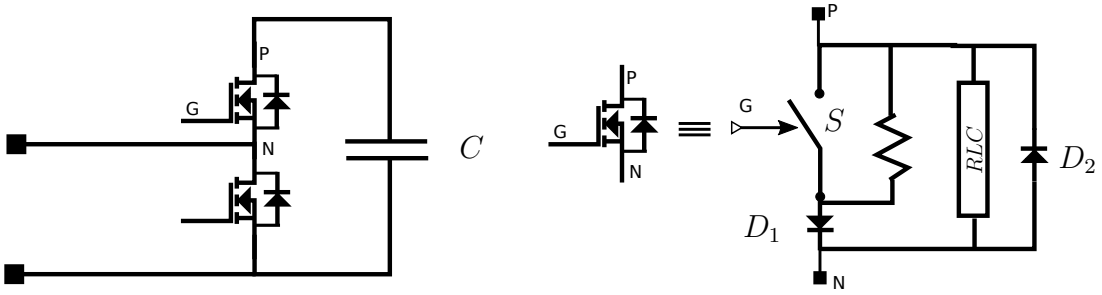

Figure 2.7.: Detailed model of the MMC module including the detailed model of the semiconductor switches used in PSCAD/EMTDC. The model of the semiconductor switch includes an ideal switch S, a snubber RLC circuit and two non linear diodes D_1 and D_2.

The results in [JJF15, RF16] show good accuracy of the Fourier series approximation with as low as two harmonic components. Moreover, it is also shown that, by increasing the harmonic components up to 17, the results are considerably improved, obtaining a very close match between the model in PSCAD/EMTDC and the approach using Fourier series. Therefore, we shall consider the model presented in this section as a good reference for the accuracy assessment of the reduced order model.

Using the Fourier series approximation, the MMC can be described by the following equation

$$\mathbf{M}(\omega)\mathbf{z} = \mathbf{U}, \tag{2.27}$$

where

$$\mathbf{M}(\omega) \triangleq \begin{bmatrix} -(R\mathbf{I} + j\omega\mathbf{n}L) & 0 & -\frac{1}{2}\mathbf{Y_u} & -\frac{1}{2}\mathbf{Y_l} \\ 0 & -(\frac{R+2R_l}{L+2L_l}\mathbf{I} + j\omega\mathbf{n}L_l) & -\frac{L_l}{L+2L_l}\mathbf{Y_u} & \frac{1}{L+2L_l}\mathbf{Y_l} \\ \frac{1}{NC}\mathbf{Y_u} & \frac{1}{2NC}\mathbf{Y_u} & -j\omega\mathbf{n}C & 0 \\ \frac{1}{NC}\mathbf{Y_l} & -\frac{1}{2NC}\mathbf{Y_l} & 0 & -j\omega\mathbf{n}C \end{bmatrix}, \tag{2.28}$$

$$\mathbf{U} \triangleq \begin{bmatrix} -\frac{1}{2}\mathbf{V_{in}} & 0 & 0 & 0 \\ 0 & \frac{2L_l}{L+2L_l}\mathbf{V^*_{ac}} & 0 & 0 \end{bmatrix}^T, \tag{2.29}$$

and

$$\mathbf{z} \triangleq \begin{bmatrix} \mathbf{I_c} & \mathbf{I_l} & \mathbf{V^u} & \mathbf{V^l} \end{bmatrix}^T, \tag{2.30}$$

are matrices constructed based on the Fourier transformation of eq. (2.3). The diagonal matrix $\mathbf{n}$ is defined as follows

$$\mathbf{n} \triangleq \ diag\left(\begin{bmatrix} -n & -(n-1) & \cdots & 0 & \dots & n-1 & n \end{bmatrix}\right) \tag{2.31}$$

where n is the number of frequency components used in the Fourier series expansion.

The variables $\mathbf{V_{in}}$, $\mathbf{V^*_{ac}}$, $\mathbf{I_c}$, $\mathbf{I_l}$, $\mathbf{V^u}$ and $\mathbf{V^l}$ are vectors that contain each of the coefficients of the Fourier series expansion of the respective variable. As an example, let us assume that $i_c(t)$ can be written as:

$$i_c(t) = \sum_{k=-n}^{n} i_c^{(k)} e^{j\omega n t}. \tag{2.32}$$

With this, the variable $\mathbf{I_c}$ can be defined as follows

$$\mathbf{I_c} \triangleq \begin{bmatrix} i_c^{(-n)} & \dots & i_c^{(0)} & \dots & i_c^{(n)} \end{bmatrix}^T, \tag{2.33}$$

where $i_c^{(j)}$ represents the coefficient corresponding to the j^{th} multiple of the natural frequency of i_c.

The matrices $\mathbf{Y_j}$ represent the Fourier decomposition of the control inputs and are defined as follows:

$$\mathbf{Y_j} \triangleq \begin{bmatrix} Y_j^{(0)} & & \dots & & Y_j^{(-2n)} \\ & \ddots & & & \\ \vdots & & Y_j^{(0)} & & \vdots \\ & & & \ddots & \\ Y_j^{(2n)} & & \dots & & Y_j^{(0)} \end{bmatrix}, \tag{2.34}$$

where $Y_j^{(k)}$ represent the coefficient corresponding to the k^{th} multiple of the natural frequency of the control signals μ^j.

With the previous definitions, the vector $\mathbf{z}$ in eq. (2.27) can be found using the following expression

$$\mathbf{z} = (\mathbf{M}(\omega))^{-1}\mathbf{U}. \tag{2.35}$$

Since the system described by eq. (2.27) is linear, it is possible to find the resonant frequencies of the system by solving for ω the following equation

$$det(\mathbf{M}(\omega)) = 0. \tag{2.36}$$

In order to illustrate the results of this method, fig. 2.8 shows the frequency response of i_c for different numbers of frequency components n. It can be seen that the resonant frequencies move and some new ones appear when the value of n is increased. In particular,

the peaks marked as "A" correspond to the resonance of the 2nd harmonic of i_c, "B" to the resonance of the 4th harmonic, "C" to the resonance of the 6th harmonic. The peaks marked as "D" correspond to the resonances dominated by the load impedance.

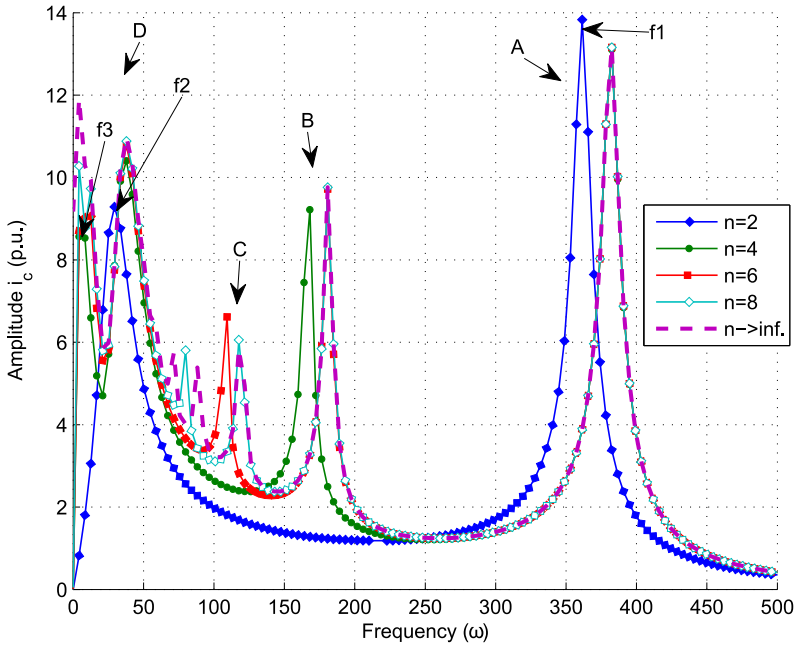

Figure 2.8.: Estimation of the amplitude of i_c using the Fourier series approximation for different values of n.

It is possible to obtain analytical expressions for some of the resonant frequencies in terms of the converter components. This can be done by solving eq. (2.36) for a given value of n. For the sake of simplicity, only the continuous control signals in eq. (2.14) are going to be considered for this analysis.

Note that the frequency response may change if the amplitude or characteristics of these control signals change due to the nonlinear properties of the system.

The results of the analysis of the frequency response using the Fourier series are shown in the sections below. For some numerical comparisons, the values in table 2.1 are used.

2.3.1. Frequency response analysis with $n = 2$

In order to begin with the analysis, matrices $\mathbf{U}$, $\mathbf{n}$, $\mathbf{Y_u}$ and $\mathbf{Y_l}$ in eqs. (2.29), (2.31) and (2.34) respectively, need to be defined using $n = 2$ and the control signals in eq. (2.14). These matrices can be used to define $M(\omega)$ (see eq. (2.28)) and then to obtain the solution $\mathbf{z}$ by applying eq. (2.35). Consequently, the resonant frequencies can be obtained using eq. (2.36).

After some algebraic manipulations, the following simplified expressions for the fre-

Table 2.2.: Comparison of the resonant frequencies f_1 and f_2 (see fig. 2.8) obtained with different methods for $n = 2$: Actual: Using eq. (2.36) with $n \to \infty$ and quantized control signals. Fourier (Num.): Using eq. (2.36) with $n = 2$ and continuous control signals. Fourier (Ana.): Using eqs. (2.37) and (2.38). Lin.: Using eqs. (2.23) and (2.26)

	Actual	Fourier (Num.)	Fourier (Ana.)	Lin.
f_1	382.6	361.4	362.4	582.4 - 823.7
f_2	50.4	29.3	28.3	0 - 265.5

quencies f_1 and f_2 in fig. 2.8 can be derived

$$f_1 = \left(\frac{28CL^2R^2 + 80CL^2RR_l + 64CL^2R_l^2}{32CL^2(L^2 + 4LL_l + 4L_l^2)} - \frac{16CLL_lR^2 + 16CL_l^2R^2 - 8L^3N - 22L^2L_lN - 12LL_l^2N}{32CL^2(L^2 + 4LL_l + 4L_l^2)} \right)^{\frac{1}{2}}, \tag{2.37}$$

$$f_2 = \mathrm{Re}\left(\sqrt{\frac{L_lN - 32CR_l^2 + 8\sqrt{16C^2R_l^4 - CL_lNR_l^2}}{64L_l^2C}} \right), \tag{2.38}$$

where Re($*$) represents the real part of the argument. Table 2.2 shows a comparison of the numerical values of the resonant frequencies obtained with different methods. It can be seen that the analytical expressions (eqs. (2.37) and (2.38)) approximate the numerical results with an error less than 4%. The approach based on linearization in section 2.2 gives a very easy method to compute these values, however the accuracy of the result is compromised. Note that the phenomenon mentioned in section 2.2 where the resonance due to f_1 is produced when the input is at $\frac{f_1}{2}$ can be seen clearly in this comparison. The linearized approach fails to model this phenomenon producing values for f_1 that are around twice as high as the actual value. Remember also that f_1 is of special importance since it could match the operating frequency of the converter and thereby producing inaccuracies in the reduced order model.

2.3.2. Frequency response analysis with $n \geqslant 4$

The complexity of the expressions obtained by solving eq. (2.36) grows exponentially with n. For $n = 4$ it is possible to obtain relatively simple analytical expressions only for f_3 (see fig. 2.8). After some algebraic manipulations, the expression for f_3 can be written as follows

$$f_3 = \mathrm{Re}\left(N \left(5\frac{23712CR_l^2 - 127L_lN}{177209344R_l^4C^3} - \frac{\sqrt{559490048C^2R_l^4 - 6022848CL_lNR_l^2 + 16129L_l^2N^2}}{177209344R_l^4C^3} \right)^{\frac{1}{2}} \right). \tag{2.39}$$

Table 2.3.: Comparison of the resonant frequencies f_3 (see fig. 2.8) obtained with different methods for $n = 4$: ((actual: Using eq. (2.36) with $n \to \infty$ and quantized control signals. Fourier (Num.): Using eq. (2.36) with $n = 4$ and continuous control signals. Fourier (Ana.): Using eq. (2.39).

	Actual	Fourier (Num.)	Fourier (Ana.)
f_3	4.2	8.4	7.88

As in the case with $n = 2$, this expression is a simplified version of the solution. Table 2.3 shows a comparison of the numerical values obtained with different methods.

For the remaining resonant frequencies, no simple closed form expression could be obtained for $n = 4$. Therefore, the solutions are computed numerically. This also applies to the cases with $n > 4$. From fig. 2.8 the numerical values for the most important frequencies for different values of n can be obtained. It is important to see that, the more terms are used in the Fourier approximation, the more resonant frequencies appear and some others change their position.

2.3.3. Effects of the quantization in the frequency response

Due to the non-linear nature of the system, the inclusion of the quantization changes the frequency response of the system. To take this effect into account, the control signals in eq. (2.15) are used for the following analysis.

Figure 2.9 shows a comparison of the frequency response of the reduced order model calculated with the Fourier approximation for $n = 2$, with and without the quantization. It can be seen how the resonant frequencies change their position and the amplitudes of the peaks are slightly attenuated. Unfortunately, it is not possible to obtain analytical expression for the resonant frequencies when the quantization is taken into account for $n \geq 2$ due to the complexity of the solution. However, they can be obtained numerically by solving eq. (2.36).

Figure 2.10 shows the results for $n = 6$. For this case, the resonant frequencies are also affected by the quantization; especially, the amplitude corresponding to the resonance of the 4th harmonic (frequency peak between 150 rad/s and 200 rad/s) is attenuated significantly once the quantization is taken into account. Moreover, the resonant frequency with the highest value is displaced around 7% due to the quantization. This displacement in frequency is less pronounced for the other resonant frequencies.

The difference of the two frequency responses in fig. 2.10 corresponds to the error caused by neglecting the quantization. Since the amplitude peaks are at slightly different locations, the difference between the two frequency responses become significant close to them. This explains the peaks obtained in the simulation already shown in fig. 2.3, where the error of the model without quantization was first illustrated.

2.4. Conclusions

The present chapter has investigated a reduced order model for Modular Multilevel Converters. Detailed methods to characterize resonant frequencies of MMCs by using ana-

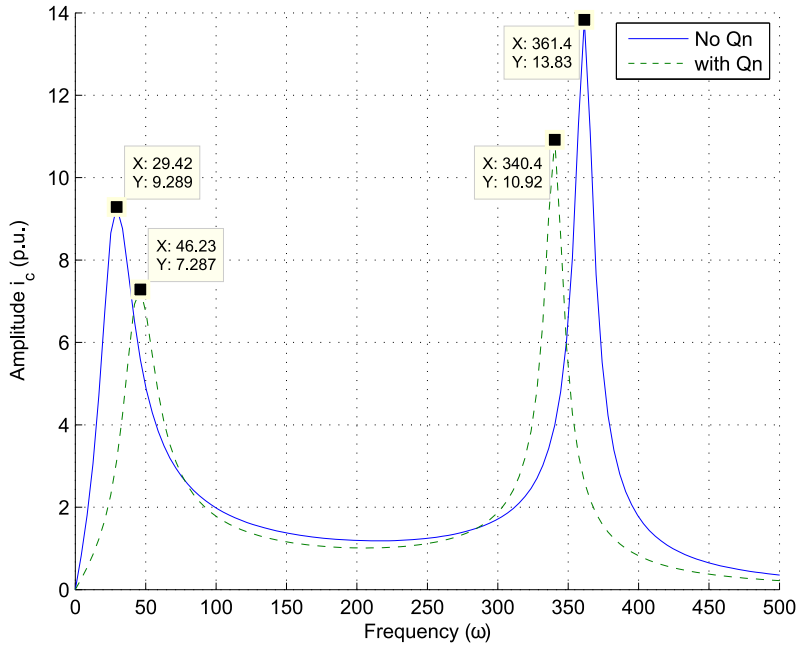

Figure 2.9.: Frequency response of the MMC for $n = 2$ with and without quantization.

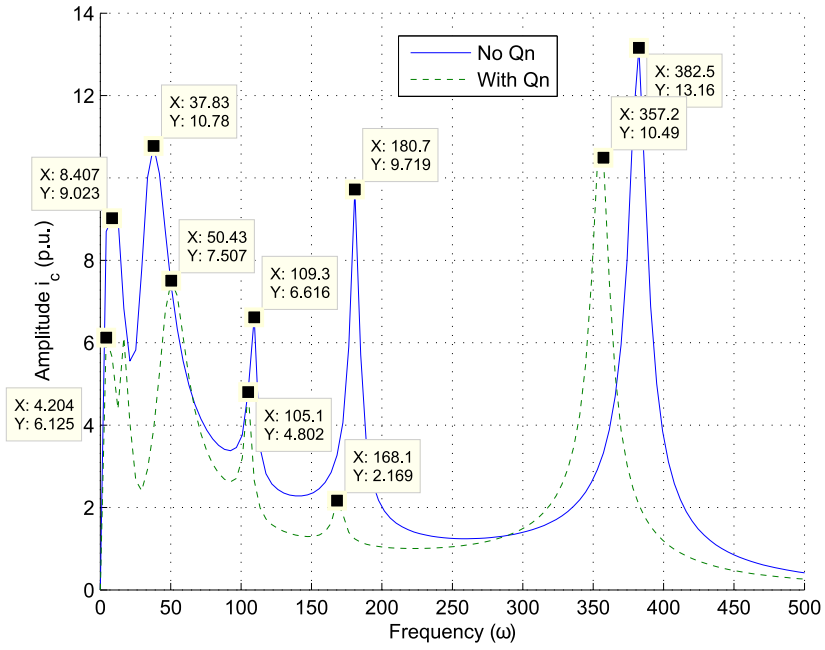

Figure 2.10.: Frequency response of the MMC for $n = 6$ with and without quantization.

lytical expressions obtained with the help of this model have been developed. This novel analysis allows one to obtain values of the resonant frequencies that have not been identi-

fied in the current literature, giving additional insight on the MMC. The results obtained here can be used to estimate beforehand if the reduced order model produces an accurate representation of the MMC. The insight gained thereby is particularly useful when working with control techniques using continuous control signals. The presented approach based on a linearized model also serves as a good starting point for evaluating the accuracy of the linearization of the MMC giving insight in how to proceed when designing any control law. The fact that the linear model fails to represent complex behavior results in an estimation of some resonant frequencies that can be twice as high as their actual value.

For the sake of accuracy, working close to any of the resonant frequencies of the converter should be avoided. This becomes more important the lower the number of used modules in the MMC, since in this case the amplitude of the quantization grows in relation with the continuous approximation of the control signals. It is also shown that the reduced order model produces the same results as the full order MMC when the quantization is taken into account. Therefore, when using control techniques with quantized variables such as finite control set MPC [GQ14b], the accuracy problem becomes less significant.

In the following chapter the reduced order model is going to be used to derive continuous analytical expressions that describe the relationship between the variables of the MMC. This will be useful to design and optimize references for control purposes.

The results presented here can also be expanded to analyse a 3-phase MMC; to see more details on this please, refer to appendix A.

3. Optimal reference design with capacitor voltage ripple reduction

This chapter proposes a method to design detailed references for MMCs. For that purpose, the reduced order model introduced in chapter 2 is used to obtain analytical expressions showing the relation between each of the variables of the converter. Additionally, it is shown how the effect of the circulating current can be modeled and manipulated to influence specifically the module capacitor voltages.

The analysis presented here evaluates the benefits of injecting harmonic components (up to an 8^{th} harmonic component) in the converter currents for minimizing the capacitor voltage ripple. Moreover, the impact of adding harmonic components to the load current to further reduce the voltage ripple is analyzed. It is shown that, if a certain Total Harmonic Distortion (THD) in the output current can be tolerated, then it is possible to reduce the voltage ripple accordingly. This trade-off is analyzed, elucidating the relation between the introduced THD and the total ripple reduction. For all the previous analyses the voltage ripple is quantified using the RMS value and the peak to peak (P2P) value, showing how the results vary depending on the figure of merit used.

To further simplify the process required to obtain the optimal values of the harmonic components in the circulating current, this work introduces an approach using linear approximations of these optimal parameters as a function of the load current parameters. The analysis shows that the linear approximations give a good result in estimating the optimal parameters for the injected currents over a wide range of operating conditions. Therefore, the linear approximations can be used in a situation where computational resources are limited.

Additionally, an analysis that illustrates the importance of the injected circulating current on the power transfer inside the converter is also presented. This and the rest of the analyses in this chapter use expressions obtained with the reduced order model presented in chapter 2. Moreover, as described in fig. 1.2 on page 5, these references can be used along with a control law to drive the MMC and achieve good performance. This topic is addressed in chapter 4 using an MPC strategy.

3.1. Voltage ripple analysis

This section illustrates how to use the reduced order model introduced in chapter 2 to derive harmonic components for the converter currents with the purpose of minimizing the capacitor voltage ripple. These harmonic components are selected using analytical expressions and a numerical optimization procedure. Extensive system simulations are not required.

3.1.1. Effect of harmonic components

Harmonics can be injected deliberately into the arm currents of the converter by means of an external control loop. This allows one to add a degree of control over the behavior of the voltage ripple in the capacitors [LQA+14, vdM13]. However, different harmonics (odd or even) can have different effects on the voltage ripple, depending on whether they appear in the circulating or in the load current. This section uses the reduced order model to analyze the effect that each harmonic component has on the voltage ripple. This leads to suggestions on which harmonics should be used in order to reduce the voltage ripple in the capacitors of the converter.

We assume that the load current (i_l), as shown in fig. 1.1 on page 2, is divided evenly between the upper and lower converter arms. Therefore, the currents in the upper arm (i^u) and in the lower arm (i^l) can be written in terms of i_c and i_l as per

$$i^u = i_c + \frac{i_l}{2}, \quad i^l = i_c - \frac{i_l}{2}. \tag{3.1}$$

They can be used to characterize the derivatives of the capacitor voltages as follows:

$$\dot{v}^u(t) = i^u(t)\frac{\mu^u(t)}{CN}, \tag{3.2}$$

$$\dot{v}^l(t) = i^l(t)\frac{\mu^l(t)}{CN}. \tag{3.3}$$

To evenly distribute the losses between the modules, we shall assume that the capacitor voltage waveform is the same in both arms but with a phase shift ϕ_v, which is to be determined. Therefore, we set $v^u(t) = v^l(t - \frac{\phi_v}{\omega})$. Using this assumption, the following expression can be obtained from eqs. (3.2) and (3.3):

$$i^u(t)\mu^u(t) = i^l\left(t - \frac{\phi_v}{\omega}\right)\mu^l\left(t - \frac{\phi_v}{\omega}\right). \tag{3.4}$$

For the sake of simplicity, we consider only continuous control signals, i.e. $\mu^u(t)$ and $\mu^l(t)$.

It is convenient to analyze (3.4) by splitting it into two different equations that relate variables of a similar nature. Therefore, we define an equation that relate the two arm currents and another equation that relate the control signals as follows:

$$i^u(t) = i^l\left(t - \frac{\phi_v}{\omega}\right), \tag{3.5}$$

$$\mu^u(t) = \mu^l\left(t - \frac{\phi_v}{\omega}\right). \tag{3.6}$$

Note that, by considering eqs. (3.5) and (3.6), eq. (3.4) is implicitly considered as well.

Let the circulating and load currents contain additional harmonic components, as per:

$$i_c(t) = i_0 + \hat{i}_k \cos(k\omega t + \phi_k),\ k \in \{2, 3, 4, \ldots\}, \tag{3.7}$$

$$i_l(t) = \hat{i}_l \cos(\omega t + \phi) + \hat{i}_n \cos(n\omega t + \phi_n),\ n \in \{2, 3, 4, \ldots\}. \tag{3.8}$$

The circulating current contains a kth order harmonic and the load current an nth order harmonic.

The currents in the upper and lower arms and the load and circulating currents can be written, using eqs. (3.7) and (3.8), as follows:

$$i^u(t) = i_c(t) + \frac{i_l(t)}{2} = i_0 + \hat{i}_k \cos(k\omega t + \phi_k) + \frac{\hat{i}_l}{2} \cos(\omega t + \phi) + \frac{\hat{i}_n}{2} \cos(n\omega t + \phi_n), \tag{3.9}$$

$$i^l(t) = i_c(t) - \frac{i_l(t)}{2} = i_0 + \hat{i}_k \cos(k\omega t + \phi_k) - \frac{\hat{i}_l}{2} \cos(\omega t + \phi) - \frac{\hat{i}_n}{2} \cos(n\omega t + \phi_n). \tag{3.10}$$

Therefore, the phase shifted version of the current in the lower arm satisfies:

$$\begin{aligned} i^l\left(t - \frac{\phi_v}{\omega}\right) = i_0 + \hat{i}_k \cos(k\omega t + \phi_k - k\phi_v) - \frac{\hat{i}_l}{2} \cos(\omega t + \phi - \phi_v) - \\ \frac{\hat{i}_n}{2} \cos(n\omega t + \phi_n - n\phi_v). \end{aligned} \tag{3.11}$$

By expanding the trigonometric functions in eq. (3.11) and isolating the effect of the angle ϕ_v, we notice that the only value of ϕ_v for which eq. (3.5) holds (see also eq. (3.9)) is $\phi_v = \pi$. With this, eq. (3.11) simplifies to

$$i^l\left(t - \frac{\pi}{\omega}\right) = i_0 + (-1)^k \hat{i}_k \cos(k\omega t + \phi_k) + \frac{\hat{i}_l}{2} \cos(\omega t + \phi) + (-1)^{n+1} \frac{\hat{i}_n}{2} \cos(n\omega t + \phi_n). \tag{3.12}$$

Therefore, eq. (3.5) holds if k is even, n is odd and $\phi_v = \pi$. Thus, eq. (3.6) must also hold. In other words, the result suggests that the circulating current should only contain even order harmonics, while the load current should contain solely odd order harmonics.

3.1.2. Analytical expressions of the capacitor voltages

For the sake of simplicity, only a second order harmonic in the circulating current is taken into account in the subsequent example (higher order harmonics will be considered in the final analysis). We thus set:

$$i_c(t) = i_0 + \hat{i}_2 \cos(2\omega t + \phi_2), \tag{3.13}$$

where $\hat{i}_2$ and ϕ_2 represent the amplitude and phase of the second harmonic of the circulating current, which are the parameters to be determined. The DC component i_0 transfers power from the DC input to the converter arms. In previous approaches, see, e.g., [QS12, PRFK12], no harmonics were taken into account and only i_0 was considered, restricting the ability to govern the capacitor voltages.

To control an MMC, a suitable reference trajectory for the state space vector x in eq. (2.33) on page 25, should be specified. We shall consider a situation where, at the load, i_l and v_l have been predefined, see eqs. (1.1) and (1.2) on page 3. The relevant design question now becomes one of specifying parameters in eq. (3.13) that reduce the

voltage ripple in the converter capacitors. These quantities are linked as specified below:

Lemma 2. *Consider the system described in eq.* (2.3) *on page 14 and the definitions of* i_c *and* i_l *in eq.* (3.13) *and eq.* (1.1) *on page 3 respectively. For a given* $\hat{i}_2$ *and* ϕ_2*, the analytical solution of eq.* (2.3) *in steady-state is given by the following equations:*

$$i_0 = \frac{v_{dc} - \sqrt{v_{dc}^2 - 8R\left(\frac{\hat{v}_l\hat{i}_l}{2}cos(\phi) + 2R\left(\frac{\hat{i}_l^2}{8} + \frac{\hat{i}_2^2}{2}\right)\right)}}{4R} \tag{3.14}$$

$$v^u(t) = \sqrt{\frac{2}{CN}\int_0^t \left(i_c(\tau) + \frac{i_l(\tau)}{2}\right) a^u(\tau)\, d\tau + (v_{DC}^u)^2} \tag{3.15}$$

$$v^l(t) = \sqrt{\frac{2}{CN}\int_0^t \left(i_c(\tau) - \frac{i_l(\tau)}{2}\right) a^l(\tau)\, d\tau + \left(v_{DC}^l\right)^2} \tag{3.16}$$

where

$$-a^u(t) = \quad (L + 2L_l)\dot{i}_l(t) + 2L\dot{i}_c(t) + 2Ri_c(t) + (R + 2R_l)i_l(t) - v_{dc} + 2v_{ac}^*(t) \tag{3.17}$$

$$a^l(t) = \quad (L + 2L_l)\dot{i}_l(t) - 2L\dot{i}_c(t) - 2Ri_c(t) + (R + 2R_l)i_l(t) + v_{dc} + 2v_{ac}^*(t) \tag{3.18}$$

and

$$v_{DC}^u = v_{DC}^l = \frac{v_{dc} - 2Ri_0}{N} \tag{3.19}$$

Proof. The component i_0 depends on the power delivered to the load and the additional power losses in the circuit; therefore, the input power produced by these current must be equal to all the power losses plus the power delivered to the load. This can be written as follows

$$v_{dc}i_0 = \frac{\hat{v}_l\hat{i}_l}{2}cos(\phi) + 2R\left(\frac{\hat{i}_l^2}{8} + \frac{\hat{i}_2^2}{2} + i_0^2\right). \tag{3.20}$$

Solving for i_0 two solutions are obtained. The positive root produces a very high value of i_0 which is often outside implementation boundaries. Therefore, the negative root is selected which leads to eq. (3.14).

Using the first two equations in eq. (2.3) ($\dot{i}_c(t)$ and $\dot{i}_l(t)$), eqs. (1.1) and (3.13), the following is obtained

$$\dot{i}_c(t) = -2\hat{i}_2 sin\left(2\omega_0 t + \phi_2\right)\omega_0, \tag{3.21}$$

$$\dot{i}_l(t) = -\hat{i}_l sin\left(\omega_0 t + \phi\right)\omega_0, \tag{3.22}$$

The desired values of the modulation functions $\mu^{u,l}$ can be obtained solving the previous set of equations, which yields

$$\mu^u(t) = \frac{1}{2}\frac{a^u(t)}{v^u(t)}, \qquad \mu^l(t) = \frac{1}{2}\frac{a^l(t)}{v^l(t)}, \tag{3.23}$$

where $a^u(t)$ and $a^l(t)$ are defined as in eqs. (3.17) and (3.18) respectively.

Using the last two equations in eq. (2.3) ($\dot{v}^u$ and $\dot{v}^l$) and the result in eq. (3.23), the following is obtained

$$\begin{aligned} \dot{v}^u(t) &= \frac{1}{CN}\left(i_c(t) + \frac{i_l(t)}{2}\right)\frac{a^u(t)}{2v^u(t)} \\ \int_0^t v^u(\tau)\dot{v}^u(\tau)\,d\tau &= \frac{1}{CN}\int_0^t \left(i_c(\tau) + \frac{i_l(\tau)}{2}\right)\frac{a^u}{2}(\tau)\,d\tau \\ \frac{v^u(t)^2}{2} &= \frac{1}{CN}\int_0^t \left(i_c(\tau) + \frac{i_l(\tau)}{2}\right)\frac{a^u}{2}(\tau)\,d\tau + \frac{(v^u_{DC})^2}{2}, \end{aligned} \tag{3.24}$$

This leads to eq. (3.15), where v^u_{DC} represents the DC value of the capacitor voltage and can be computed as in eq. (3.19)

An analogous procedure can be followed to compute v^l, leading to eq. (3.16) □

Note that all the previous expressions are composed of known integrable and differentiable functions, implying that analytical explicit expressions can be obtained. These expressions can be used to select the values of $\hat{i}_2$, ϕ_2 to satisfy a variety of design objectives.[1]

With the previous results it is easy to study the effect of several design variables, such as current amplitudes and phase angles, on the behaviour of the converter. In the following sections, we focus our efforts into analysing the particular case of the relation between the voltage ripple and the circulating current harmonics.

3.2. Numerical studies

In order to evaluate the effect of the current harmonic components on the capacitor voltages, the RMS and the peak to peak (P2P) values are used as figures of merit. These quantities are defined as follows:

$$v^u_{RMS} = \frac{1}{T}\sqrt{\int_0^T (v^u(t))^2 dt}, \tag{3.25}$$

$$v^u_{P2P} = \max(v^u(t)) - \min(v^u(t)), \tag{3.26}$$

where $T = \frac{2\pi}{\omega}$ represents the fundamental period and $t \in [0, T]$. The RMS and P2P values for v^l are defined accordingly. For this analysis, the modulation signals μ^u and μ^l are assumed to be continuous (see chapter 2). Figure 3.1 shows the effect of $\hat{i}_2$ and ϕ_2 on the RMS and P2P values of the capacitor voltage ripple. It is possible to see that both plots are similar. However, when the RMS function is used, a smoother plot is obtained. The RMS value is directly related with the energy stored in the capacitor. Therefore, by minimizing this value the average energy fluctuation in the capacitors is also minimized.

Note that, since the proposed method is based on analytical expressions, the RMS or P2P values can be easily obtained simply by evaluating numerically the corresponding

[1] Note that the expressions in eqs. (3.27) and (3.28) can also be used, taking into account more harmonic components. This will be analyzed in section 3.2.

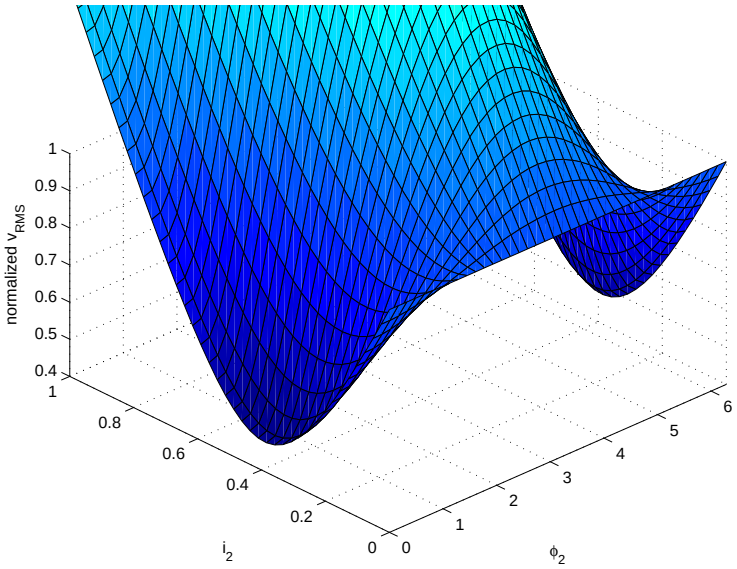

(a) RMS

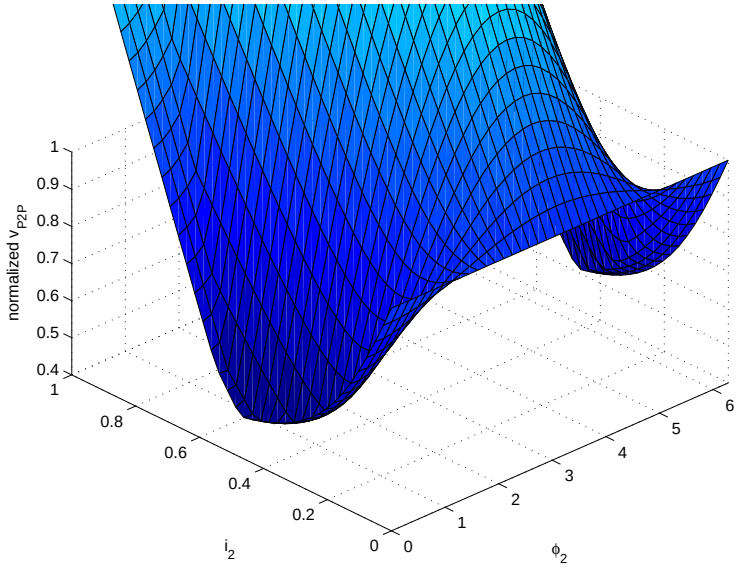

(b) P2P

Figure 3.1.: RMS and P2P values of the voltage ripple of each capacitor as a function of the second harmonic of the circulating current i_c with $P.F. = 1$ ($P.F.$ stands for power factor).

expression. In contrast, alternative methods that lack analytical expressions, require significantly more computational effort [PPC+13].

In the preceding analysis, a simplified case with just a second harmonic in the circulating

Table 3.1.: Optimal harmonics in the circulating current and their effect on the voltage ripple (cost function: RMS) when operating at $\hat{i}_l = 1$ p.u.. The RMS and P2P values are normalized.

	i_c								Performance	
	$\hat{i}_2$	ϕ_2	$\hat{i}_4$	ϕ_4	$\hat{i}_6$	ϕ_6	$\hat{i}_8$	ϕ_8	$v^{u,l}RMS$	$v^{u,l}P2P$
Case 0	0	0	0	0	0	0	0	0	1	1
Case 1	0.390	0.046	0	0	0	0	0	0	0.478	0.524
Case 2	0.396	0.043	−0.106	0.370	0	0	0	0	0.467	0.560
Case 3	0.396	0.043	−0.109	0.370	0.029	1.003	0	0	0.466	0.569
Case 4	0.396	0.043	−0.109	0.370	0.031	1.018	0.012	−1.173	0.466	0.569

current was investigated. It is possible to also consider additional harmonic components in the circulating current and in the load current as follows:

$$i_c(t) = i_0 + \hat{i}_2 \cos(2\omega t + \phi_2) + \hat{i}_4 \cos(4\omega t + \phi_4) + \hat{i}_6 \cos(6\omega t + \phi_6) + \hat{i}_8 \cos(8\omega t + \phi_8), \quad (3.27)$$

$$i_l(t) = \hat{i}_l \cos(\omega t + \phi) + \hat{i}_3 \cos(3\omega t + \phi_3) + \hat{i}_5 \cos(5\omega t + \phi_5). \quad (3.28)$$

The subsequent numerical results take into account eqs. (3.27) and (3.28) and aim to find amplitudes and phases of the harmonic components, which minimize capacitor voltage ripple. Note that, as long as the reduced order model is accurate, the calculation of the harmonic components in the converter currents does not depend on the control or modulation technique used (see chapter 2 for details on the accuracy and limitations of the reduced order model). Therefore, the same harmonic components can be used in different control set-ups.

3.2.1. Optimal harmonic components in the circulating current

For this case, the values of table 2.1 on page 17 are used and the additional harmonic components in the load current are assumed zero. Therefore, we set $\hat{i}_3 = \hat{i}_5 = 0$ in eq. (3.28). The harmonic components of the circulating current are added as shown in tables 3.1 and 3.2 (see also eq. (3.27)). A trust-region optimization algorithm was used to compute the amplitudes and phases of the harmonic components such that the cost function (RMS or P2P value) is minimized. Different sets of harmonic components and cost functions are taken into account. Table 3.1 shows the resulting amplitudes and phases using the RMS value of the capacitor voltage ripple as a cost function for the optimization. It can be seen that the addition of the second harmonic produces a significant reduction in the RMS value. However, the addition of the 6th and 8th harmonic only improves the result by 1%. For the instances presented in table 3.2, where the P2P value is used as the cost function, a similar behavior can be observed. Adding the 6th and 8th harmonic improves the result of case 2 in table 3.2 by less than 2%. It can be concluded that, for the situations examined, harmonics up to and including 4th order suffice.

Figure 3.2 shows the relation between the RMS value of the AC components of the circulating current and the P2P value of the voltage ripple. It can be seen that, in order to reduce the P2P value, it is necessary to increase the RMS value of the circulating current, thereby increasing the losses in the converter. If desired, the circulating current RMS can be considered in the cost function used for the numerical optimization to directly

Table 3.2.: Optimal harmonics in the circulating current and their effect on the voltage ripple (cost function: P2P) when operating at $\hat{i}_l = 1$ p.u.. The RMS and P2P values are normalized.

	i_c								Performance	
	$\hat{i}_2$	ϕ_2	$\hat{i}_4$	ϕ_4	$\hat{i}_6$	ϕ_6	$\hat{i}_8$	ϕ_8	$v^{u,l}RMS$	$v^{u,l}P2P$
Case 0	0	0	0	0	0	0	0	0	1	1
Case 1	0.494	0.088	0	0	0	0	0	0	0.534	0.497
Case 2	0.458	0.071	0.067	0	0	0	0	0	0.521	0.461
Case 3	0.444	0.078	0.063	0	−0.080	0	0	0	0.513	0.455
Case 4	0.449	0.087	0.079	0.001	−0.088	0.002	0.089	0.002	0.519	0.447

consider this trade-off [EDD11].

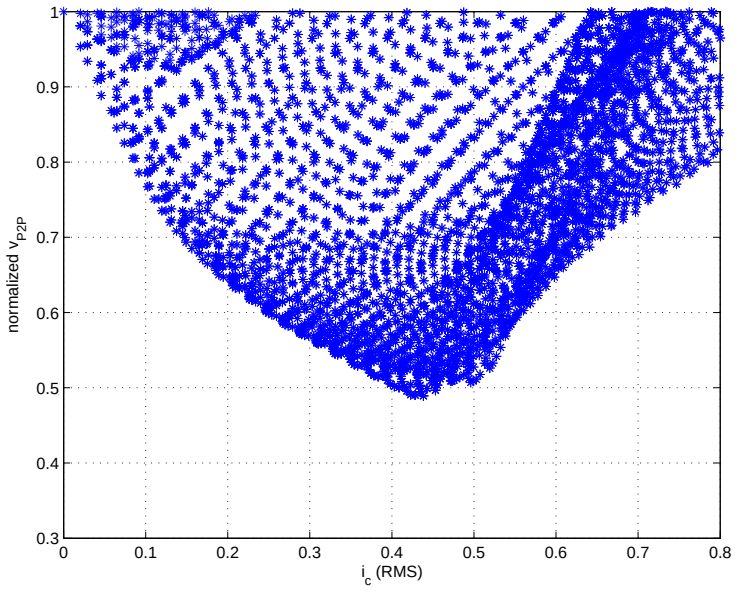

Figure 3.2.: Normalized P2P value of the voltage ripple for several combinations of $\hat{i}_2$, ϕ_2, $\hat{i}_4$, ϕ_4. Each instance corresponds to a different combination of values.

It is worth noting that when the RMS value is used in the cost function, the numerical optimization converges to the minimum independently of the initial conditions. However, with the P2P function the convergence depends, in some cases, on the initial conditions.

3.2.2. Optimal harmonic components in the load current

It is well known that adding harmonic components to the load current increases the THD and reduces the power quality. However, adding these components may serve to further reduce the voltage ripple in the capacitors. The goal in this section is to evaluate how successful these components are in reducing the voltage ripple in the capacitors by finding optimal values of amplitudes and phases. Our findings allow one to shed light into the trade-off between the THD in the load current and the capacitor voltage ripple reduction.

Table 3.3.: Optimal harmonics in the load current and their effect on the voltage ripple (cost function: RMS) when operating at $\hat{i}_l = 1$ p.u.. The RMS and P2P values are normalized.

	i_c				i_l				Performance		
	$\hat{i}_2$	ϕ_2	$\hat{i}_4$	ϕ_4	$\hat{i}_3$	ϕ_3	$\hat{i}_5$	ϕ_5	$v^{u,l}RMS$	$v^{u,l}P2P$	THD
Case 0	0	0	0	0	0	0	0	0	1	1	0%
Case 1	0.440	−0.067	0.176	−0.689	−0.548	0.943	0	0	0.364	0.509	54.8%
Case 2	0.447	−0.056	0.175	−1.014	−0.593	0.978	0.347	1.516	0.319	0.453	68.7%

Table 3.4.: Optimal harmonics in the load current and their effect on the voltage ripple (cost function: P2P) when operating at $\hat{i}_l = 1$ p.u.. The RMS and P2P values are normalized.

	i_c				i_l				Performance		
	$\hat{i}_2$	ϕ_2	$\hat{i}_4$	ϕ_4	$\hat{i}_3$	ϕ_3	$\hat{i}_5$	ϕ_5	$v^{u,l}RMS$	$v^{u,l}P2P$	THD
Case 0	0	0	0	0	0	0	0	0	1	1	0%
Case 1	0.407	−0.008	0.106	0.035	−0.306	0.583	0	0	0.422	0.406	30.5%
Case 2	0.381	0.011	0.150	−0.090	−0.221	0.670	−0.152	−0.003	0.444	0.385	26.7%

As in the previous case, the parameter values of table 2.1 on page 17 are used. Table 3.3 shows the results when 3rd and 5th harmonics are added to the load current (see eq. (3.28)) and the voltage RMS value is used as the cost function. For this case, the parameters of the circulating current harmonics are also optimized along with the parameters in the load current. It can be seen that the addition of optimal 3rd and 5th harmonics (table 3.3) reduces the RMS value by more than 22% in comparison with the results in table 3.1 (Case 2), producing a THD of up to 68.7%.

Table 3.4 shows the results when the voltage P2P value is used as a cost function. Note that for this case, adding both harmonics improves the results by around 21% in comparison with the results of Case 2 in table 3.2. The THD, when the 3rd and 5th harmonics are included, is 27%. This value is lower than in all the other cases evaluated.

Although, as shown in the previous examples, the additional harmonics in the load current can be used to reduce further the voltage ripple, they should be used in combination with the right set of harmonics in the circulating current. In order to illustrate this critical aspect, fig. 3.3 shows the THD of the load current for different values of amplitudes and phases of its harmonic components with the corresponding normalized P2P value of the voltage ripple. For this example, no harmonic component in the circulating current is used. It can be seen that a reduction in the voltage P2P value of around 7% can be achieved, with a THD of 31%.

Figure 3.4 shows results for the same setup, but with the harmonic components in the circulating current carefully selected. It can be seen that the relative improvement is better (around 22%) with around 30% THD. In both cases, the lowest voltage P2P value for a given THD decreases almost linearly with the increase of its respective THD. The injection of large harmonic components to the load currents might be prohibited in MMC applications. The analysis done in this section could thus be deemed to be of a rather theoretical value. However, any PWM method introduces small low-order harmonics into the load current. It might be possible to design a PWM method that injects low-order harmonics with amplitudes and phases that help minimize the capacitor voltage ripple. The analysis proposed in this section could be used for this purpose.

3.3. Linear aproximation of the optimal circulating current parameters

This section presents a simple approach to obtain approximated values of the optimal parameters of the second harmonic in the circulating current. For the example examined in this section the RMS value is used as a cost function. The circulating current is limited to contain only a second order harmonic component.

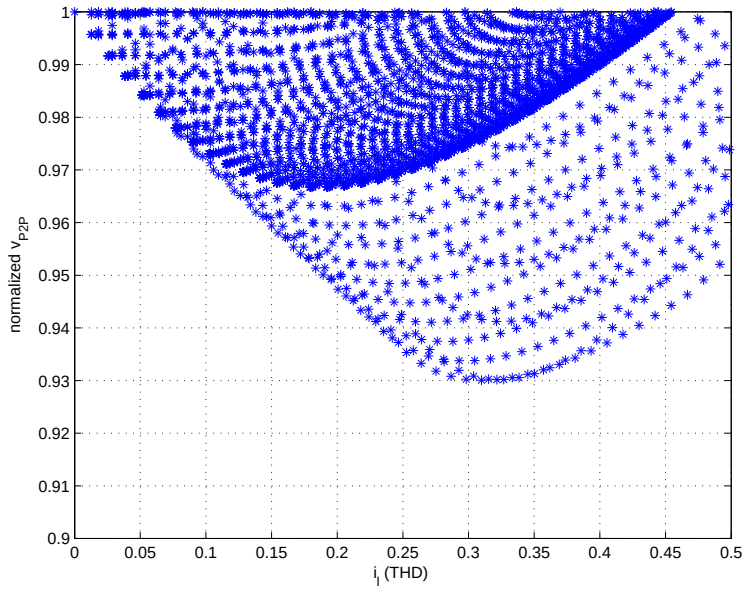

Figure 3.3.: Normalized P2P values of the voltage ripple for several combinations of $\hat{i}_3$, ϕ_3, $\hat{i}_5$ and ϕ_5. All the harmonic components in the circulating current are taken as zero. Each instance corresponds to a different combination of values.

3.3.1. Dependence of the optimal harmonic components with the load current parameters

The voltage ripple reduction obtained by injecting additional harmonic components into the circulating current depends strongly on the load current (amplitude and phase). This can be seen in more detail in fig. 3.5; here the reduction of the voltage ripple fluctuates between 38% and 54%, depending on the load current.

The values of amplitude and phase of the second harmonic of the circulating current that correspond to the results in fig. 3.5 are shown in figs. 3.6 and 3.7. As expected, the relationships between the amplitude and phase of the load current, and the optimal amplitude and phase of the second harmonic of the circulating current are non-linear. To simplify the analysis and design, we will next derive an approximation based on linear relations between the variables in order to derive the optimal values.

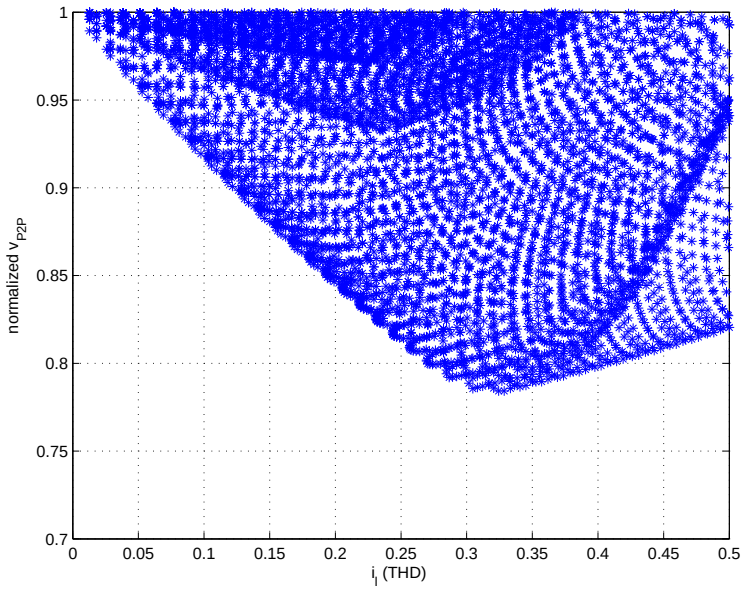

Figure 3.4.: Normalized P2P values of the voltage ripple for several combinations of $\hat{i}_3$, ϕ_3, $\hat{i}_5$ and ϕ_5. The harmonic components in the circulating current are considered as in table 3.2 Case 2. The P2P values are also normalized with respect to table 3.2 Case 2. Each instance corresponds to a different combination of values.

For that purpose let us consider a linear relationship of the following form

$$\hat{f}(\hat{i}_l, \phi) = a\hat{i}_l + b\phi + c. \tag{3.29}$$

In table 3.5 the optimal values of a, b and c are shown. These values are selected such that the RMS error:

$$e_{RMS} = \sqrt{\frac{1}{n}\sum_{i=1}^{n}(\hat{f}(z_i) - f(z_i))^2}, \tag{3.30}$$

is minimized. In eq. (3.30), n stands for the number of data points, z_i for a pair of values $(\hat{i}_l, \phi)$ contained in the empirical data and $f(z_i)$ for the non-linear relationship to be approximated (i.e. figs. 3.6 and 3.7). The function $f(\bullet)$ represents a generic function, which represents either the amplitude or the phase angle of the second harmonic in table 3.5.

The results show a strong dependence between the optimal amplitude of the second harmonic and the amplitude of the load current (i.e. the parameter a takes a large value). Although the amplitude of the second harmonic is also affected by the phase of the load current, this relation is weaker. On the other hand, the phase of the second harmonic of the circulating current is very similar to the phase of the load current (i.e. $b \approx 1$).

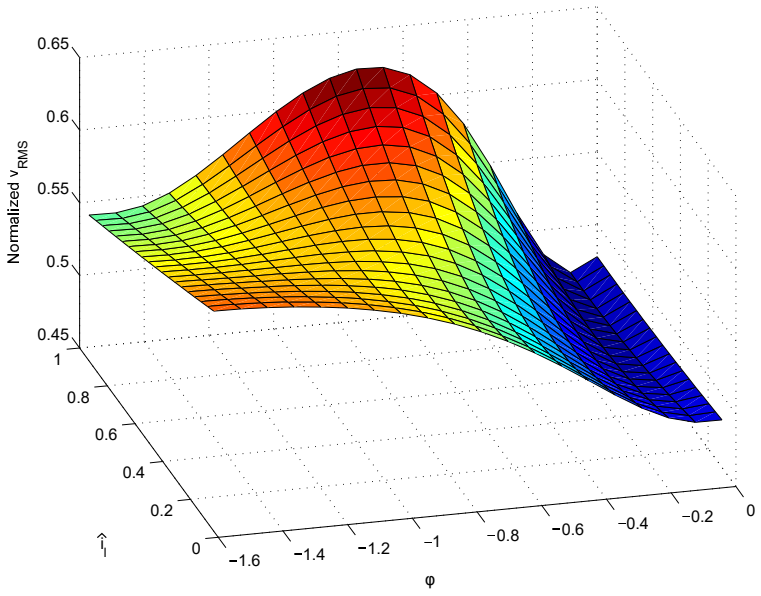

Figure 3.5.: Optimal normalized RMS capacitor voltage with a second harmonic in the circulating current as a function of the amplitude and phase of the load current.

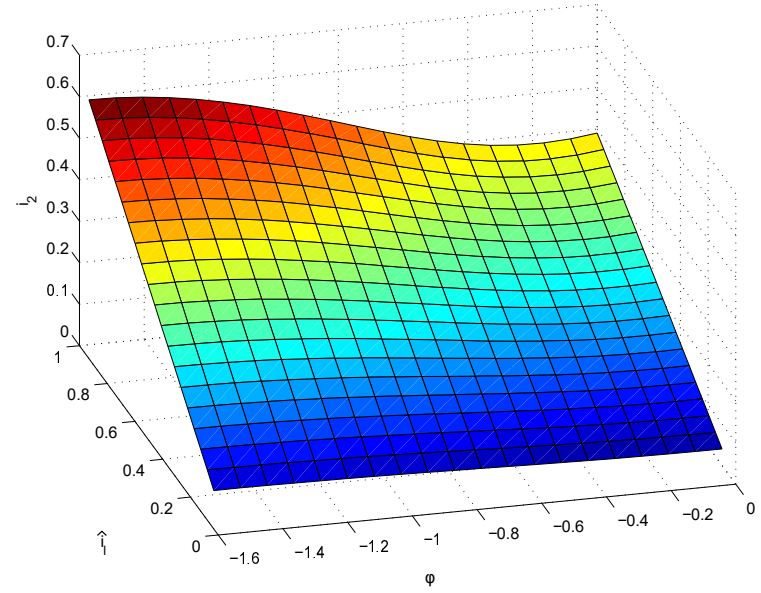

Figure 3.6.: Optimal amplitude of the second harmonic of the circulating current as a function of the amplitude and phase of the load current.

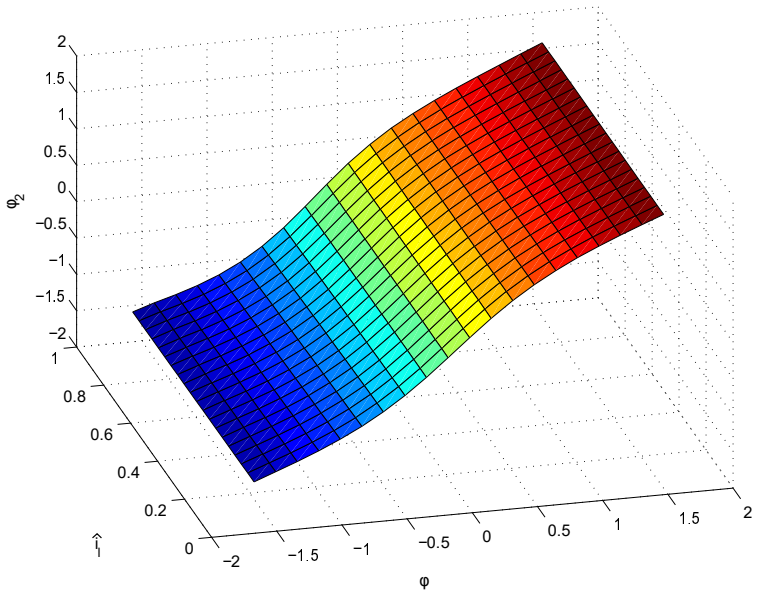

Figure 3.7.: Optimal phase of the second harmonic of the circulating current as a function of the amplitude and phase of the load current.

Table 3.5.: Parameters of the linear approximation of the optimal components of the second harmonic of the circulating current.

$\hat{f}(\bullet)$	a	b	c	e_{RMS}
$\hat{i}_2(\bullet)$	0.4809	−0.08846	−0.06841	0.0234
$\phi_2(\bullet)$	−0.02366	1.108	−0.0002	0.1208

3.3.2. Additional results including a 4th harmonic in the circulating current

In order to complement the previous results, an additional 4th harmonic is included in the circulating current. Figures 3.8 and 3.9 show the optimal amplitude and phase of the 4th harmonic for different values of the load amplitude and phase. It can be seen that these results can be approximated by linear functions with a relatively small error, similar to the case presented in the previous section. Table 3.6 shows the results of this linear approximation (see eq. (3.29)). Note that the results for the second harmonic are very similar to the situation considered in table 3.5.

3.3.3. Analysis using the P2P value

In the previous results, the RMS was used as the cost function due to the fact that its numerical convergence is more robust to the set of initial conditions; the P2P function on the other hand, produces less consistent results.

To further examine this issue, the optimal amplitudes and phases of the second and fourth harmonic of the circulating current are found using the P2P value as the cost

Table 3.6.: Parameters of the linear approximation of the optimal components of the second and fourth harmonic of the circulating current.

$\hat{f}(\bullet)$	a	b	c	e_{RMS}
$\hat{i}_2(\bullet)$	0.4928	−0.09226	−0.07234	0.02553
$\phi_2(\bullet)$	−0.02537	1.108	0.0002	0.1113
$\hat{i}_4(\bullet)$	0.161	−0.03266	−0.03427	0.009958
$\phi_4(\bullet)$	−0.2175	1.149	−0.003069	0.1702

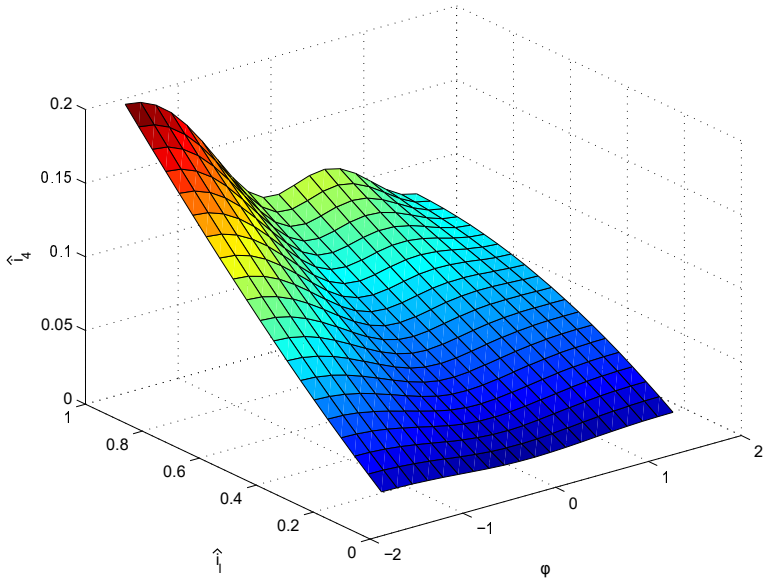

Figure 3.8.: Optimal amplitude of the fourth harmonic of the circulating current as a function of the amplitude and phase of the load current.

function. The results are illustrated in figs. 3.10 to 3.14. The surfaces obtained for this case are not as smooth as in the case of the RMS value. However, it can be clearly seen that they can be well approximated by a linear function. It is worth noting that the results obtained for the amplitude of the fourth harmonic (see fig. 3.14) are not sufficiently smooth to deduce any shape.

The results of the linear approximation are shown in table 3.7. Note that the RMS error is smaller than in table 3.6 except for the case of describing the amplitude of $\hat{i}_4$.

In order to evaluate the effectiveness of the linear approximation of the optimal harmonic parameters, the error in the voltage ripple produced when the parameters of tables 3.6 and 3.7 are used, is shown in figs. 3.15 and 3.16. This error is computed as follows

$$Error = \frac{|v^u_{RMS} - \tilde{v}^u_{RMS}|}{v^u_{RMS}}, \tag{3.31}$$

where v^u_{RMS} and $\tilde{v}^u_{RMS}$ represent the RMS values of the voltage ripple, calculated using the exact parameters for the circulating current harmonics and using the linear approximation

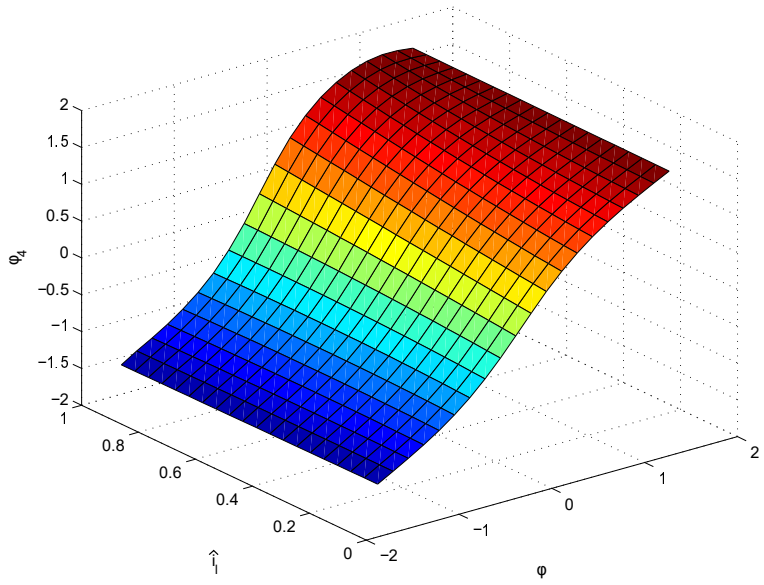

Figure 3.9.: Optimal phase of the fourth harmonic of the circulating current as a function of the amplitude and phase of the load current.

Table 3.7.: Parameters of the linear approximation of the optimal components of the second and fourth harmonic of the circulating current using the P2P value as cost function.

$\hat{f}(\bullet)$	a	b	c	e_{RMS}
$\hat{i}_2(\bullet)$	0.3717	0.01568	0.02835	0.01991
$\phi_2(\bullet)$	−0.02312	1.033	0.006358	0.08614
$\hat{i}_4(\bullet)$	0.1213	−0.03841	−0.04009	0.01805
$\phi_4(\bullet)$	0.1994	1.137	0.01452	0.2014

respectively.

It can be seen in fig. 3.15 that the error for $\hat{i}_l = 1$ lies between 7% and 15%. For values of $\hat{i}_l$ close to 0, the error of the approximation is higher, with values between 5% and 35%. On the other hand, in the case where the P2P value is used (see fig. 3.16), the error seems to depend more on the load phase ϕ. The error reaches values of around 20% for values of ϕ around $-\pi/2$, and values around 2% for values of ϕ around 0. However, for $\hat{i}_l$ close to 0, the error of the approximation increases drastically, reaching values of up to 50%.

3.4. Circulating current analysis

In order to take a deeper look at the role of circulating current in the converter, the reduced order model is used to provide simplified expressions that ease the analysis. In this section, these expressions are computed showing the role of the circulating current on the power flow in the converter. Using the reduced order model, the modulation functions

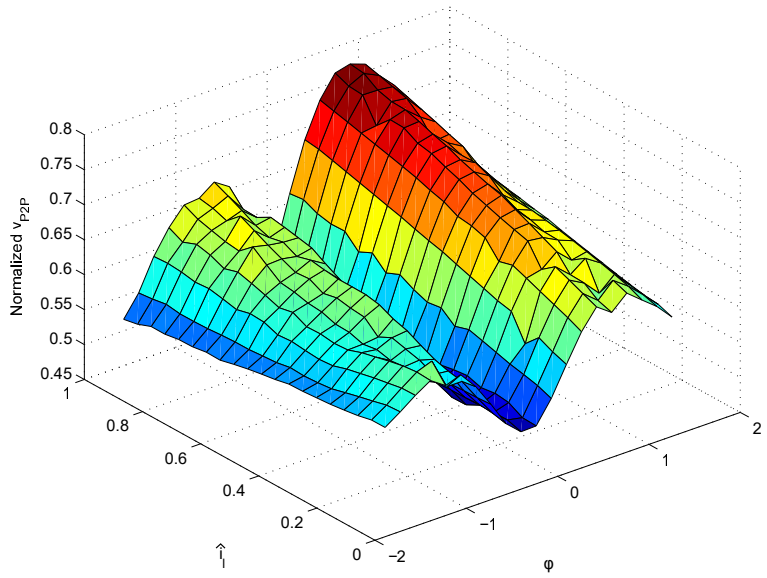

Figure 3.10.: Optimal normalized capacitor voltage P2P with a second and fourth harmonic in the circulating current as a function of the amplitude and phase of the load current.

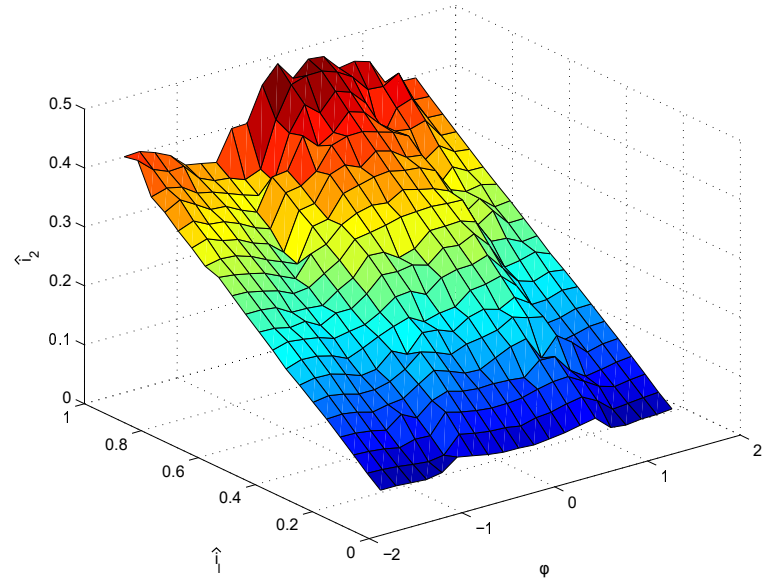

Figure 3.11.: Optimal amplitude of the second harmonic of the circulating current as a function of the amplitude an phase of the load current using the P2P value as cost function.

for each arm can be easily obtained as in eq. (3.23). These modulation functions depend

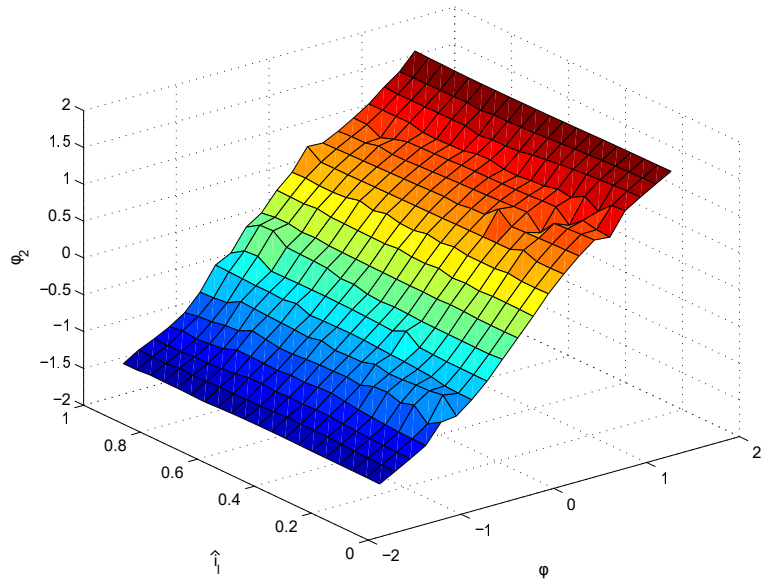

Figure 3.12.: Optimal phase of the second harmonic of the circulating current as a function of the amplitude and phase of the load current using the P2P value as cost function.

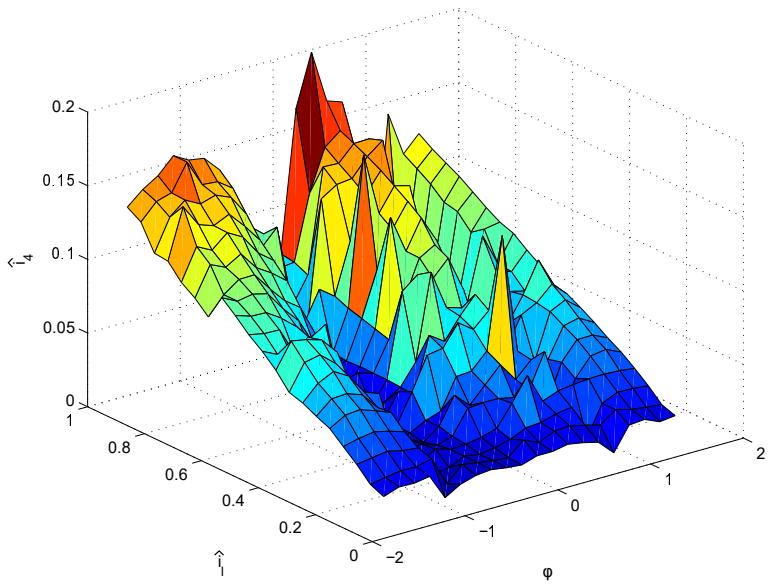

Figure 3.13.: Optimal amplitude of the fourth harmonic of the circulating current as a function of the amplitude and phase of the load current using the P2P value as cost function.

on the desired values of the circulating and load current. For the sake of simplicity $v_{ac}^{*} = 0$

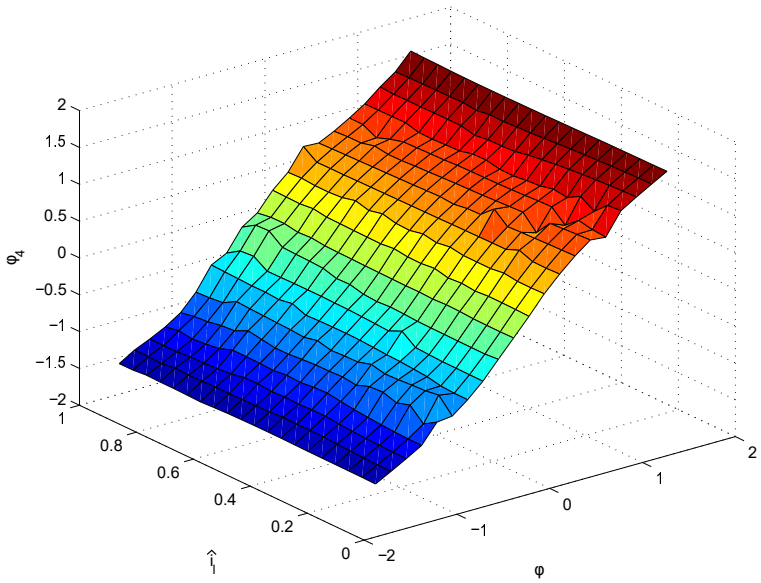

Figure 3.14.: Optimal phase of the fourth harmonic of the circulating current as a function of the amplitude and phase of the load current using the P2P value as cost function.

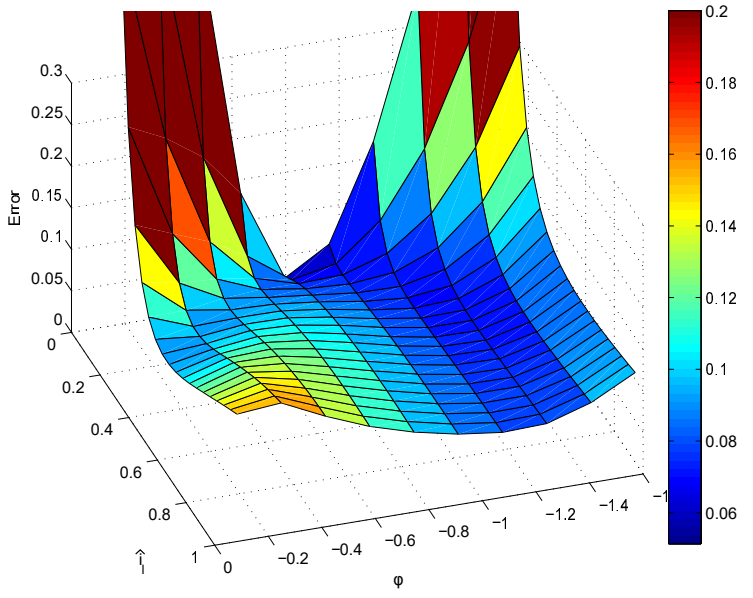

Figure 3.15.: Error of the RMS obtained with the linear approximation of the optimal circulating current harmonic components in comparison with the optimal RMS.

is assumed. Therefore, they can be written as:

$$\mu^u(t) = \frac{1}{2v^u(t)}\left(\left(\frac{di_l(t)}{dt} + 2\frac{di_c(t)}{dt}\right)L - (i_l(t) + 2i_c(t))R + \frac{di_l(t)}{dt}L_l + 2i_l(t)R_l + v_{dc}\right), \tag{3.32}$$

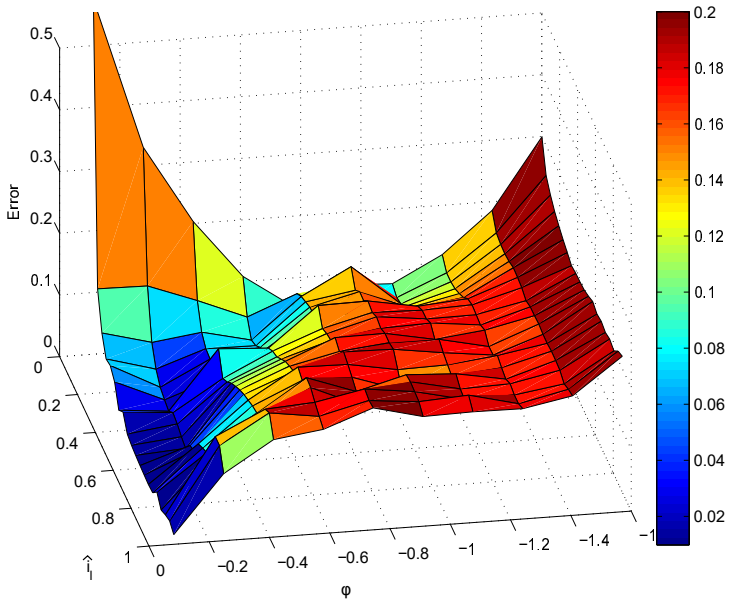

Figure 3.16.: Error of the P2P obtained with the linear approximation of the optimal circulating current harmonic components in comparison with the optimal P2P.

$$\mu^l(t) = -\frac{1}{2v^l(t)}\left(\left(\frac{di_l(t)}{dt} - 2\frac{di_c(t)}{dt}\right)L - (i_l(t) - 2i_c(t))R + \frac{di_l(t)}{dt}L_l - 2i_l(t)R_l - v_{dc}\right). \tag{3.33}$$

The modulation functions can be used to compute the voltages of the capacitors and the power on them by multiplying the capacitor voltage and current using the equations described in eq. (2.3) on page 14. This can be written as:

$$P^u(t) = \frac{dE^u(t)}{dt} = \left(i_c(t) + \frac{i_l(t)}{2}\right)\frac{\mu^u(t)v^u(t)}{CN}, \tag{3.34}$$

$$P^l(t) = \frac{dE^l(t)}{dt} = \left(i_c(t) - \frac{i_l(t)}{2}\right)\frac{\mu^l(t)v^l(t)}{CN}, \tag{3.35}$$

where $E^u(t)$ and $E^l(t)$ represent the energy in each capacitor in the upper and lower arm respectively. Computing the energy of the capacitors in both arms, the power difference between them can be defined as

$$P^{\Delta}(t) \triangleq P^u(t) - P^l(t). \tag{3.36}$$

This term represents the power transferred between the two arms. The total power represents the power transferred from the arms to other elements in the converter, and can be defined as

$$P^T(t) \triangleq P^u(t) + P^l(t). \tag{3.37}$$

Note that all the capacitor voltages in the upper and lower arm are considered to be balanced. Therefore, the total power in the upper or lower arm can be calculated by multiplying the power in the capacitor by a factor N. Using the results in eqs. (3.32) and (3.33), and computing eq. (3.36) and (3.37) the following is obtained

$$CNP^{T}(t) = v_{dc}i_c(t) - 2\left(i_c(t)R + \frac{di_c(t)}{dt}L\right)i_c(t) - \left(R_l i_l(t) + \frac{di_l(t)}{dt}L_l\right)i_l(t), \quad (3.38)$$

$$CNP^{\Delta}(t) = -2\left(R_l i_l(t) + \frac{di_l(t)}{dt}L_l\right)i_c(t) + \frac{v_{dc}i_l(t)}{2} - \left(i_c(t)R + \frac{di_c(t)}{dt}L\right)i_l(t). \quad (3.39)$$

For the sake of simplicity, let us assume that the circulating current in eq. (3.7) contains only a second harmonic, and the load current in eq. (3.8) contains no harmonics. The total power in eq. (3.38) contains the squares of $i_c(t)$ and $i_l(t)$, which when multiplied with the DC values produce active power. This can be written as:

$$CNP^{T}_{\text{active}}(t) = v_{dc}i_0 - 2Ri_0^2 - 2R\hat{i}_2^2\cos(2\omega_0 t + \phi_2)^2 - R_l\hat{i}_l^2\cos(\omega_0 t + \phi)^2 - \frac{R\hat{i}_l^2}{2}\cos(\omega_0 t + \phi)^2. \quad (3.40)$$

The active power contains a DC part and a second and fourth harmonic produced by the square of the cosine functions. The remaining terms are reactive power, and can be written as:

$$\begin{aligned} &CNP^{T}_{\text{reactive}}(t) = v_{dc}\hat{i}_2\cos(2\omega_0 t + \phi_2) - 4i_0\hat{i}_2\cos(2\omega_0 t + \phi_2) + \\ &4\omega_0 L\hat{i}_2^2\sin(2\omega_0 t + \phi_2)\cos(2\omega_0 t + \phi_2) - \omega_0 L_l\hat{i}_l^2\sin(\omega_0 t + \phi)\cos(\omega_0 t + \phi). \end{aligned} \quad (3.41)$$

The reactive power only contains AC terms. These terms are only the second and fourth harmonics and most of them are produced by the injection of a second harmonic in the circulating current.

On the other hand, eq. (3.39) contains the product between $i_c(t)$ and $i_l(t)$. Since these currents or their derivatives share no common harmonics, all the power in eq. (3.39) is purely reactive and can be expressed as follows

$$\begin{aligned} CNP^{\Delta}_{\text{reactive}}(t) = &\left(\frac{v_{dc}}{2} - 2R_l i_0 - 2Ri_0\right)\hat{i}_l\cos(\omega_0 t + \phi) + \omega_0 i_0(2L_l + L)\hat{i}_l\sin(\omega_0 t + \phi) \\ &+ \frac{\hat{i}_2}{2}\Big[\omega_0(3L + 2L_l)\hat{i}_l\sin(3\omega_0 t + \phi + \phi_2) + \omega_0(L - 2L_l)\hat{i}_l\sin(\omega_0 t - \phi + \phi_2) \\ &- 2(R + R_l)\hat{i}_l\cos(\omega_0 t - \phi + \phi_2) - 2(R + R_l)\hat{i}_l\cos(3\omega_0 t + \phi + \phi_2)\Big]. \end{aligned} \quad (3.42)$$

This expression contains only odd order harmonics (first and third). The third order harmonic is generated by the injection of the second harmonic in the circulating current.

When the voltage ripple of the capacitors is reduced, the total power fluctuation is also reduced. However, the higher the amplitude of the circulating current, the higher the peak value of the power.

It can be seen in eqs. (3.40) to (3.42), that the second harmonic injected into the circulating current is present in both the reactive and active power. However, in the

active power, this harmonic only appears due to the power losses in the resistor R, which usually can be neglected compared with the power dissipated in R_l (see eq. (3.40)). In the reactive power in eqs. (3.41) and (3.42), the circulating current plays an important role generating most of its components. Note how the frequency components on the reactive part of the total power are only even order harmonics, while in the difference ($P^{\Delta}(t)$) they are only odd order harmonics.

3.5. Conclusions

A novel method to compute reference signals for MMCs has been investigated. The method allows one to take into account AC components of the circulating current and capacitor voltages for a more accurate control of the MMC. Using analytical expressions that describe the converter dynamics, the behaviour of the system can be easily studied and optimized.

Here we aim to reduce the voltage ripple of the module capacitors by injecting additional harmonics into the circulating and load currents. The analytical expressions allow one to describe the voltage ripple as a function of the harmonic components in the currents. These expressions are then used to derive the optimal amplitude and phase of the harmonics by means of a numerical optimization. Two figures of merit are evaluated in the optimization, namely the RMS and the P2P voltage ripple.

The addition of harmonics to the load current reduces the voltage ripple in the capacitors even further. The trade-off between the additional THD in the load current and the ripple reduction is evaluated. The results show that the effect of these harmonic components is highly dependent on the circulating current components. Moreover, the relation between the lowest voltage ripple for a given THD and the corresponding THD is almost linear until the optimal point is reached as shown in figs. 3.3 and 3.4.

The injection of harmonics in the circulating and load current can be used to reduce the voltage ripple by more than 60% for the evaluated cases. However, these results strongly depend on the load parameters, with the ripple reduction varying between 30% and 60%. The relation between the parameters of the optimal second harmonic component injected in the circulating current with the phase and amplitude of the output current is non-linear. Interestingly, a linear approximation closely matches the results, thus easing the calculation of the optimal components significantly. The reference design technique presented here does not depend on the control or modulation technique used, allowing applications with other control strategies.

Furthermore, the circulating current can be understood by analyzing the power transfer between arms using the analytical expressions provided by the reduced order model.

It has been shown here that, by carefully designing references for an MMC, its performance can be improved. However, a control law is required to drive the MMC to follow the references properly. In the following chapter, the references presented here and the reduced order model in chapter 2 are going to be employed to implement and analyze MPC strategies.

The results presented here can also be expanded to analyse a 3-phase MMC, please refer to appendix A.

4. MPC for bilinear systems: convexity and application to power converters

MPC is a very intuitive and popular control technique that uses a cost function and future predictions of the system behaviour to decide the optimal control action. It covers a broad range of applications. In power electronics, particularly in switched power converters, it is possible to apply the MPC in two different ways. The most direct option is to allow the MPC to drive the converter switches directly, implying that the decision variables are binary (i.e. Finite Control Set (FCS)). This chapter starts by illustrating the use of the reference design technique, introduced in chapter 3, in the application of an FCS MPC. Here, a comparison with more simplistic reference design approaches is shown, demonstrating the importance of well selected references. Moreover, some drawbacks of the FCS approach are discussed explaining the motivation to move towards the use of MPC with PWM.

The rest of this chapter discusses more in detail the problem of MPC with PWM, addressing the problem of the convexity of the associated optimization problem as defined in section 1.3.2. Here, convex constraints are assumed, therefore only the convexity of the cost function is left to be analyzed. Conditions to guarantee this convexity are developed in terms of the system model parameters. Finally, an application to the MMC shows how the results in chapters 2 and 3 can be used along with the developed conditions to achieve good performance with reduced complexity.

4.1. Application of FCS MPC

For the application of the FCS MPC, the MMC model in section 1.1.1 with binary control variables is used. Moreover, in order to obtain a discrete time system representation, the Euler method is employed. By doing this it is possible to obtain an MPC problem as the one described in section 1.3.2. However, here the allowed control decision values are binary, which represents a non-convex constraint set.

In order to decide the control action, an optimal switching combination is found using the cost function J (see section 1.3.2). For the sake of this example the following is set: $\mathcal{H} = 1$ and $\lambda_h^\dagger = 0$. Moreover, the MMC parameters in table 2.1 on page 17 are used. For the case presented here, the MMC with $N = 8$ modules per arm has 65536 (2^{2N}) possible switching combinations, and one of them has to be selected as the optimal. A traditional approach to find the optimal switching combination involves brute force search, evaluating every possible combination and then selecting the one with the lowest cost function value. Less computationally tasking methods include using a restricted control set [PRFK12], indirect FCS [VBSH15], or sphere decoding techniques [GQ14b, GQ14a].

In order to show the advantages of the reference design approach, introduced in chapter 3, in comparison with a simplified approach used in the literature [QS12, PRFK12], three different sets of references are used along with a FCS MPC and tested via simulations. The first set of references consider the case where no harmonic components are injected in the circulating current. The other two set of references are selected optimally to reduce the RMS and the P2P value of the capacitor voltage ripple as shown in chapter 3 (see tables 3.1 and 3.2)

Figure 4.1 shows the response of the controlled converter to all sets of references. The results show that with no injection of harmonics in the circulating current, the capacitor voltage ripple is twice as high in comparison with the other two cases. Using the results in chapter 3, the capacitor voltage ripple can be optimally reduced.

For short horizon approaches, as the one shown above, FCS MPC can be efficiently implemented. However, let us consider the case where a longer prediction horizon is required (i.e. $\mathcal{H} = 20$). Then, for an MMC as described in chapter 2, 320 different binary control variables and more than 2×10^{96} switch combinations have to be considered to find the optimal control action. By using the reduced order model presented in chapter 2 and a set of PWMs, it is possible to simplify this problem and only consider 40 continuous control variables. The fact that the control variables are continuous facilitates the problem, giving information about the optimal solution through differentiation. Although more efficient and better methods to solve these kinds of FCS problems are proposed every day, the binary nature of its variables make them inherently a significantly more difficult problem than the PWM counterpart [D'A10, GQ14b]. This motivates the analysis presented in the following sections.

4.2. MPC with PWM

In the following sections, a general kind of problem that often appears with the application of MPC is analyzed. This problem consists of a quadratic cost function of bilinear systems using an arbitrary prediction horizon, convex constraints and continuous decision variables (i.e. PWM). This set of characteristics frequently appear in MPC for power electronics where most of the popular power converters are bilinear systems [BvdBV01, BMC$^+$09, KPKL14, Gey09, AG94]. This bilinearity can become a problem when the MPC uses a large prediction horizon, producing a non-convex problem and therefore, requiring a high computational effort to get to an optimal solution. If convexity can be guaranteed by manipulating the cost function, simpler and more efficient optimization algorithms can be used. The following sections aim to develop conditions over a weighting parameter in the cost function that guarantees the convexity of the optimization problem. In this case, this term (λ_h) penalizes the error of the control inputs with their respective references (see section 1.3.2). A detailed analysis of the cost function for an arbitrary prediction horizon is carried out. This analysis allows one to find bounds for the value of the weighting factor that can be estimated with a simple analytical expression. These bounds give us useful information if the goal is to obtain a convex optimization problem. Two cases are considered, one that guarantees convexity for a wide range of the state space, and one that is restricted only to a neighborhood around the reference values. Numerical and analytical results are compared for both cases showing the advantages and disadvantages of each.

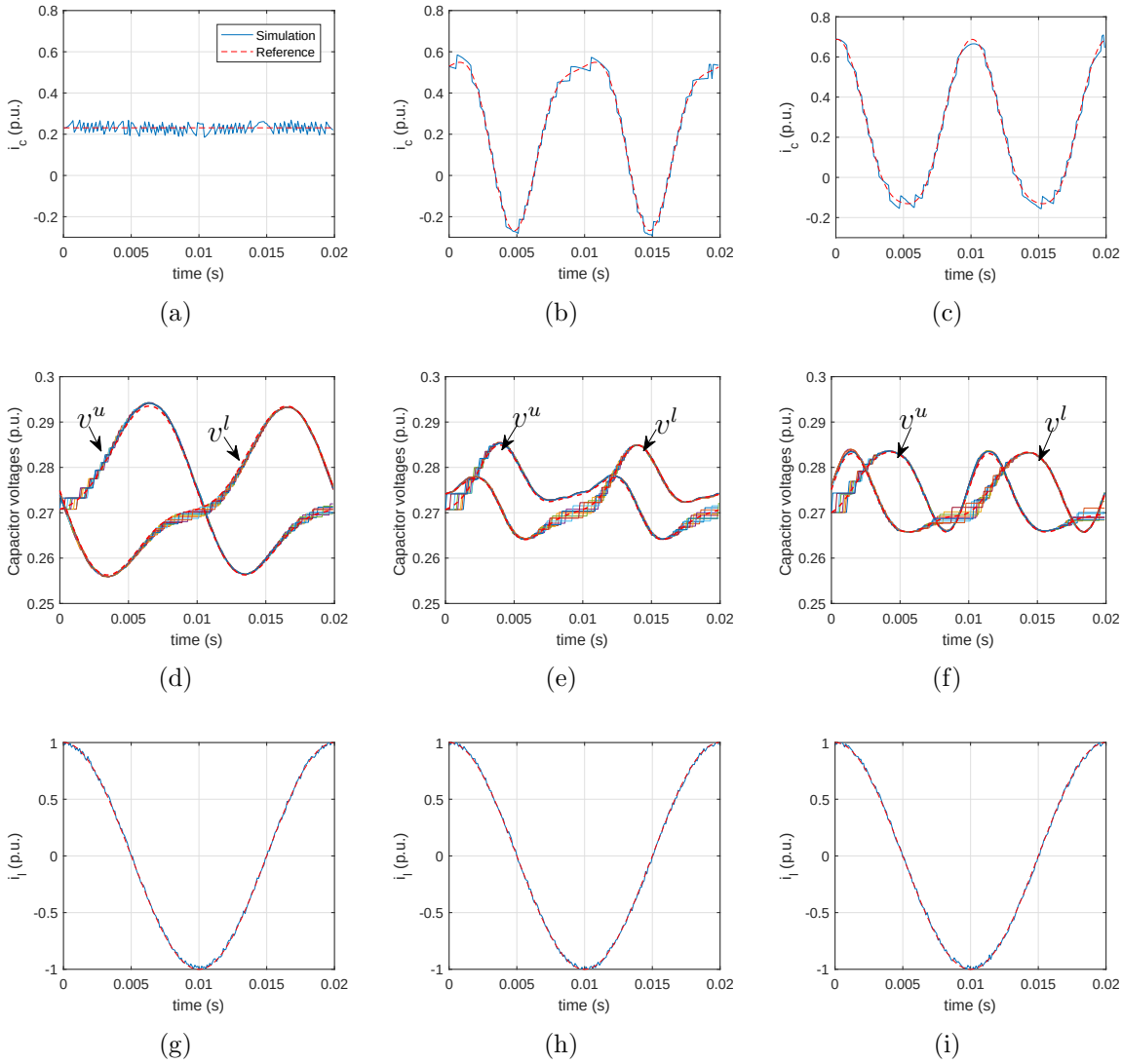

Figure 4.1.: Response of the FCS-MPC for three different cases: In (a), (d) and (g), no harmonics are injected in the circulating current. In (b), (e) and (h), harmonics to reduce the RMS value of the capacitors voltage ripple are used (i.e. table 3.1 Case 2). In (c), (f) and (i), harmonics to reduce the P2P value of the capacitors voltage ripple are used (i.e. table 3.2 Case 2). With $M = \text{diag}([20 \quad 17 \quad 40 \times 10^3 \quad 40 \times 10^3])$ and sampling time 1ms.

Examples using a Boost converter and an MMC are shown to illustrate numerically the proposed procedure.

First, let us address details about the discrete time model and the definition of the MPC problem that are going to be used throughout this chapter to simplify the analysis of the optimization problem.

4.2.1. Discrete system modeling

In section 1.3.1, basics of the discrete time modeling were described. Based on this model, and in order to simplify the analysis presented in this work, let us consider a new state space vector $x(k)$ defined as

$$x(k) = \begin{bmatrix} z(k)^T & 1 \end{bmatrix}^T, \tag{4.1}$$

with the following associated state dynamics

$$x(k+1) = \left(A(k) + \sum_{i \in \mathbb{I}} B_i(k) u_i(k) \right) x(k) \tag{4.2}$$

where

$$u_i(k) = \frac{1}{\delta_i} \upsilon_i(k), \tag{4.3}$$

and

$$A(k) = \begin{bmatrix} \mathcal{A}(k) & \mathcal{C}(k) \\ 0 & I \end{bmatrix}, \quad B_i(k) = \begin{bmatrix} \delta_i \mathcal{B}_i(k) & 0 \\ 0 & 0 \end{bmatrix}. \tag{4.4}$$

In eq. (4.3), δ_i is a weighting parameter such that

$$\max_k |u_i(k)| = \rho, \quad \forall i \in \mathbb{I}. \tag{4.5}$$

where ρ is an arbitrary constant. More details on the purpose of δ_i will be discussed in section 4.4 (see Remark 3).

Using the model presented in eq. (4.2), the analysis of the MPC can be simplified. Note that, in contrast with the model in eq. (1.11), all the terms are multiplied by the state space vector. The model in eq. (4.2) is also going to be used in the following section to describe details of MPC.

4.2.2. MPC Problem

The basic MPC problem were discussed in section 1.3.2. Here, a description of the problem that allows one to reduce the analytical complexity of the analysis is presented. This will be particularly useful later in this chapter.

Based on the MPC problem presented in section 1.3.2, the cost function in eq. (1.12) can be equivalently written as

$$J(x(0), ..., x(\mathcal{H}), u_i(0), .., u_i(\mathcal{H}-1)) = \sum_{h=1}^{\mathcal{H}} J_h(x(h), u_i(h-1)), \quad \forall i \in \mathbb{I}, \tag{4.6}$$

where

$$J_h(x(h), u_i(h-1)) = \|x(h) - \bar{x}(h)\|_M^2 + \frac{\lambda_h}{2} \sum_{i \in \mathbb{I}} \|\mathbf{u}_i(h-1) - \bar{\mathbf{u}}_i(h-1)\|^2, \quad \forall i \in \mathbb{I}, \tag{4.7}$$

and

$$\begin{aligned}\mathbf{u}_i(h-1) &= \begin{bmatrix} u_i(0) & u_i(1) & \dots & u_i(h-1) \end{bmatrix}^T, \\ \bar{\mathbf{u}}_i(h-1) &= \begin{bmatrix} \bar{u}_i(0) & \bar{u}_i(1) & \dots & \bar{u}_i(h-1) \end{bmatrix}^T.\end{aligned} \tag{4.8}$$

In eq. (4.7) $\bar{\mathbf{u}}_i(h)$ represents the control input references and $\lambda_h \in \mathbb{R}$, $\lambda_h \geq 0$. Note that eqs. (1.12) and (4.6) are equivalent if $\lambda_h^\dagger = \lambda_h + \lambda_{h+1} + \cdots + \lambda_{\mathcal{H}}$. The definition of J as in eq. (4.6) is going to be useful for its analysis later in this chapter. Note that the Hessian of J_h, contains only λ_h on its diagonal, which is convenient when analyzing the MPC problem (see section 4.3). Therefore, the following analyses are going to be based on the cost function defined as in eq. (4.6). Moreover, the cost function $J(x(0), ..., x(\mathcal{H}), u_i(0), .., u_i(\mathcal{H}-1))$ and the stage cost $J_h(x(h), u_i(h-1))$ will be referred to simply as J and J_h when convenient.

It is possible then to write the goal of the MPC as an optimization problem subject to constraints as follows:

$$\begin{aligned} \min_{\mathbf{u}_i(\mathcal{H}-1), \forall i \in \mathbb{I}} \quad & J(x(0), ..., x(\mathcal{H}), u_i(0), .., u_i(\mathcal{H}-1)) \\ & h(\mathbf{u}_i(\mathcal{H}-1)) = 0 \\ \text{s.t.} \quad & g(\mathbf{u}_i(\mathcal{H}-1)) \leq 0, \qquad \forall i \in \mathbb{I} \\ & u_i(k) \in \mathbb{U} \end{aligned} \tag{4.9}$$

Remark 1. *In the analysis presented in this work, only convex constraints $h(\mathbf{u}_i(\mathcal{H}-1))$, $g(\mathbf{u}_i(\mathcal{H}-1))$ and $\mathbb{U}$ are going to be considered. Therefore, if J is convex, the optimization problem in eq.* (4.9) *is also convex.*

The following sections address the problem of the convexity of the optimization problem of the MPC with PWM as defined in here. Since convex constraints are assumed, only the convexity of the cost function is left to be analyzed. Conditions to guarantee this convexity are developed in terms of the system model parameters. Finally, an application to the MMC shows how the results in chapters 2 and 3 can be used along with the developed conditions to achieve good performance with reduced complexity.

Throughout the following sections, the matrix properties described in appendix B are going to be used.

4.3. Convexity of the cost function

In this section, conditions for the convexity of the cost function J are discussed. It is clear that, due to the bilinear nature of the system in eq. (4.2), the cost function in eqs. (4.6) and (4.7) with $\lambda_h = 0$ is in general not convex. On the other hand, as the value of λ_h moves towards infinity, the cost function J reduces to the quadratic term $\frac{\lambda_h}{2} \sum_{i \in \mathbb{I}} \|\mathbf{u}_i(h-1) - \bar{\mathbf{u}}_i(h-1)\|^2$, which is a convex function. Therefore, there is a range of values of λ_h for which the cost function J is convex [Ber79]. The following theorem focuses on identifying the range of values of λ_h for which this occurs. This is done by identifying the lower bound of this set of values, which we call ζ_h, and elucidating its relation with the system parameters, including the prediction horizon of the MPC.

In the analysis carried out to find the bounds ζ_h, a dependency on the control input $\mathbf{u}_i(\mathcal{H}-1)$ has been identified. Note that this variable is the decision variable in the

optimization problem in eq. (1.14). To overcome this issue, worst cases of $\mathbf{u}_i(\mathcal{H}-1)$ are considered to find ζ_h. These worst cases are restricted by the constraints in eq. (1.14). By doing this, the direct dependency of ζ_h on the decision variable is overcome and, at the same time, the validity of ζ_h for all possible values of $\mathbf{u}_i(\mathcal{H}-1)$ is guaranteed. A similar consideration has to be done for the state vector $x(k)$ and its reference. For these, the worst case is considered by the use of the variable $x_{\max}$, which is particulary useful when analytical estimates of the convexity bound are required. More details on this will be addressed in section 4.4.

Theorem 1. *Consider the state space system in eq.* (4.2) *and a cost function J associated with an MPC problem as in eq.* (4.6)*. Then J is convex if*

$$\lambda_1 \geq 0 \text{ and } \lambda_h \geq \begin{cases} \zeta_h & 0 \preceq Z_{k,v} \preceq I\zeta_h \quad \forall k,v \in \{1,2,...,h\}, \\ (h-1)\zeta_h & -I\zeta_h \preceq Z_{k,v} \preceq I\zeta_h \quad \forall h \in \{2,3,...,\mathcal{H}\}. \end{cases} \tag{4.10}$$

where

$$\zeta_h = \max_{k,v} \left(\|Z_{k,v}\| \right), \tag{4.11}$$

$$Z_{k,v} = 2 \begin{bmatrix} x_e^T M \frac{\partial^2 x_e}{\partial u_1(k)\partial u_1(v)} & x_e^T M \frac{\partial^2 x_e}{\partial u_1(k)\partial u_2(v)} & \cdots & x_e M \frac{\partial^2 x_e}{\partial u_1(k)\partial u_\jmath(v)} \\ x_e^T M \frac{\partial^2 x_e}{\partial u_1(k)\partial u_2(v)} & x_e^T M \frac{\partial^2 x_e}{\partial u_2(k)\partial u_2(v)} & & \\ \vdots & & \ddots & \vdots \\ x_e^T M \frac{\partial^2 x_e}{\partial u_1(k)\partial u_\jmath(v)} & & \cdots & x_e^T M \frac{\partial^2 x_e}{\partial u_\jmath(k)\partial u_\jmath(v)} \end{bmatrix}, \tag{4.12}$$

$$x_e = x(h) - \bar{x}(h), \quad x(h) = \prod_{j=0}^{h-1} \chi_{\{\emptyset\}}(j)x(0), \quad \frac{\partial^2 x_e}{\partial u_\iota(k)\partial u_\ell(v)} = \prod_{j=0}^{h-1} \chi_{\{(\iota,k),(\ell,v)\}}(j)x(0) \tag{4.13}$$

and

$$\chi_{\{(i_1,j_1),(i_2,j_2),...\}}(j) \triangleq \begin{cases} B_{i_n}(j) & j = j_n \\ A(j) + \sum_{i\in\mathbb{I}} B_i(j)u_i(j) & otherwise \end{cases}. \tag{4.14}$$

The norm $\|\cdot\|$ is defined as the maximum singular value for matrices and the absolute value for scalars.

Proof. To guarantee convexity of the cost function J, it is sufficient to prove that J_h in eq. (4.7) is convex for all $h \in \mathbb{N}$. In order to verify this, it is possible to proceed by using induction over the variable h. Let us first verify the convexity for the case where $h = 1$:

- Analyzing J_1

  Using eqs. (4.2) and (4.7) we have

$$J_1 = \left\| \left(A(0) + \sum_{i\in\mathbb{I}} B_i(0)u_i(0) \right) x(0) - \bar{x}(1) \right\|_M^2 + \frac{\lambda_1}{2} \sum_{i\in\mathbb{I}} \|\mathbf{u}_i(0) - \bar{\mathbf{u}}_i(0)\|^2 \tag{4.15}$$

  The Hessian of J_1 can be expressed as

$$H_1 = \mathbf{h}_1 \mathbf{h}_1^T + I\lambda_1 \tag{4.16}$$

where

$$\mathbf{h}_1 = \begin{bmatrix} M^{\frac{1}{2}}B_1(0)x(0) & M^{\frac{1}{2}}B_2(0)x(0) & \cdots & M^{\frac{1}{2}}B_I(0)x(0) \end{bmatrix}^T \tag{4.17}$$

For J_1 to be convex it is necessary that $H_1 \succ 0$. Therefore, since $\mathbf{h}_1\mathbf{h}_1^T$ is always positive, the following can be easily deduced from eq. (4.16):

$$\lambda_1 > 0. \tag{4.18}$$

- Analyzing J_h for $h \geq 2$

  In general, J_h can be written as

$$J_h = \left\| \prod_{j=0}^{h-1} \chi_j x(0) - \bar{x}(h) \right\|_M^2 + \frac{\lambda_h}{2} \sum_{i \in \mathbb{I}} \|\mathbf{u}_i(h) - \bar{\mathbf{u}}_i(h)\|^2. \tag{4.19}$$

  The corresponding second order derivatives of J_h are

$$\frac{\partial^2 J_h}{\partial u_i(k)^2} = 2 \left\| \prod_{j=0}^{h-1} \chi_{\{(i,k)\}}(j) x(0) \right\|_M^2 + \lambda_h \tag{4.20}$$

$$\frac{\partial^2 J_h}{\partial u_i(k) \partial u_\ell(k)} = 2 \left(\prod_{j=0}^{h-1} \chi_{\{(i,k)\}}(j) x(0) \right)^T M \prod_{j=0}^{h-1} \chi_{\{(\ell,k)\}}(j) x(0) \tag{4.21}$$

$$\begin{aligned} \frac{\partial^2 J_h}{\partial u_i(k) \partial u_\ell(v)} =& 2 \left(\prod_{j=0}^{h-1} \chi_{\{(i,k)\}}(j) x(0) \right)^T M \prod_{j=0}^{h-1} \chi_{\{(\ell,v)\}}(j) x(0) + \\ & 2 \left(\prod_{j=0}^{h-1} \chi_{\{\emptyset\}}(j) x(0) - \bar{x}(h) \right)^T M \prod_{j=0}^{h-1} \chi_{\{(i,k),(\ell,v)\}}(j) x(0) \end{aligned} \tag{4.22}$$

  The Hessian matrix associated with J_h can be constructed as

$$H_h = \begin{bmatrix} H^{1,1} & H^{1,2} & \cdots & H^{1,h} \\ H^{2,1} & H^{2,2} & & \\ \vdots & & \ddots & \vdots \\ H^{h,1} & & \cdots & H^{h,h} \end{bmatrix}, \tag{4.23}$$

  where

$$H^{k,v} = \begin{bmatrix} \frac{\partial^2 J_h}{\partial u_1(k) \partial u_1(v)} & \frac{\partial^2 J_h}{\partial u_1(k) \partial u_2(v)} & \cdots & \frac{\partial^2 J_h}{\partial u_1(k) \partial u_\jmath(v)} \\ \frac{\partial^2 J_h}{\partial u_1(k) \partial u_2(v)} & \frac{\partial^2 J_h}{\partial u_2(k) \partial u_2(v)} & & \\ \vdots & & \ddots & \vdots \\ \frac{\partial^2 J_h}{\partial u_1(k) \partial u_\jmath(v)} & & \cdots & \frac{\partial^2 J_h}{\partial u_\jmath(k) \partial u_\jmath(v)} \end{bmatrix}. \tag{4.24}$$

  It is convenient to write H_h as follows

$$H_h = \mathbf{h}_h \mathbf{h}_h^T + \tilde{H} \tag{4.25}$$

where

$$\mathbf{h}_h = \begin{bmatrix} \sqrt{\frac{\partial^2 J_h}{\partial u_1(1)^2} - \lambda_h} \\ \sqrt{\frac{\partial^2 J_h}{\partial u_2(1)^2} - \lambda_h} \\ \vdots \\ \sqrt{\frac{\partial^2 J_h}{\partial u_\jmath(1)^2} - \lambda_h} \\ \sqrt{\frac{\partial^2 J_h}{\partial u_1(2)^2} - \lambda_h} \\ \sqrt{\frac{\partial^2 J_h}{\partial u_2(2)^2} - \lambda_h} \\ \vdots \\ \sqrt{\frac{\partial^2 J_h}{\partial u_\jmath(h)^2} - \lambda_h} \end{bmatrix}, \qquad \tilde{H} = \begin{bmatrix} I\lambda_h & Z_{1,2} & \cdots & Z_{1,h} \\ Z_{2,1} & I\lambda_h & & Z_{2,h} \\ \vdots & & \ddots & \vdots \\ Z_{h,1} & Z_{h,2} & \cdots & I\lambda_h \end{bmatrix}, \tag{4.26}$$

and $Z_{k,v}$ is defined in eq. (4.12). Note that $Z_{k,v} = Z_{v,k}^T$

Consider now ζ_h as in eq. (4.11), and a set $\mathbf{Z}_h$ containing all the possible values of $Z_{k,v}$ as

$$\mathbf{Z}_h = \{Z_{k,v} | Z_{k,v} \text{ satisfies eq. (4.12)} \quad \forall k, v \in \{1, 2, ..., h\}\}. \tag{4.27}$$

The parameter ζ_h will be used to define bounds later in the demonstration.

For J_h to be convex, H_h must be positive definite. Note that the term $\mathbf{h}_h \mathbf{h}_h^T$ in eq. (4.25) is at least positive semidefinite. Therefore, it is sufficient to guarantee that $\tilde{H}$ is positive definite for the Hessian to be positive definite. Let us define $\tilde{H}_\ell$ as the ℓ^{th} leading principal submatrix of $\tilde{H}$ constructed by blocks as follows: $\tilde{H}_1 = I\lambda_h$, $\tilde{H}_2 = \begin{bmatrix} I\lambda_h & Z_{1,2} \\ Z_{2,1} & I\lambda_h \end{bmatrix}$ and so on, up to $\tilde{H}_h = \tilde{H}$. Using Fact B.2 and B.7, and induction over the variable ℓ, conditions over λ_h for $\tilde{H}$ to be positive definite can be obtained. Let us start analyzing the first two cases $\ell = 1$ and $\ell = 2$:

1. Principal submatrix $\tilde{H}_1$

   It is trivial to see that for $\tilde{H}_1$ we get the basic condition

   $$\lambda_h > 0. \tag{4.28}$$

2. Principal submatrix $\tilde{H}_2$

   In order to guarantee $\tilde{H}_2$ to be positive definite, Fact B.7 can be used. Note that, with the conditions imposed over $\tilde{H}_1$, the block $A_{1,1}$ (see details in Fact B.7) in $\tilde{H}_2$ is guaranteed to be positive definite. Therefore the remaining condition goes as follows

   $$I\lambda_h - Z_{2,1}^T (I\lambda_h)^{-1} Z_{2,1} \succ 0, \quad \forall Z_{1,2} \in \mathbf{Z_2}. \tag{4.29}$$

   Using Facts B.4 and B.5, and ζ_h in eq. (4.11), the following can be written

   $$I\lambda_h - \frac{Z_{2,1}^T Z_{1,2}}{\lambda_h} \succeq I\lambda_h - \frac{I\zeta_h^2}{\lambda_h} \quad \forall Z_{1,2} \in \mathbf{Z_2}. \tag{4.30}$$

Therefore, to guarantee eq. (4.29), the following condition is sufficient

$$I\lambda_h - \frac{I\zeta_h^2}{\lambda_h} \succ 0, \tag{4.31}$$

which leads to

$$\lambda_h > \zeta_h. \tag{4.32}$$

Note that, for eq. (4.29) to be true for all values of $Z_{1,2}$, it is necessary to consider the worst case, which is given by the bound in eq. (4.12). A consequence of this fact is that, for the analyses of the following principal leading submatrices $\tilde{H}_3$, $\tilde{H}_4$, ..., $\tilde{H}_j$, the value of $Z_{1,2}$ will be substituted for the one corresponding to its bound, i.e. ζ_h. Analagous to this, we will see that from the analyses of $\tilde{H}_3$, $\tilde{H}_4$, and up to $\tilde{H}_j$, it is concluded that for $Z_{k,v}$, $\forall k, v \in \{1, 2, ..., j\}$ the worst case is also given by ζ_h.

3. Principal submatrix $\tilde{H}_{j+1}$

The induction hypothesis states that

$$\tilde{H}_j \succ 0. \tag{4.33}$$

In order to prove that

$$\tilde{H}_{j+1} \succ 0, \tag{4.34}$$

Fact B.7 is used and its two necessary conditions are verified. Note that $A_{1,1} = \tilde{H}_j \succ 0$ (see details in Fact B.7) is given by the induction hypothesis. Therefore, to guarantee eq. (4.34), it is sufficient to guarantee the following

$$I\lambda_h - \begin{bmatrix} Z_{1,j+1} \\ \vdots \\ Z_{j,j+1} \end{bmatrix}^T \tilde{H}_j^{-1} \begin{bmatrix} Z_{1,j+1} \\ \vdots \\ Z_{j,j+1} \end{bmatrix} \succ 0, \forall Z_{k,v} \in \mathbf{Z}_h. \tag{4.35}$$

Note that, as mentioned previously, the worst case scenario for the values in $\tilde{H}_j$ (i.e. $Z_{k,v}$, $\forall k, v \in \{1, 2, ..., j\}$) is given by the matrix $\tilde{H}_j^\dagger$ defined as follows

$$\tilde{H}_j^\dagger = \begin{bmatrix} I\lambda_h & I\zeta_h & \cdots & I\zeta_h \\ I\zeta_h & I\lambda_h & & I\zeta_h \\ \vdots & & \ddots & \vdots \\ I\zeta_h & I\zeta_h & \cdots & I\lambda_h \end{bmatrix}. \tag{4.36}$$

Moreover, we can write $\tilde{H}_j^\dagger$ as

$$\tilde{H}_j^\dagger = \Xi_j + \lambda_h I, \tag{4.37}$$

where Ξ_j is an $j\mathfrak{I} \times j\mathfrak{I}$ matrix defined as follows:

$$\Xi_j = \begin{bmatrix} 0 & I\zeta_h & \cdots & I\zeta_h \\ I\zeta_h & 0 & & I\zeta_h \\ \vdots & & \ddots & \vdots \\ I\zeta_h & I\zeta_h & \cdots & 0 \end{bmatrix}, \tag{4.38}$$

where $\mathfrak{I}$ represent the number of control inputs.

By substituting the worst case given by eq. (4.36) in eq. (4.35), the following sufficient condition to guarantee eq. (4.34) can be obtained

$$I\lambda_h - \begin{bmatrix} Z_{1,j+1} \\ \vdots \\ Z_{j,j+1} \end{bmatrix}^T \left(\tilde{H}_j^\dagger\right)^{-1} \begin{bmatrix} Z_{1,j+1} \\ \vdots \\ Z_{j,j+1} \end{bmatrix} \succ 0, \quad \forall Z_{k,j+1} \in \mathbf{Z}_h \tag{4.39}$$

So far, the definition of Ξ_j in eq. (4.38) has been written in terms of ζ_h, a positive value as defined in eq. (4.11). However, considering a general case where $-I\zeta_h \preceq Z_{k,i} \preceq I\zeta_h$, $\forall k, i$, it is necessary to consider also $\pm\Xi_j$. Let us start by analysing first the less general case where $0 \preceq Z_{k,i} \preceq I\zeta_h$ (i.e. $+\Xi_j$).

Using eq. (4.37) and Fact B.8, the quadratic form in eq. (4.39) can be rewritten as

$$\begin{aligned} &\begin{bmatrix} Z_{1,j+1} \\ \vdots \\ Z_{j,j+1} \end{bmatrix}^T \left(\tilde{H}_j^\dagger\right)^{-1} \begin{bmatrix} Z_{1,j+1} \\ \vdots \\ Z_{j,j+1} \end{bmatrix} = \\ &\qquad \begin{bmatrix} Z_{1,j+1} \\ \vdots \\ Z_{j,j+1} \end{bmatrix}^T \left(\sum_{i=0}^{\infty} (-1)^i \Xi_j^{-1} (\lambda_h \Xi_j^{-1})^i\right) \begin{bmatrix} Z_{1,j+1} \\ \vdots \\ Z_{j,j+1} \end{bmatrix}. \end{aligned} \tag{4.40}$$

Applying Fact B.4 to eq. (4.40) we obtain

$$\begin{aligned} &\begin{bmatrix} Z_{1,j+1} \\ \vdots \\ Z_{j,j+1} \end{bmatrix}^T \left(\tilde{H}_j^\dagger\right)^{-1} \begin{bmatrix} Z_{1,j+1} \\ \vdots \\ Z_{j,j+1} \end{bmatrix} \preceq \\ &\qquad - \begin{bmatrix} Z_{1,j+1} \\ \vdots \\ Z_{j,j+1} \end{bmatrix}^T \left(\sum_{i=0}^{\infty} \lambda_h^i (I\Lambda_{\min}(-\Xi_j^{-1}))^{i+1}\right) \begin{bmatrix} Z_{1,j+1} \\ \vdots \\ Z_{j,j+1} \end{bmatrix}. \end{aligned} \tag{4.41}$$

Moreover, using the bound ζ_h leads to

$$-\begin{bmatrix} Z_{1,j+1} \\ \vdots \\ Z_{j,j+1} \end{bmatrix}^T \begin{bmatrix} Z_{1,j+1} \\ \vdots \\ Z_{j,j+1} \end{bmatrix} \sum_{i=0}^{\infty} \lambda_h^i (\Lambda_{\min}(-\Xi_j^{-1}))^{i+1} \preceq \\ -jI\zeta_h^2 \sum_{i=0}^{\infty} \lambda_h^i (\Lambda_{\min}(-\Xi_j^{-1}))^{i+1}, \quad \forall Z_{k,j+1} \in \mathbf{Z}_h \tag{4.42}$$

From eqs. (4.41) and (4.42) we conclude that

$$\begin{bmatrix} Z_{1,j+1} \\ \vdots \\ Z_{j,j+1} \end{bmatrix}^T \left(\tilde{H}_j^{\dagger}\right)^{-1} \begin{bmatrix} Z_{1,j+1} \\ \vdots \\ Z_{j,j+1} \end{bmatrix} \preceq -jI\zeta_h^2 \sum_{i=0}^{\infty} \lambda_h^i (\Lambda_{\min}(-\Xi_j^{-1}))^{i+1}, \\ \forall Z_{k,j+1} \in \mathbf{Z}_h. \tag{4.43}$$

Note that the conclusion from eq. (4.42) that led to eq. (4.43) goes in line with the statement made at the end of item 2 which says that the worst cases for $Z_{k,v}$ are given by ζ_h.

With the definition of Ξ_j in eq. (4.38), it is possible to compute $\Lambda_{\min}(-\Xi_j^{-1})$ as

$$\Lambda_{\min}(-\Xi_j^{-1}) = -\frac{1}{(j-1)\zeta_h}. \tag{4.44}$$

Substituting eq. (4.44) into the scalar part of the sum in eq. (4.43) leads to

$$-j\zeta_h^2 \sum_{i=0}^{\infty} \lambda_h^i \left(-\frac{1}{(j-1)\zeta_h}\right)^{i+1} = j\sum_{i=0}^{\infty} (-1)^i \lambda_h^i \left(\frac{1}{\zeta_h}\right)^{i-1} \left(\frac{1}{j-1}\right)^{i+1}, \tag{4.45}$$

by changing the variable ($i = 2\ell$) in the sum, we obtain

$$\begin{aligned} -j\zeta_h^2 \sum_{i=0}^{\infty} \lambda_h^i \left(-\frac{1}{(j-1)\zeta_h}\right)^{i+1} = \\ = j\sum_{\ell=0}^{\infty} \lambda_h^{2\ell} \left(\frac{1}{\zeta_h}\right)^{2\ell-1} \left(\frac{1}{j-1}\right)^{2\ell+1} - \lambda_h^{2\ell+1} \left(\frac{1}{\zeta_h}\right)^{2\ell} \left(\frac{1}{j-1}\right)^{2\ell+2} \\ = \frac{j}{j-1}\left(\zeta_h - \frac{\lambda_h}{j-1}\right) \sum_{\ell=0}^{\infty} \left(\frac{\lambda_h^2}{\zeta_h^2 (j-1)^2}\right)^{\ell}. \end{aligned} \tag{4.46}$$

From eqs. (4.43) and (4.46) we obtain that

$$I\lambda_h - \begin{bmatrix} Z_{1,j+1} \\ \vdots \\ Z_{j,j+1} \end{bmatrix}^T \left(\tilde{H}_j^{\dagger}\right)^{-1} \begin{bmatrix} Z_{1,j+1} \\ \vdots \\ Z_{j,j+1} \end{bmatrix} \succeq I\lambda_h - I\frac{j}{j-1}\left(\zeta_h - \frac{\lambda_h}{j-1}\right)\sum_{\ell=0}^{\infty}\left(\frac{\lambda_h^2}{\zeta_h^2(j-1)^2}\right)^{\ell}, \quad \forall z_{k,j+1} \in \mathbf{Z}_h. \tag{4.47}$$

Therefore, to guarantee eq. (4.39), it is sufficient to guarantee that

$$I\lambda_h - I\frac{j}{j-1}\left(\zeta_h - \frac{\lambda_h}{j-1}\right)\sum_{\ell=0}^{\infty}\left(\frac{\lambda_h^2}{\zeta_h^2(j-1)^2}\right)^{\ell} \succ 0, \tag{4.48}$$

which is equivalent to the following scalar inequality

$$\lambda_h - \frac{j}{j-1}\left(\zeta_h - \frac{\lambda_h}{j-1}\right)\sum_{\ell=0}^{\infty}\left(\frac{\lambda_h^2}{\zeta_h^2(j-1)^2}\right)^{\ell} > 0. \tag{4.49}$$

Now consider a constant $\kappa > 0$ such that $\lambda_h = \kappa\zeta_h$. With this, we can rewrite eq. (4.49) for $\left|\frac{\kappa}{j-1}\right| < 1$ as follows

$$\kappa\zeta_h - \frac{j}{j-1}\left(\zeta_h - \frac{\kappa\zeta_h}{j-1}\right)\frac{1}{1-\frac{\kappa^2}{(j-1)^2}} > 0. \tag{4.50}$$

After some algebraic manipulations we obtain

$$\frac{(\kappa-1)(\kappa+j)}{\kappa+j-1} > 0, \tag{4.51}$$

concluding that $\kappa > 1$ and, since $\lambda_h = \kappa\zeta_h$, we have that

$$\lambda_h > \zeta_h, \quad \forall h \in \{2, 3, ..., \mathcal{H}\}, \tag{4.52}$$

where $\mathcal{H}$ represents the prediction horizon. Therefore, for eq. (4.25) to be positive definite (i.e. convex cost function (eq. (4.6))), given that $0 \preceq Z_{k,i} \preceq I\zeta_h$, the condition in eq. (4.52) sufficient.

Now, let us consider the general case where $-I\zeta_h \preceq Z_{k,i} \preceq I\zeta_h$ (i.e. $\pm\Xi_j$ is used

instead of $+\Xi_j$). Then eq. (4.40) can be rewritten using Fact B.8 as follows

$$\begin{bmatrix} Z_{1,j+1} \\ \vdots \\ Z_{j,j+1} \end{bmatrix}^T \left(\tilde{H}_j^{\dagger}\right)^{-1} \begin{bmatrix} Z_{1,j+1} \\ \vdots \\ Z_{j,j+1} \end{bmatrix} = \begin{bmatrix} Z_{1,j+1} \\ \vdots \\ Z_{j,j+1} \end{bmatrix}^T \left(\sum_{i=0}^{\infty} (-1)^i \lambda_h^{-1} ((\pm\Xi_j)\lambda_h^{-1})^i\right) \begin{bmatrix} Z_{1,j+1} \\ \vdots \\ Z_{j,j+1} \end{bmatrix}. \tag{4.53}$$

In an analogous procedure, an upper bound is found using Fact B.3 and considering the following

$$\Lambda_{\max}(-(\pm\Xi_j)) = (j-1)\zeta_h. \tag{4.54}$$

Solving the sum in eq. (4.53) and, as in the previous case, using a constant $\kappa > 0$ such that $\lambda_h = \kappa\zeta_h$, leads to the condition

$$-\frac{(1+\kappa)(j-\kappa)}{\kappa-(j-1)} > 0, \tag{4.55}$$

where we conclude that $\kappa > j-1$.

The variable j represents the principal submatrix being analyzed. Since eq. (4.55) must be true for all j, we consider the worst case $j = h$, which corresponds to the last principal submatrix. Therefore we conclude that

$$\lambda_h > (h-1)\zeta_h, \quad \forall h \in \{2, 3, ..., \mathcal{H}\}, \tag{4.56}$$

It is now possible to say that, for eq. (4.25) to be positive definite (i.e. convex cost function (eq. (4.6))) given that $-I\zeta_h \preceq Z_{k,i} \preceq I\zeta_h$, the condition in eq. (4.56) sufficient.

□

The previous theorem provides sufficient conditions over the parameters λ_h for which the convexity of J is guaranteed. The following section focuses into elucidating analytical estimates of these conditions as a function of the system model parameters.

4.4. Analytical estimation of the convexity bound

As a direct consequence of Theorem 1, the following Corollary (Convexity for a wide operation range) provides an analytical estimate of ζ_h for an admissible set of state space values and inputs.

Corollary 3 (Convexity for a wide range of operation)**.** An estimate of ζ_h can be defined as follows

$$\hat{\zeta}_h = 2\frac{(\alpha^h+1)\alpha^h}{\alpha^2}\|M\|x_{\max}^2\beta, \tag{4.57}$$

where

$$\beta = \left\| \begin{bmatrix} \beta_1^2 & \beta_1\beta_2 & \cdots & \beta_1\beta_{\mathfrak{I}} \\ \beta_1\beta_2 & \beta_2^2 & & \\ \vdots & & \ddots & \vdots \\ \beta_1\beta_{\mathfrak{I}} & & \cdots & \beta_{\mathfrak{I}}^2 \end{bmatrix} \right\| \tag{4.58}$$

and

$$\begin{aligned} x_{\max} &= \max_k(\|x(0)\|, \|\bar{x}(k)\|), \quad \alpha = \max_k \left(\left\| A(k) + \sum_{i=1}^{\mathfrak{I}} B_i(k)u_i(k) \right\| \right), \\ \beta_i &= \max_k(\|B_i(k)\|). \end{aligned} \tag{4.59}$$

The norm $\|\cdot\|$ is defined as the maximum singular value for matrices and the absolute value for scalars.

Proof. Based on Theorem 1 and using eqs. (4.12) and (4.13), each of the elements of $Z_{k,v}$ can be written as

$$x_e^T M \frac{\partial^2 x_e}{\partial u_\iota(k)\partial u_\ell(v)} = \left(\prod_{j=0}^{h-1} \chi_{\{\emptyset\}}(j)x(0) - \bar{x}(h) \right)^T M \prod_{j=0}^{h-1} \chi_{\{(\iota,k),(\ell,v)\}}(j)x(0) \tag{4.60}$$

Applying Fact B.1 to each of the elements described in eq. (4.60), using Fact B.6 and the definition of ζ_h in eq. (4.11), the following holds

$$\begin{aligned} 2\frac{(\alpha^h+1)\alpha^h}{\alpha^2}\|M\|x_{\max}^2\beta &\geq \max_{k,v}(\|Z_{k,v}\|) \\ &\geq \zeta_h, \end{aligned} \tag{4.61}$$

where β, α, β_i and $x_{\max}$ are defined in eqs. (4.58) and (4.59) respectively. Therefore, $\hat{\zeta}_h$ as defined in eq. (4.57), represents an estimate of ζ_h in eq. (4.11). □

The following result (Convexity for local operation) presents an analytical expression that relates the values of the convexity bound with the differences between the references and the values of the state. Therefore, convexity is merely guaranteed in a neighborhood around the reference values. The value of the bound obtained for local operation is typically lower than the one for wide operation range, impliying a less restrictive condition for the controller.

Corollary 4 (Convexity for local operation)**.** It is possible to obtain an estimate of ζ_h by limiting the error between the reference and the predicted states as follows

$$\hat{\zeta}_h = 2e_{\max}\alpha^{h-2}x_{\max}\beta, \tag{4.62}$$

where β, α, β_i and $x_{\max}$ are defined in eqs. (4.58) and (4.59) respectively, and

$$e_{\max} = \max_k(\|Mx_e\|) \tag{4.63}$$

Proof. Using eqs. (4.12) and (4.13), each of the elements of $Z_{k,v}$ can be written as

$$x_e^T M \frac{\partial^2 x_e}{\partial u_\iota(k)\partial u_\ell(v)} = x_e^T M \prod_{j=0}^{h-1} \chi_{\{(\iota,k),(\ell,v)\}}(j)x(0) \tag{4.64}$$

In an analogous procedure to that of Corollary 3, $\hat{\zeta}_h$ as defined in eq. (4.62) represents an estimate of the convexity bound. □

Remark 2. *The analytical expressions obtained in Corollary 3 and 4 are an estimate. This comes from using the inequality $\|Ax\| \leq \|A\|\|x\|$ (see Fact B.1). In the general case, when the values of A, B, $x(k)$ and $\bar{x}(k)$ are matrices and vectors respectively, the value $\|A\|\|x\|$ could be considerably higher than the one of $\|Ax\|$, giving as a result a loose estimate of the actual bounds. The estimate becomes looser, the higher the dimension of the state space. In the specific case where A, B, $x(k)$ and $\bar{x}(k)$ are scalars, the analytical expressions provide an accurate result. This can be verified by using numerical techniques along with eqs.* (4.11) *and* (4.15).

Remark 3. *The transformation of the state space system from the original model in eq.* (1.11) *to the model in eq.* (4.2) *serves the purpose of easing the analysis done in Theorem 1 and, consequently, in Corollary 3 and 4. The introduction of the parameter δ_i in eq.* (4.3) *is particulary useful when using the estimates in Corollary 3 and 4. This parameter can be used to take into account constraints and differences in the range of the different control inputs $u_i(k)$ for a better analytical estimate of ζ_h.*

As an example, let us assume that two control inputs are available, and the constraints $-1 \leq \upsilon_1(k) \leq 1$ and $-1 \leq \upsilon_2(k) \leq 1$ are taken into account. In this case $\delta_1 = \delta_2 = 1$ can be selected. Leading to the new inputs $u_1(k)$ and $u_2(k)$ in eq. (4.3)*, to share the same constraints as the original inputs.*

Now consider the case where the constraints over $\upsilon_2(k)$ are $-\frac{1}{2} \leq \upsilon_2(k) \leq \frac{1}{2}$. In this case it is possible to set $\delta_1 = 2\delta_2 = 1$. Transforming the constrains on the new inputs $u_1(k)$ and $u_2(k)$ to $-1 \leq u_1(k) \leq 1$ and $-1 \leq u_2(k) \leq 1$.

A reasonable choice of the parameter ρ in eq. (4.5) *can be $\rho = 1$ or, alternatively, $\rho = \max_i(\max_k(|\upsilon_i(k)|))$.*

4.5. Application to a Boost converter

In order to illustrate numerically the results obtained in sections 4.3 and 4.4, and before turning to the MMC, let us consider a switched power converter in Boost configuration as in fig. 4.2 [EM01]. This power converter consists of a DC power supply V_{dc}, an inductive element L, a capacitor C, a load resistor R_l and two ideal switches S_1 and S_2. The two switches, S_1 and S_2, are complementary. This leads to the two possible circuit configurations shown in fig. 4.3.

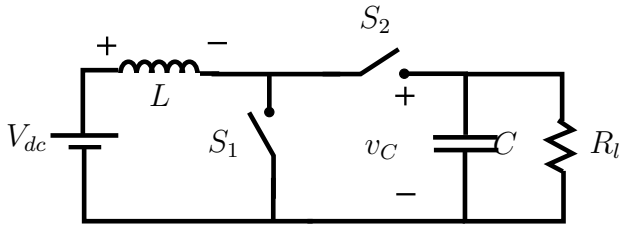

Figure 4.2.: Boost converter

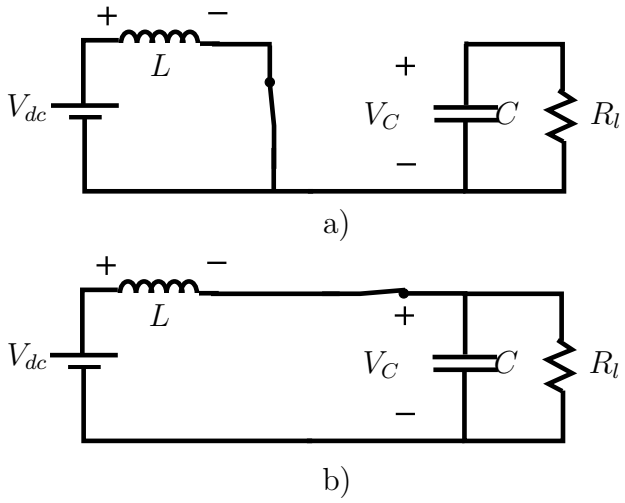

Figure 4.3.: Possible circuit configurations of the Boost converter. a) S_1 ON and S_2 OFF, b) S_1 OFF and S_2 ON

By manipulating the times in which the converter stays in each of the two possible circuit configurations, it is possible to regulate the voltage in the capacitor C (i.e. v_c).

4.5.1. Converter modeling

It is common practice to use a PWM at constant frequency to drive the switches S_1 and S_2 in these types of converters. This also allows one to apply average modeling techniques to obtain a continuous model of the converter [MC76, LPDP13]. Therefore, a discrete dynamic model of the Boost converter can be written as follows

$$z(k+1) = (\mathcal{A} + \mathcal{B}d(k))z(k) + \mathcal{C} \tag{4.65}$$

where

$$\mathcal{A} = \begin{bmatrix} 0 & -\frac{1}{L} \\ \frac{1}{C} & -\frac{1}{R_l C} \end{bmatrix} T_s + I, \quad \mathcal{B} = \begin{bmatrix} 0 & \frac{1}{L} \\ -\frac{1}{C} & 0 \end{bmatrix} T_s, \quad \mathcal{C} = \begin{bmatrix} \frac{V_{dc}}{L} \\ 0 \end{bmatrix} T_s \tag{4.66}$$

and

$$z(k) = \begin{bmatrix} i_L(k) & v_C(k) \end{bmatrix}^T. \tag{4.67}$$

In eqs. (4.65) and (4.66), $d(k)$ and T_s represents the duty cycle of the converter and the sampling time of the MPC respectively. Additionally $0 \leq d(k) \leq 1, \quad \forall k \geq 0$. In

eq. (4.67), $i_L(k)$ and $v_C(k)$ represent inductor current and the capacitor voltage respectively.

In order to transform the system in eq. (4.65) into the system in eq. (4.2), eq. (4.4) can be used to obtain matrices A and B as follows

$$A = \begin{bmatrix} 1 & -\frac{T_s}{L} & \frac{V_{dc}}{L}T_s \\ \frac{T_s}{C} & -\frac{T_s}{R_l C}+1 & 0 \\ 0 & 0 & 1 \end{bmatrix}, \quad B = \begin{bmatrix} 0 & \frac{T_s}{L} & 0 \\ -\frac{T_s}{C} & 0 & 0 \\ 0 & 0 & 0 \end{bmatrix} \tag{4.68}$$

and

$$x(k) = \begin{bmatrix} i_L(k) & v_C(k) & 1 \end{bmatrix}^T. \tag{4.69}$$

For the sake of this example, the numerical values shown in table 4.1 are used.

Table 4.1.: Numerical values of the parameters of the Boost converter

V_{dc}	L	C	R_l	T_s	$x_{\max}$	$e_{\max}$	$\mathcal{H}$	M
10V	450μH	220μF	76Ω	42μs	$\|[7 \quad 35]^T\|$	$\|M[0.057 \quad 15]^T\|$	12	$\begin{bmatrix} 10^{-3} & 0 \\ 0 & 1 \end{bmatrix}$

4.5.2. Definition of the control objective

The objective of the controller is to regulate the state vector to a constant reference value. This constant reference can be defined as

$$\bar{x}(k) = \begin{bmatrix} \bar{i}_L & \bar{v}_C & 1 \end{bmatrix}^T, \quad \bar{d}(k) = \bar{d}, \quad \forall k \geq 0 \tag{4.70}$$

where $\bar{i}_L$, $\bar{v}_C$ and $\bar{d}$ represent the individual reference values of each of the state space variables and the control input respectively. With the references in eq. (4.70), the help of eqs. (4.2), (4.6), (4.7), (4.68) and (4.69), and given that there is only one available input ($u_1(k) = d(k)$), it is possible to compute the cost function J for a finite prediction horizon $\mathcal{H}$. Therefore, the optimization problem associated with the MPC for the Boost converter can be written as follows

$$\begin{aligned} \min_{d(k),\forall k\geq 0} \quad & J(x(0), ..., x(\mathcal{H}), d(0), .., d(\mathcal{H}-1)) \\ \text{s.t.} \quad & 0 \leq d(k) \leq 1, \quad \forall k \geq 0 \end{aligned} \tag{4.71}$$

Note that, for the optimization problem in eq. (4.76) to be convex, the values of λ_h should meet the requirements given by Theorem 1.

4.5.3. Values of the weighting parameter λ_h

In this section we aim to use the results in Theorem 1, Corollary 3 and Corollary 4 to calculate and compare the bounds ζ_h for the two cases presented in section 4.4 (wide operation range and local operation). The results using the analytical expressions obtained in Corollary 3 and Corollary 4 are compared with results obtained numerically (see. fig. 4.4).

The results in fig. 4.4 show that, as expected, the bounds for a wide operation range present a higher value than those for local operation. Moreover, the numerical results for both wide operation and local operation are below the analytical counterparts (see Remark 2).

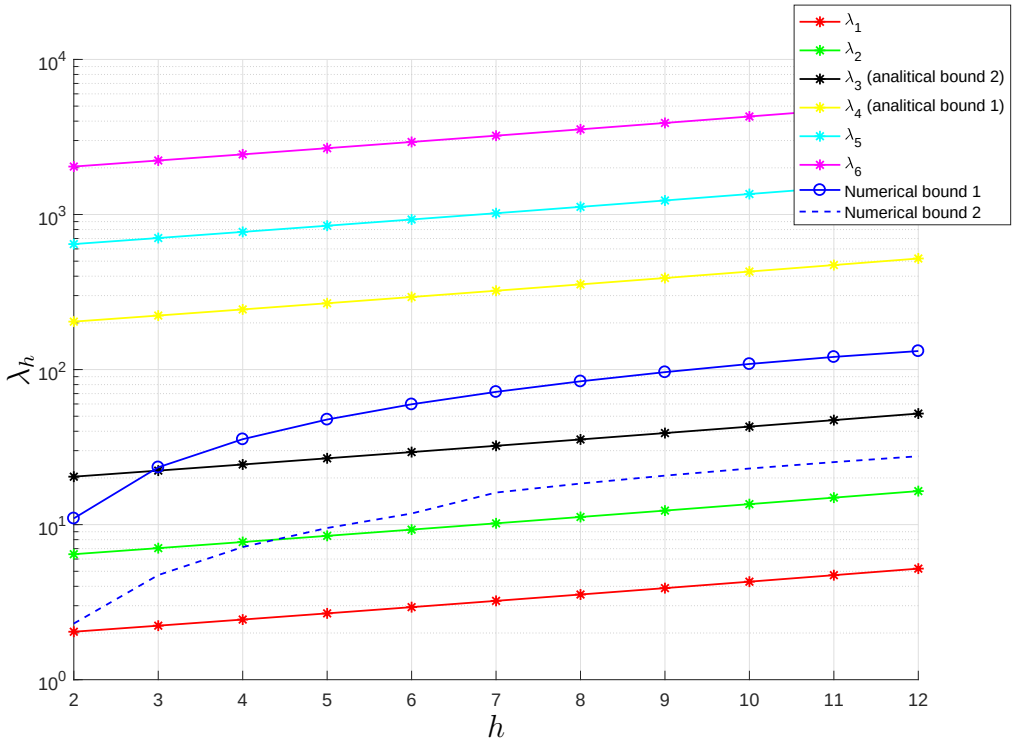

Figure 4.4.: Comparison of the values of the bound ζ_h as a function of h (the vales were obtained analytically and numerically). Bound 1 is found considering a wide range of possible values of the state space vector (see. eq. (4.57)) and Bound 2 is found considering a restricted set of values of the state space vector around the reference (see eq. (4.62))). Additional values of λ_h used for simulation are shown.

4.5.4. Evaluation of the controlled system performance

In order to evaluate how the selection of λ_h influences the performance of the controller, fig. 4.5 (a) show the system response from zero initial conditions using the different values of λ_h shown in fig. 4.4. Additionally, in fig. 4.5 (b) the response starting from non-zero initial conditions using the the same λ_h values is shown. For all these tests the parameters in table 4.1 are used. Moreover, the simulation uses average models of the switching devices [EM01].

It can be seen how the response of the controller changes in fig. 4.5 when convexity is guaranteed. For lower values of λ_h the system tends to oscillate significantly around the solution. This can be seen more clearly with $\lambda_h = 0$. The more the value of λ_h increases, the more the oscillations are reduced. Moreover, the overshoot and the settling

time increase. It is important to note that, for large values of λ_h, the controlled response gets closer to an open loop response. This can be seen more clearly in fig. 4.5 (b) where the control action d equals the reference almost the entire time.

We can conclude that, the set of values of λ_h that guarantees convexity according to the local operation numerical bound is λ_3. The values of λ_2 are close to convexity showing a similar response. It can be seen that non-convex optimization problems lead to an increase in the oscillations of the controlled variables.

4.6. Application to an MMC

For this example, the MMC and the reduced order model introduced in chapter 2 are employed. The numerical values of its components can be found in table 2.1 on page 17.

Taking this into account, a reduced order model of the MMC in discrete time can be written as:

$$z(k+1) = \left(\mathcal{A} + \mathcal{B}_1\mu^u(k) + \mathcal{B}_2\mu^l(k)\right) z(k) + \mathcal{C}(k), \tag{4.72}$$

where

$$\begin{aligned} \mathcal{A} &\triangleq \begin{bmatrix} -\frac{R}{L} & 0 & 0 & 0 \\ 0 & -\frac{R+2R_l}{L+2L_l} & 0 & 0 \\ 0 & 0 & 0 & 0 \\ 0 & 0 & 0 & 0 \end{bmatrix} T_s + I, \quad \mathcal{B}_1 \triangleq \begin{bmatrix} 0 & 0 & -\frac{1}{2L} & 0 \\ 0 & 0 & -\frac{1}{L+2L_l} & 0 \\ \frac{1}{NC} & \frac{1}{2NC} & 0 & 0 \\ 0 & 0 & 0 & 0 \end{bmatrix} T_s, \\ \mathcal{B}_2 &\triangleq \begin{bmatrix} 0 & 0 & 0 & -\frac{1}{2L} \\ 0 & 0 & 0 & \frac{1}{L+2L_l} \\ 0 & 0 & 0 & 0 \\ \frac{1}{NC} & -\frac{1}{2NC} & 0 & 0 \end{bmatrix} T_s, \quad \mathcal{C}(k) \triangleq \begin{bmatrix} \frac{1}{2L}v_{dc} & 0 \\ 0 & -\frac{2}{L+2L_l}v^*_{ac} \\ 0 & 0 \\ 0 & 0 \end{bmatrix} T_s \end{aligned} \tag{4.73}$$

and the state space vector is given by

$$z(k) \triangleq \begin{bmatrix} i_c(k) & i_l(k) & v^u(k) & v^l(k) \end{bmatrix}^T. \tag{4.74}$$

In this model, the control inputs (modulation functions) $\mu^u(k)$ and $\mu^l(k)$ represent the number of modules inserted in the upper and lower arms of the converter respectively ($0 \leq \mu^u(k), \mu^l(k) \leq N$). For the sake of simplicity $\mu^u(k)$ and $\mu^l(k)$ are treated as smooth functions, which is especially useful when using a control law with a PWM (see chapter 2).

The values of $A(k)$, $B_i(k)$, the new state vector $x(k)$ and its respective state space model can be constructed as in eqs. (4.1), (4.2) and (4.4) on page 56. Here we consider $u_1(k) = \mu^u(k)$ and $u_2(k) = \mu^l(k)$.

4.6.1. Reference design

In order to properly control the MMC, it is necessary to track all the state space variables adequately. Therefore, references for the state have to be carefully designed considering the converter dynamics. In order to do this, the results in chapter 3 are used.

Table 3.2 on page 38 (case 2) shows the optimal values of the phase and amplitudes of the circulating current components aiming to reduce the P2P value of the capacitors

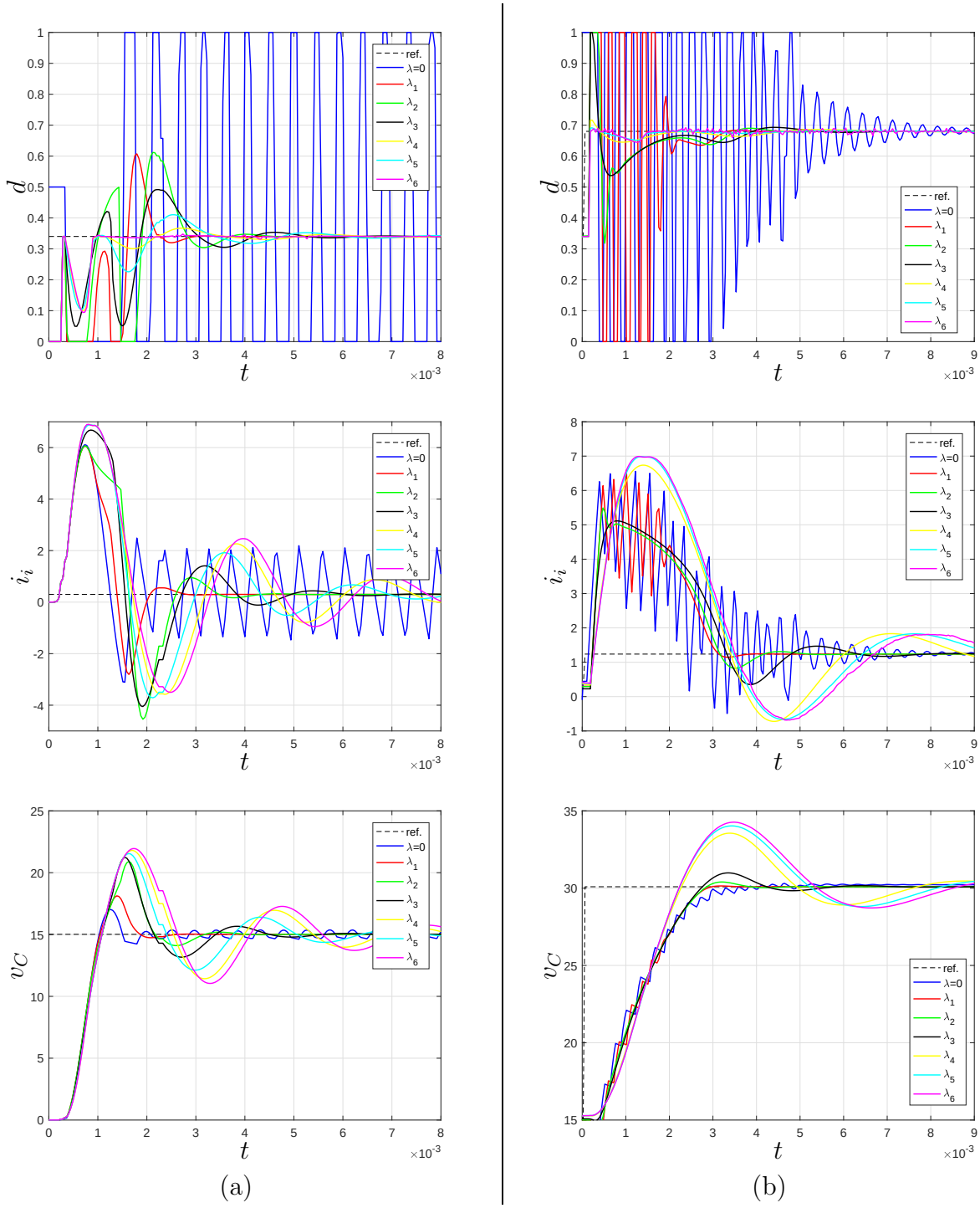

Figure 4.5.: Response of the controlled Boost converter for different values of λ_h, (a) shows the response form zero initial conditions. (b) shows the response to a voltage reference change (from $v_C = 15$ to $v_C = 30$).

voltage ripple. These values are going to be considered for the sake of this example.

4.6.2. Definition of the control objective

The objective of the controller is to track the state reference, which can be defined as:

$$\bar{x}(k) = \begin{bmatrix} \bar{i}_c(k) & \bar{i}_l(k) & \bar{v}^u(k) & \bar{v}^l(k) & 1 \end{bmatrix}^T, \quad \bar{\mu}^u(k), \quad \bar{\mu}^l(k), \quad \forall k \geq 0, \tag{4.75}$$

where $\bar{i}_c(k)$, $\bar{i}_l(k)$, $\bar{v}^u(k)$, $\bar{v}^l(k)$, $\bar{\mu}^u(k)$ and $\bar{\mu}^l(k)$ represent the individual reference values for each of the state space variables and the inputs $\mu^u(k)$ and $\mu^l(k)$. With the references presented in chapter 3, the help of eqs. (4.6) and (4.7), and given that we consider $u_1(k) = \mu^u(k)$ and $u_2(k) = \mu^l(k)$, it is possible to write the cost function J of the MPC problem for a finite prediction horizon $\mathcal{H}$. Therefore, the optimization problem associated with the MPC can be written as follows

$$\begin{aligned} \min_{\mu^u(k),\mu^l(k),\forall i \in k \geq 0} \quad & J(x(0), ..., x(\mathcal{H}), \mu^u(0), \mu^l(0), .., \mu^u(\mathcal{H}-1), \mu^l(\mathcal{H}-1)) \\ \text{s.t.} \quad & \begin{matrix} 0 \leq \mu^u(k) \leq N, \\ 0 \leq \mu^l(k) \leq N. \end{matrix} \quad \forall k \geq 0 \end{aligned} \tag{4.76}$$

Note that for the optimization problem in eq. (4.76) to be convex, the values of λ_h in J (see eq. (4.7)) should meet the requirements given by Theorem 1. The numerical parameters used for the controller implementation can be found in table 4.2. Here the value of M is calculated such that the relative error is considered equitably for all the variables in the state.

A phase shift of $\frac{2\pi}{N}$ is applied to the PWM between two consecutive modules of the same arm. Moreover, a voltage balancing algorithm is implemented to guarantee the assumptions of the reduced order model introduced in chapter 2. The block diagram in fig. 4.6 illustrates the structure of the controller.

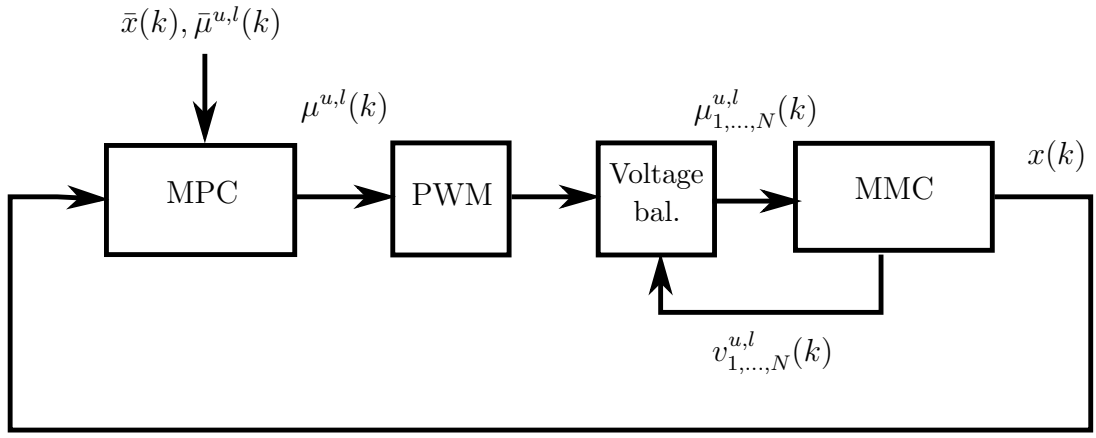

Figure 4.6.: Control scheme of the MMC including a PWM and a voltage balance algorithm. $\mu^{u,l}(k)$ represent continuous control signals while $\mu^{u,l}_{1,...,N}(k)$ represent a set of binary control signals.

Table 4.2.: Controller parameter values. $x_{\max}$ represents the maximum allowed value of the state space vector. $e_{\max}$ the weighted maximum allowed error of the state space vector with respect to its reference where convexity is guaranteed (local operation) . M represents the a weighting matrix in the quadratic term in the cost function.

T_s	f_{PWM}	Horizon $\mathcal{H}$	$x_{\max}$	$e_{\max}$	M
500μ s	250 Hz	20	$\left\Vert \begin{bmatrix} 1 \\ 1 \\ 0.3 \\ 0.3 \end{bmatrix} \right\Vert$	$\left\Vert M \begin{bmatrix} 0.2 \\ 0.2 \\ 0.004 \\ 0.004 \end{bmatrix} \right\Vert$	$\begin{bmatrix} 20 & 0 & 0 & 0 \\ 0 & 17 & 0 & 0 \\ 0 & 0 & 40 \cdot 10^3 & 0 \\ 0 & 0 & 0 & 40 \cdot 10^3 \end{bmatrix}$

4.6.3. Value of the weighting parameter λ_h

In section 4.4, the concept of convexity for wide operation range and local operation was introduced. In order to obtain convexity for a wider range of operation the values of λ_h are typically higher. This implies that the controller has less freedom to act against the error in the state vector. Therefore, in order to reduce the restrictions in the controller, limiting the convexity to a neighborhood around the references is a reasonable option. Moreover one can select the values of λ_h equal to those of the bound required for convexity to reduce the controller restrictions further.

Tests have shown that, in the case of this MMC, the parameters λ_h to guarantee convexity for a wide operation range are too restrictive, degrading the controller performance. Moreover, the analytical estimates of the convexity bound for local operation is affected significantly by the fact mentioned in Remark 2. For these reasons, only convexity for local operation (found numerically) is going to be considered in this example. This can be found using the results in Theorem 1, specifically eqs. (4.11) and (4.15), and considering the constraints in the control signals, in the state space vector and its distance to the reference ($e_{\max}$), as shown in table 4.2. We consider values of λ_h equal to the bound required for convexity. The results are shown in fig. 4.7.

4.6.4. Evaluation of the controlled system performance

The impact on the system response is evaluated using the values of λ_h equal to zero (Case 1) and the values in fig. 4.7 (Case 2). Case 1 is used as a baseline for performance comparison in the tests presented in the following section. Here, a comparison of the controller performance in steady state (fig. 4.8 (a)) and the response to changes in the state references (fig. 4.8 (b)) is shown. It can be seen that Case 1 and Case 2 present similar performance in all the tests. A good tracking in steady state along with good response to reference changes is shown. This implies that local convexity can be achieved without impacting significantly the controller performance.

In fig. 4.8 (b) the amplitude of i_l is decreased by 20% of its maximum value (1 p.u.) at $t = 0.06$s. Note that this small change in the reference allows the converter to stay always close enough to it to guarantee convexity in Case 2.

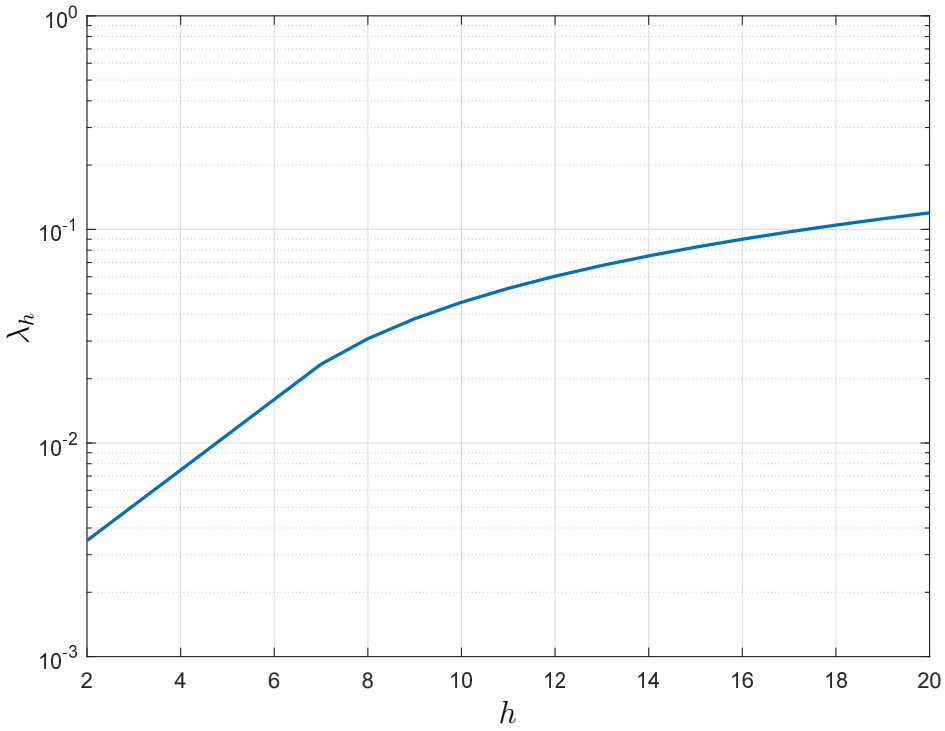

Figure 4.7.: Values of λ_h as a function of the stage cost h (Case 2). Case 1 refers to $\lambda_h = 0$

4.7. Conclusions

The MPC problem using FCS and PWM was compared, showing the advantages of the PWM approach. Moreover, a detailed analysis of the convexity of quadratic cost functions for bilinear systems using PWM was presented. The analysis addresses the case of an MPC problem where prediction horizons longer than one are required. With this analysis, conditions to guarantee convexity of the optimization problem with convex constraints were derived. These conditions are expressed in terms of the parameters of the system and the controller. Two different scenarios were taken into account, wide range of operation and local operation. Local operation guarantees convexity in a limited neighborhood close to the reference values, and restricts the control action less in comparison with the wide range case. Analytical estimates of the conditions for convexity for both cases were obtained and compared with their actual values (found numerically). The results showed that, for the matrix case, the conditions obtained with the analytical expressions are more restrictive than those obtained numerically.

Numerical examples using a Boost converter and an MMC were presented. In the case of the Boost converter, the impact on the controller performance when the controller operates close to the convexity bound was shown. For the MMC, with the help of the model in chapter 2 and the references in chapter 3, it was possible to obtain a long-horizon controller whose performance is not affected when convexity is guaranteed in a region close to the references.

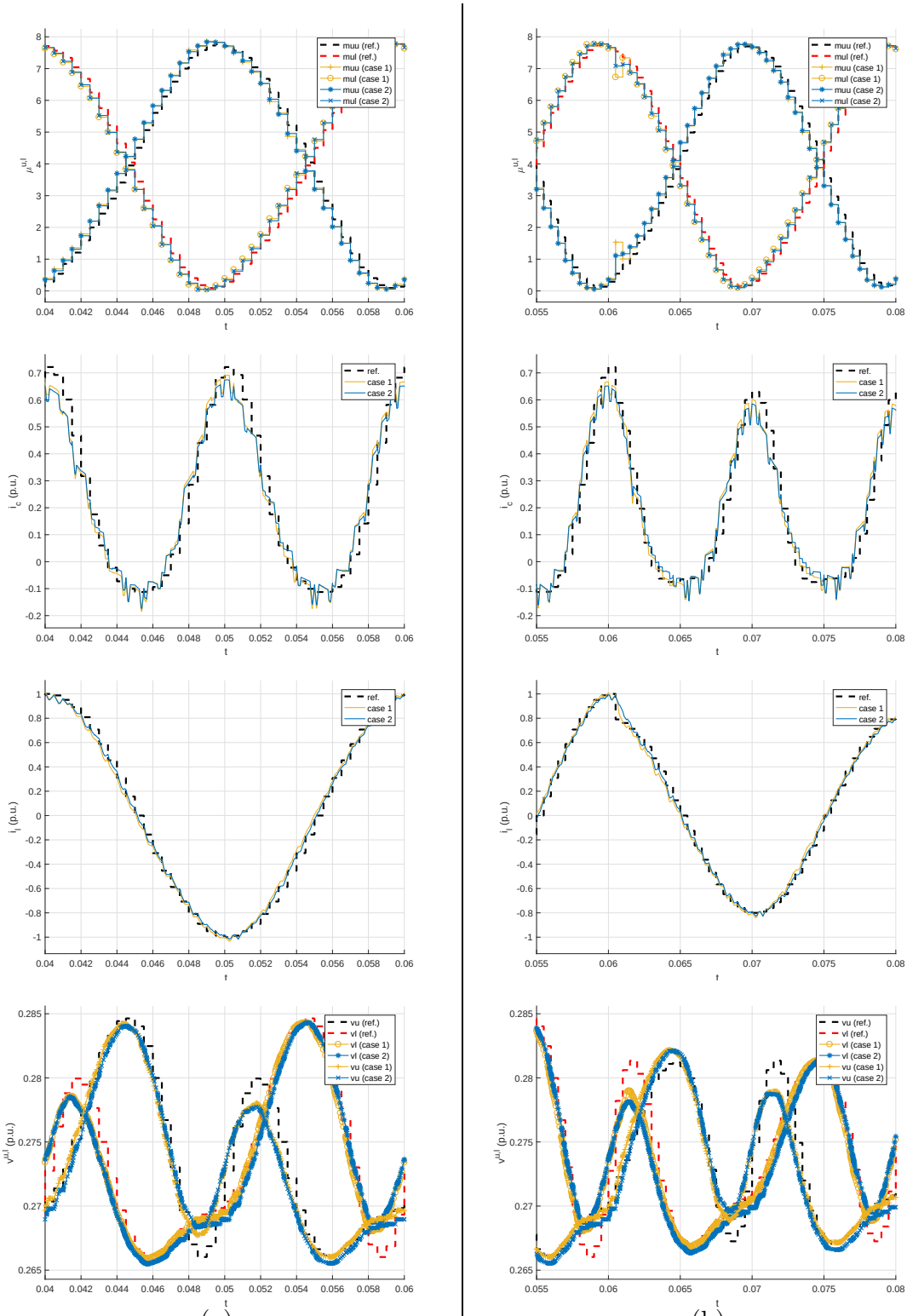

Figure 4.8.: Response of the controlled MMC, (a) shows the response at steady state and (b) the response to a current reference change (-20% on i_l at $t = 0.06$). Averages of all the modules for each arm are shown in both cases.

5. General conclusions and future work

In this work, a deep analysis of the MMC and the problem that arises with the application of MPC was presented. The MMC is a widely popular converter topology that gives several advantages in high voltage DC applications over more traditional topologies. Its modular structure gives the MMC the flexibility to adapt to the requirements of the application and allows one to use (relatively) low voltage components to handle high voltage outputs. Power quality and efficiency are also part of the MMC advantages, giving the possibility to use low switching frequencies while producing low harmonic distortion.

The analysis of the behaviour of the MMC has shown to be a challenge due to its numerous discontinuous control inputs and the high number of state space variables. This makes the obtention of explicit analytical relationships between the converter variables hard to find, making approximations such as considering infinite capacitances, an easy but low accuracy alternative. Chapter 2 presented a reduced order model that was shown to be a good alternative to obtain simplified analytical expression of the MMC and to understand its behaviour. This model conserves all the non-linearities of the original MMC and at the same time, it simplifies the analysis by considering only continuous control signals with a reduced number of state space and control variables. Situations where the accuracy of the model is compromised have been properly identified, showing that close to some specific frequencies, the error of the model increases. However, if one stays sufficiently far from these frequencies, then the reduced order model can be highly accurate even for a low number of modules. The accuracy of the model was also tested when capacitor voltages were out of balance, showing that it is not necessary to obtain perfect balance to get good model accuracy.

The reduced order model was also shown to be useful when designing detailed references for control applications as shown in chapter 3. The fact that the model can be treated as continuous, opened the possibility to obtain analytical expressions by simply solving a set of differential equations. Moreover, it has been shown that these references can be carefully selected to reduce module voltage ripple successfully. This is done by injecting harmonic components in the circulating current of the converter that are selected by means of numerical optimization. This numerical optimization uses the analytical expression obtained with the reduced order model which makes it faster than other methods using simulation approaches. To reduce even further the task of obtaining these optimal harmonic components, a linear approximation as a function of the load current parameters was presented. It showed very good accuracy for most of the cases, making it a good alternative when computational resources are limited. Injection of harmonic components in the load current was also considered. Although this approach could diminish power quality, the analysis can be taken as a proof of concept and can be considered as an alternative when the application allows it. Voltage ripple reduction can be potentially used to reduce capacitance requirements, alleviating monetary costs and reducing the size of

an implementation.

Chapter 4 showed that all the previous results can be applied when designing an MPC for MMCs. Here, conditions that have been successfully applied to exploit the properties of convexity in the optimization process associated with the MPC are provided. These conditions are developed for a general class of bilinear systems, opening the path for it to be used in other applications. The reduced complexity provided by the reduced order model, the design technique of detailed references for each of the voltages and currents of the MMC, and being able to guarantee that the complexity of the optimization associated with the MPC is merely the one of a convex problem, have shown to be successful in maintaining good tracking performance while allowing one to increase the prediction horizon of the controller.

Future work

In order to continue and complement the work presented in this thesis, the following points present some key ideas that can be used as starting points for new research projects.

Extension to 3-phase MMCs

Although the analysis presented in this work focused on a single phase MMC, it has been shown that the results of the reduced order model and reference design can be extended to a 3-phase converter (see appendix A). Since the guarantees for convexity are presented for a general bilinear system, their extension to 3-phase converters is also straightforward. However, a more detailed simulation and analytical study to corroborate the performance of the controller using the method proposed here, is still required. The evaluation of the impact of problems associated only with a 3-phase implementation, such as load imbalances, is also still pending.

Experimental verification

This work addressed the problem from a theoretical viewpoint, limiting its verification to a simulation environment. To verify more in detail the applicability of the methods presented here, an experimental set-up is still required.

Optimization of the control optimization method for hardware implementation

The convexity guarantees allow one to use well studied and less computationally intensive algorithms for the optimization associated with the MPC. In a real life application these algorithms have to be implemented in hardware with limited resources. A detailed analysis on how these convexity guarantees can help to reduce algorithm execution times and how they can be implemented successfully, can help significantly to evaluate the practical value of the method.

Exploiting the convexity properties for different purposes and applications

The analysis presented here also opens the possibility to exploit the properties derived from convexity on other power converters, or bilinear systems in other areas. This can be an advantage, not only for using better optimization algorithms, but for the application of other control schemes.

Distributed control

Particulary, the application of distributed control techniques can be significantly simplified due to convexity. Distributed control techniques, along with the modularity and flexibility of the MMC, can be used in order to obtain a significantly more robust system, which is particulary useful on industrial applications.

A. Extension to 3-phase MMC

The analysis presented here illustrates how the results in chapters 2 and 3 can be extended to a 3-phase converter. This is done by showing a simplified version of the procedures that were first applied to a single phase MMC, including the definition of a reduced order model, the implications of using continuous control signals and the design of optimal references injecting circulating current harmonics.

A.1. 3-phase Modular Multilevel Converter

MMC are a series connection of several independently controlled modules. Due to its high power capabilities 3-phase applications are very common. In fig. A.1, a 3-phase MMC with N modules per arm is shown.

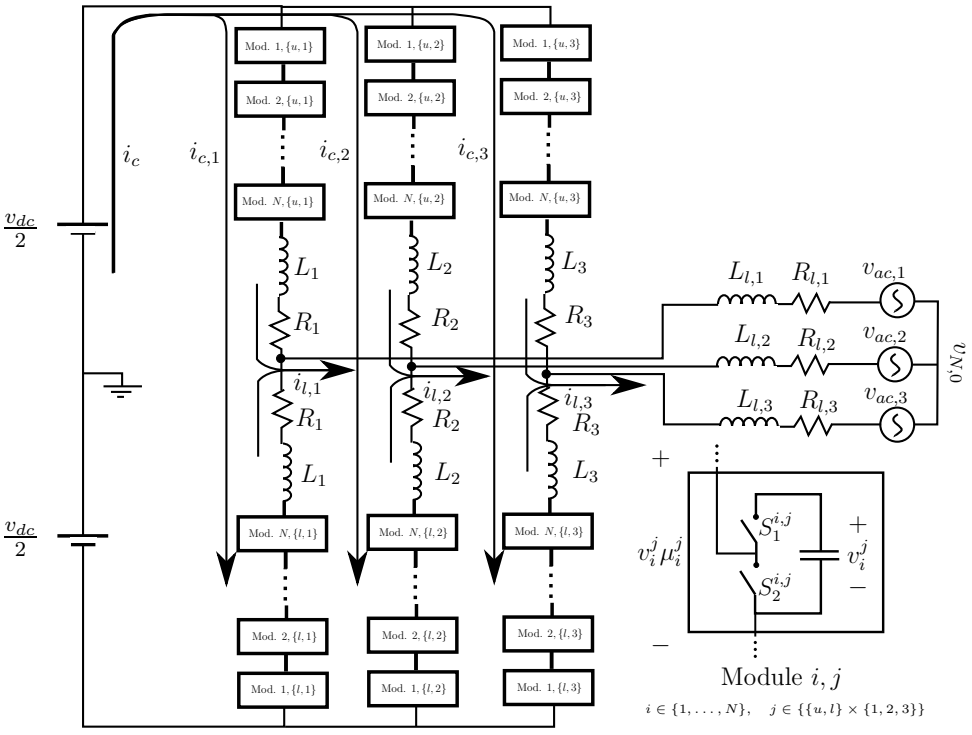

Figure A.1.: 3-phase MMC configuration with N modules per arm. μ_i^j is a binary switching function

For the sake of simplicity the following is assumed

$$R_1 = R_2 = R_3 = R, \tag{A.1}$$

and

$$L_1 = L_2 = L_3 = L. \tag{A.2}$$

The relation of the currents in the converter can be described as follows

$$i_c(t) = i_{c,1}(t) + i_{c,2}(t) + i_{c,3}(t), \tag{A.3}$$

and

$$i_{l,3}(t) = -i_{l,1}(t) - i_{l,2}(t). \tag{A.4}$$

Using circuit analysis, the following equations that describe the behavior of the circuit in Fig. A.1 can be obtained:

$$\frac{di_{c,1}(t)}{dt} = -\frac{Ri_{c,1}(t)}{L} - \frac{1}{2L}\sum_{n=1}^{N}\mu_n^{l,1}(t)v_n^{l,1}(t) - \frac{1}{2L}\sum_{n=1}^{N}\mu_n^{u,1}(t)v_n^{u,1}(t) + \frac{v_{dc}}{2L}, \tag{A.5}$$

$$\frac{di_{c,2}(t)}{dt} = -\frac{Ri_{c,2}(t)}{L} - \frac{1}{2L}\sum_{n=1}^{N}\mu_n^{l,2}(t)v_n^{l,2}(t) - \frac{1}{2L}\sum_{n=1}^{N}\mu_n^{u,2}(t)v_n^{u,2}(t) + \frac{v_{dc}}{2L}, \tag{A.6}$$

$$\frac{di_{c,3}(t)}{dt} = -\frac{Ri_{c,3}(t)}{L} - \frac{1}{2L}\sum_{n=1}^{N}\mu_n^{l,3}(t)v_n^{l,3}(t) - \frac{1}{2L}\sum_{n=1}^{N}\mu_n^{u,3}(t)v_n^{u,3}(t) + \frac{v_{dc}}{2L}, \tag{A.7}$$

$$\begin{aligned}\alpha\frac{di_{l,1}(t)}{dt} = &-\beta_{1,2}i_{l,1}(t) - \gamma_2 i_{l,2}(t) + (\zeta_2+\zeta_3)\sum_{n=1}^{N}\mu_n^{l,1}(t)v_n^{l,1}(t) - \\ &\zeta_3\sum_{n=1}^{N}\mu_n^{l,2}(t)v_n^{l,2}(t) - \zeta_2\sum_{n=1}^{N}\mu_n^{l,3}(t)v_n^{l,3}(t) - (\zeta_2+\zeta_3)\sum_{n=1}^{N}\mu_n^{u,1}(t)v_n^{u,1}(t) + \\ &\zeta_3\sum_{n=1}^{N}\mu_n^{u,2}(t)v_n^{u,2}(t) + \zeta_2\sum_{n=1}^{N}\mu_n^{u,3}(t)v_n^{u,3}(t) - 2(\zeta_2+\zeta_3)v_{ac,1}(t) + \\ &2\zeta_3 v_{ac,2}(t) + 2\zeta_2 v_{ac,3}(t),\end{aligned} \tag{A.8}$$

$$\begin{aligned}\alpha\frac{di_{l,2}(t)}{dt} = &-\gamma_1 i_{l,1}(t) - \beta_{2,1}i_{l,2}(t) - \zeta_3\sum_{n=1}^{N}\mu_n^{l,1}(t)v_n^{l,1}(t) + \\ &(\zeta_1+\zeta_3)\sum_{n=1}^{N}\mu_n^{l,2}(t)v_n^{l,2}(t) - \zeta_1\sum_{n=1}^{N}\mu_n^{l,3}(t)v_n^{l,3}(t) + \zeta_3\sum_{n=1}^{N}\mu_n^{u,1}(t)v_n^{u,1}(t) - \\ &(\zeta_1+\zeta_3)\sum_{n=1}^{N}\mu_n^{u,2}(t)v_n^{u,2}(t) + \zeta_1\sum_{n=1}^{N}\mu_n^{u,3}(t)v_n^{u,3}(t) + 2\zeta_3 v_{ac,1}(t) - \\ &2(\zeta_1+\zeta_3)v_{ac,2}(t) + 2\zeta_1 v_{ac,3}(t),\end{aligned} \tag{A.9}$$

where

$$\alpha = 3L^2 + 4LL_{l,1} + 4LL_{l,2} + 4LL_{l,3} + 4L_{l,1}L_{l,2} + 4L_{l,1}L_{l,3} + 4L_{l,2}L_{l,3}, \tag{A.10}$$

$$\beta_{\lambda,\delta} = 3LR + 4LR_{l,\lambda} + 2LR_{l,3} + 4L_{l,\delta}R + 4L_{l,\delta}R_{l,\lambda} + 4L_{l,\delta}R_{l,3} + 2L_{l,3}R + 4L_{l,3}R_{l,\lambda}, \tag{A.11}$$

$$\gamma_\delta = -2LR_{l,\delta} + 2LR_{l,3} + 2L_{l,\delta}R + 4L_{l,\delta}R_{l,3} - 2L_{l,3}R - 4L_{l,3}R_{l,\delta}, \tag{A.12}$$

$$\zeta_\delta = L + 2L_{l,\delta}. \tag{A.13}$$

The previous values are true for $\lambda, \delta \in \{1, 2, 3\}$. λ and δ are used to distinguish the parameters of the three branches of the converter.

The dynamics of the capacitor voltages are given by the following expressions

$$\begin{aligned} \frac{dv_i^{u,\delta}(t)}{dt} &= \frac{\mu_i^{u,\delta}(t)}{C}\left(i_{c,\delta}(t) + \frac{i_{l,\delta}(t)}{2}\right), \\ \frac{dv_i^{l,\delta}(t)}{dt} &= \frac{\mu_i^{l,\delta}(t)}{C}\left(i_{c,\delta}(t) - \frac{i_{l,\delta}(t)}{2}\right), \end{aligned} \quad \forall\delta \in \{1,2,3\} \wedge \forall i \in \{1,\ldots,N\} \tag{A.14}$$

Based on the previous equations, the dynamics of the 3-phase MMC can be described in state space form as follows

$$\frac{d\mathbf{x}(t)}{dt} = \mathcal{A}(\vec{\mu}_i^j(t))\mathbf{x}(t) + \mathcal{B}\mathbf{u}(t), \tag{A.15}$$

where the state vector $\mathbf{x}$, the input $\mathbf{u}$ and the matrix $\mathcal{B}$ are defined as

$$\begin{aligned} \mathbf{x}(t) = \big[&i_{c,1}(t) \quad i_{c,2}(t) \quad i_{c,3}(t) \quad i_{l,1}(t) \quad i_{l,2}(t) \\ &\vec{v}^{u,1}(t) \quad \vec{v}^{l,1}(t) \quad \vec{v}^{u,2}(t) \quad \vec{v}^{l,2}(t) \quad \vec{v}^{u,3}(t) \quad \vec{v}^{l,3}(t)\big]^T, \end{aligned} \tag{A.16}$$

$$\mathbf{u}(t) = \begin{bmatrix} v_{ac,1}(t) & v_{ac,2}(t) & v_{ac,3}(t) & v_{dc} \end{bmatrix}^T, \tag{A.17}$$

$$\mathcal{B} = \begin{bmatrix} 0 & 0 & 0 & \frac{1}{2L} \\ 0 & 0 & 0 & \frac{1}{2L} \\ 0 & 0 & 0 & \frac{1}{2L} \\ -2\frac{\zeta_2+\zeta_3}{\alpha} & 2\frac{\zeta_3}{\alpha} & 2\frac{\zeta_2}{\alpha} & 0 \\ 2\frac{\zeta_3}{\alpha} & -2\frac{\zeta_1+\zeta_3}{\alpha} & 2\frac{\zeta_1}{\alpha} & 0 \\ 0 & 0 & 0 & 0 \\ \vdots & \vdots & \vdots & \vdots \\ 0 & 0 & 0 & 0 \end{bmatrix}, \tag{A.18}$$

where

$$\vec{v}^j(t) = \begin{bmatrix} v_1^j(t) & \ldots & v_N^j(t) \end{bmatrix}. \tag{A.19}$$

The matrix $\mathcal{A}(\vec{\mu}_i^j)(t)$ is given by:

$$\mathcal{A}(\vec{\mu}_i^j(t)) = \begin{bmatrix} \mathcal{A}_1 & \begin{bmatrix}\mathcal{A}_2(\vec{\mu}_i^j(t))\\ \mathcal{A}_3(\vec{\mu}_i^j(t))\end{bmatrix} \\ \mathcal{A}_4(\vec{\mu}_i^j(t)) & 0 \end{bmatrix}, \tag{A.20}$$

where

$$\mathcal{A}_1 = \begin{bmatrix} -\frac{R}{L} & 0 & 0 & 0 & 0 \\ 0 & -\frac{R}{L} & 0 & 0 & 0 \\ 0 & 0 & -\frac{R}{L} & 0 & 0 \\ 0 & 0 & 0 & -\frac{\beta_{1,2}}{\alpha} & -\frac{\gamma_2}{\alpha} \\ 0 & 0 & 0 & -\frac{\beta_{2,1}}{\alpha} & -\frac{\gamma_1}{\alpha} \end{bmatrix}, \tag{A.21}$$

$$\mathcal{A}_2(\vec{\mu}_i^j(t)) = \begin{bmatrix} -\frac{1}{2L}\vec{\mathbf{M}}_1^+ & 0 & 0 \\ 0 & -\frac{1}{2L}\vec{\mathbf{M}}_2^+ & 0 \\ 0 & 0 & -\frac{1}{2L}\vec{\mathbf{M}}_3^+ \end{bmatrix}, \tag{A.22}$$

$$\mathcal{A}_3(\vec{\mu}_i^j(t)) = \frac{1}{\alpha}\begin{bmatrix} -(\zeta_2+\zeta_3)\vec{\mathbf{M}}_1^- & \zeta_3\vec{\mathbf{M}}_2^- & \zeta_2\vec{\mathbf{M}}_3^- \\ \zeta_3\vec{\mathbf{M}}_1^- & -(\zeta_1+\zeta_3)\vec{\mathbf{M}}_2^- & \zeta_1\vec{\mathbf{M}}_3^- \end{bmatrix}, \tag{A.23}$$

$$\mathcal{A}_4(\vec{\mu}_i^j(t)) = \begin{bmatrix} \frac{1}{C}\vec{\mathbf{M}}_1^+ & 0 & 0 \\ 0 & \frac{1}{C}\vec{\mathbf{M}}_2^+ & 0 \\ 0 & 0 & \frac{1}{C}\vec{\mathbf{M}}_3^+ \\ \frac{1}{2C}\vec{\mathbf{M}}_1^- & 0 & -\frac{1}{2C}\vec{\mathbf{M}}_3^- \\ 0 & \frac{1}{2C}\vec{\mathbf{M}}_2^- & -\frac{1}{2C}\vec{\mathbf{M}}_3^- \end{bmatrix}^T, \tag{A.24}$$

and

$$\vec{\mu}^j(t) = \begin{bmatrix}\mu_1^j(t) & \dots & \mu_N^j(t)\end{bmatrix}, \quad \mu_i^j(t) \in \{0,1\}, \forall i \in \{1,\dots,N\}, \tag{A.25}$$

$$\vec{\mathbf{M}}_\delta^\pm = \begin{bmatrix}\vec{\mu}^{u,\delta}(t) & \pm\vec{\mu}^{l,\delta}(t)\end{bmatrix}, \forall \delta \in \{1,2,3\}. \tag{A.26}$$

A.2. Reduced Order Model

In order to simplify the modeling of the MMC, and as in chapter 2, let us assume balanced voltages on each arm of the converter as follows

$$v_n^j(t) = v_m^j(t) = v^j(t), \quad \forall n,m \in \{1,\dots,N\}. \tag{A.27}$$

This allows one to simplify the equations that describe the behavior of the converter using the following procedure: let μ^j be a new control variable defined as follows

$$\mu^j(t) = \sum_{n=1}^{N} \mu_n^j(t), \quad \mu^j(t) \in \{0,\dots,N\}. \tag{A.28}$$

Using the new variable, the derivative of $i_{c,1}$ in (A.5) can be re-written as

$$\frac{di_{c,1}(t)}{dt} = -\frac{Ri_{c,1}(t)}{L} - \frac{v^{l,1}(t)\mu^{l,1}(t)}{2L} - \frac{v^{u,1}(t)\mu^{u,1}(t)}{2L} + \frac{v_{dc}}{2L}. \tag{A.29}$$

The expressions in eqs. (A.6) to (A.9) can also be re-written analogously using eqs. (A.27) and (A.28). Following the procedure for eq. (A.8) leads to

$$\begin{aligned}\alpha\frac{di_{l,1}(t)}{dt} = &-\beta_{1,2}i_{l,1}(t) - \gamma_2 i_{l,2}(t) + (\zeta_2+\zeta_3)\mu^{l,1}(t)v^{l,1}(t) - \zeta_3\mu^{l,2}(t)v^{l,2}(t) - \\ &\zeta_2\mu^{l,3}(t)v^{l,3}(t) - (\zeta_2+\zeta_3)\mu^{u,1}(t)v^{u,1}(t) + \zeta_3\mu^{u,2}(t)v^{u,2}(t) + \zeta_2\mu^{u,3}(t)v^{u,3}(t) - \\ &2(\zeta_2+\zeta_3)v_{ac,1}(t) + 2\zeta_3 v_{ac,2}(t) + 2\zeta_2 v_{ac,3}(t).\end{aligned} \tag{A.30}$$

In order to re-write eq. (A.14), it is necessary to add up all the voltages in one arm. The procedure is shown only for the equations of the upper arm. For the lower arm the same steps can be followed. Adding the derivatives of all the voltages in the same arm the following is obtained

$$\sum_{i=1}^{N}\frac{dv_i^{u,\delta}(t)}{dt} = \sum_{i=1}^{N}\frac{\mu_i^{u,\delta}(t)}{C}\left(i_{c,\delta}(t) + \frac{i_{l,\delta}(t)}{2}\right),\ \forall\delta\in\{1,2,3\}. \tag{A.31}$$

Since the current going through the modules is the same in all of them, eqs. (A.27) and (A.28) can be used to re-write the latter expression as follows

$$\frac{dv^{u,\delta}(t)}{dt} = \frac{\mu^{u,\delta}(t)}{NC}\left(i_{c,\delta}(t) + \frac{i_{l,\delta}(t)}{2}\right),\ \forall\delta\in\{1,2,3\}. \tag{A.32}$$

With all the equations that define the dynamics of the converter re-written, a new state space model with a reduced number of state space variables and control signals μ, can be defined as follows

$$\frac{d\mathbf{x}(t)}{dt} = A(\mu^j(t))\mathbf{x}(t) + B\mathbf{u}(t), \tag{A.33}$$

where the state space vector is defined as

$$\begin{aligned}\mathbf{x}(t) = [&i_{c,1}(t) \quad i_{c,2}(t) \quad i_{c,3}(t) \quad i_{l,1}(t) \quad i_{l,2}(t) \\ &v^{u,1}(t) \quad v^{l,1}(t) \quad v^{u,2}(t) \quad v^{l,2}(t) \quad v^{u,3}(t) \quad v^{l,3}(t)\big]^T,\end{aligned} \tag{A.34}$$

and the state space matrices are defined in eqs. (A.35) and (A.36).

Note that the number of control variables is reduced from $6N$ binary signals to 6 continuous signals in the interval $[0, N]$. Moreover, the number of state space variables is reduced from $6N + 5$ to 11. The number of state space variables and control signals in the reduced order model is independent of the number of modules N.

$$A(\mu^j(t)) = \begin{bmatrix}
-\frac{R}{L} & 0 & 0 & 0 & 0 & -\frac{\mu^{u,1}(t)}{2L} & -\frac{\mu^{u,1}(t)}{2L} & 0 & 0 & 0 & 0 \\
0 & -\frac{R}{L} & 0 & 0 & 0 & 0 & 0 & -\frac{\mu^{u,2}(t)}{2L} & -\frac{\mu^{u,2}(t)}{2L} & 0 & 0 \\
0 & 0 & -\frac{R}{L} & 0 & 0 & 0 & 0 & 0 & 0 & -\frac{\mu^{u,3}(t)}{2L} & -\frac{\mu^{u,3}(t)}{2L} \\
0 & 0 & 0 & -\frac{\beta_{1,2}}{\alpha} & -\frac{\gamma_2}{\alpha} & -(\zeta_2+\zeta_3)\frac{\mu^{u,1}(t)}{\alpha} & (\zeta_2+\zeta_3)\frac{\mu^{l,1}(t)}{\alpha} & \zeta_3\frac{\mu^{u,2}(t)}{\alpha} & -\zeta_3\frac{\mu^{l,2}(t)}{\alpha} & \zeta_2\frac{\mu^{u,3}(t)}{\alpha} & -\zeta_2\frac{\mu^{l,3}(t)}{\alpha} \\
0 & 0 & 0 & -\frac{\beta_{2,1}}{\alpha} & -\frac{\gamma_1}{\alpha} & \zeta_3\frac{\mu^{u,1}(t)}{\alpha} & -\zeta_3\frac{\mu^{l,1}(t)}{\alpha} & -(\zeta_2+\zeta_3)\frac{\mu^{u,2}(t)}{\alpha} & (\zeta_2+\zeta_3)\frac{\mu^{l,2}(t)}{\alpha} & \zeta_1\frac{\mu^{u,3}(t)}{\alpha} & -\zeta_1\frac{\mu^{l,3}(t)}{\alpha} \\
\frac{\mu^{u,1}(t)}{NC} & 0 & 0 & \frac{\mu^{u,1}(t)}{2NC} & 0 & 0 & 0 & 0 & 0 & 0 & 0 \\
\frac{\mu^{l,1}(t)}{NC} & 0 & 0 & -\frac{\mu^{l,1}(t)}{2NC} & 0 & 0 & 0 & 0 & 0 & 0 & 0 \\
0 & \frac{\mu^{u,2}(t)}{NC} & 0 & 0 & \frac{\mu^{u,2}(t)}{2NC} & 0 & 0 & 0 & 0 & 0 & 0 \\
0 & \frac{\mu^{l,2}(t)}{NC} & 0 & 0 & -\frac{\mu^{l,2}(t)}{2NC} & 0 & 0 & 0 & 0 & 0 & 0 \\
0 & 0 & \frac{\mu^{u,3}(t)}{NC} & -\frac{\mu^{u,3}(t)}{2NC} & -\frac{\mu^{u,3}(t)}{2NC} & 0 & 0 & 0 & 0 & 0 & 0 \\
0 & 0 & \frac{\mu^{l,3}(t)}{NC} & \frac{\mu^{l,3}(t)}{2NC} & \frac{\mu^{l,3}(t)}{2NC} & 0 & 0 & 0 & 0 & 0 & 0
\end{bmatrix}, \tag{A.35}$$

$$B = \begin{bmatrix} 0 & 0 & 0 & \frac{1}{2L} \\ 0 & 0 & 0 & \frac{1}{2L} \\ 0 & 0 & 0 & \frac{1}{2L} \\ -2\frac{\zeta_2+\zeta_3}{\alpha} & 2\frac{\zeta_3}{\alpha} & 2\frac{\zeta_2}{\alpha} & 0 \\ 2\frac{\zeta_3}{\alpha} & -2\frac{\zeta_1+\zeta_3}{\alpha} & 2\frac{\zeta_1}{\alpha} & 0 \\ 0 & 0 & 0 & 0 \\ 0 & 0 & 0 & 0 \\ 0 & 0 & 0 & 0 \\ 0 & 0 & 0 & 0 \\ 0 & 0 & 0 & 0 \\ 0 & 0 & 0 & 0 \end{bmatrix}. \tag{A.36}$$

Implications of using continuous control signals

In order to obtain a continuous model of the MMC, the quantization effect produced by the switching of the modules is neglected. To evaluate the effect of this approximation, the response of the models with and without the quantization are compared. It is worth mentioning that the response of the reduced order model when the quantization is taken into account is identical to the response of the full order model as long as the voltages in the modules of the converter are balanced properly. In order to evaluate the effect of the quantization, the following continuous control signals are used

$$\begin{aligned} \mu^{u,\delta}(t) &= N\frac{1+\cos(\omega t + \frac{2\pi}{3}(1-\delta))}{2}, \\ \mu^{l,\delta}(t) &= N\frac{1-\cos(\omega t + \frac{2\pi}{3}(1-\delta))}{2}, \\ &\qquad \forall \delta \in \{1,2,3\}. \end{aligned} \tag{A.37}$$

These control signals produce a sinusoidal output current on each phase.

The model is tested with different numbers of modules N. The quantized inputs are generated by considering a nearest integer approximation of the expressions in eq. (A.37). The simulated steady state waveforms of the model without the quantization are compared with the waveforms of the model with the quantization using the following expression

$$Error = \frac{\|y_Q - y\|}{\|y_Q\|}, \tag{A.38}$$

where, y is the response of the model without the quantization, y_Q the response of the model with the quantization, and $\| * \|$ represents the Euclidian norm of the argument.

In fig. A.2 the results of the validation of the reduced order model are shown for different frequencies. It is possible to see that for some particular frequencies the error increases significantly. The frequencies where this happens are dependent on the number of modules used, these frequencies are higher the higher the number of modules. In addition, the higher the number of modules the lower the magnitude of the error peaks.

The frequencies where the error between the two responses is higher, are directly related

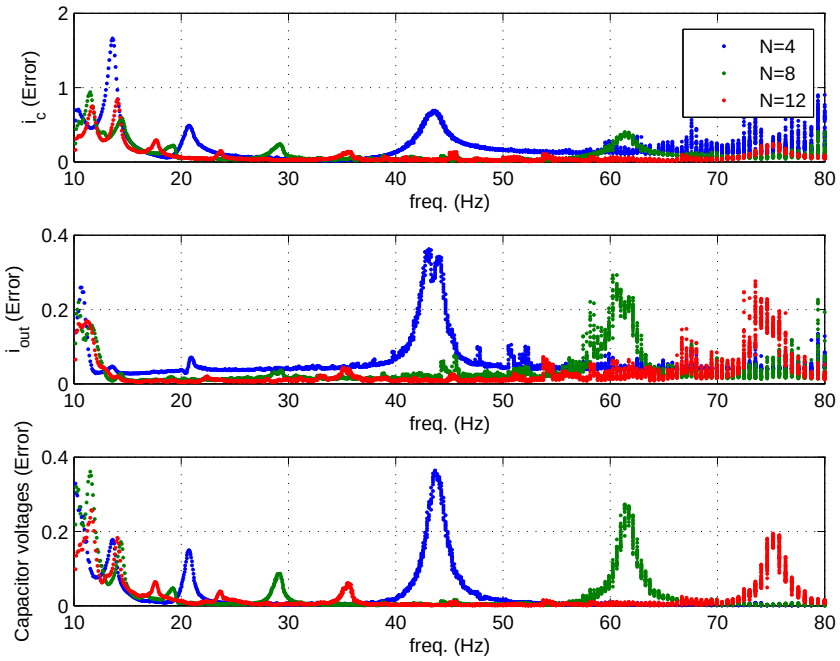

Figure A.2.: Validation of the reduced order model for different number of modules per arm

with the resonant frequencies of the converter. Figures A.3 and A.4 show the amplitude of the response of the models with and without the quantization. It can be seen that the amplitude of the circulating current is significantly affected by the resonances in the circuit. Around the resonant frequencies the error in fig. A.2 appears in all the variables (load current and module voltages) almost equally.

In order to estimate these frequencies easily, one can consider an approach based on linearization. However, as seen in chapter 2, the error of this approach can be significantly higher. Therefore, here we limit the analysis to a numerical comparison between the resonant frequencies obtained with and without the quantization using simulation tools.

Table A.1 shows a numerical comparison of one of the resonant frequencies with and without considering the quantization. This particular frequency is analyzed since it can match the operating frequency of the converter, typically 50Hz or 60Hz. It can be seen that including the quantization moves the resonant frequencies to a lower value. Moreover, this effect is more noticeable the lower the number of modules used.

Table A.1.: Numerical comparison of resonant frequencies (Hz)

N	w. Quant.(fig. A.3)	w/o. Quant. (fig. A.4)
4	42.29	44.35
8	61.4	62.1
12	75.19	75.76

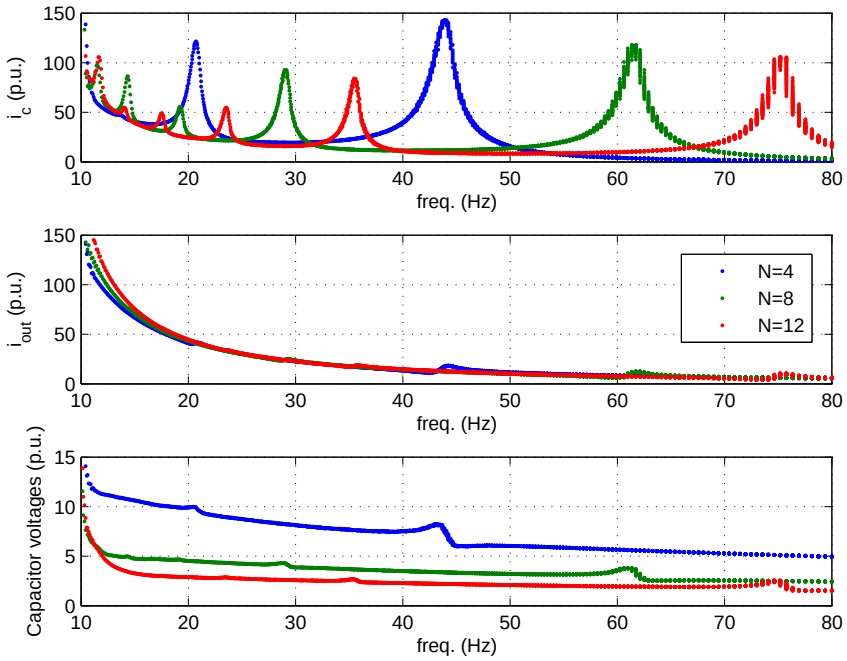

Figure A.3.: Amplitude of the MMC variables for different frequency values with quantization

A.3. Reference design with voltage ripple reduction

In order to be able to manipulate and analyze the behaviour of the converter, the reduced order model can be used to obtain analytical expressions that further describe its behavior. Here we aim to find expressions that relate the converter currents with the module voltages in order to be able to freely manipulate module voltage ripple.

Let us start by defining the circulating currents as follows

$$\begin{aligned} i_{c,\delta}(t) =& i_{0,\delta} + \hat{i}_{2,\delta}\cos(2\omega t + \phi_{2,\delta}) + \hat{i}_{4,\delta}\cos(4\omega t + \phi_{4,\delta}) + \\ & \hat{i}_{6,\delta}\cos(6\omega t + \phi_{6,\delta}),\ \forall\delta \in \{1,2,3\}, \end{aligned} \tag{A.39}$$

where the value $i_{0,\delta}$ represents the DC component in charge of transferring the energy from the DC voltage source to the modules, and finally to the load. $\hat{i}_{2,\delta}$, $\hat{i}_{4,\delta}$ and $\hat{i}_{6,\delta}$ represent the amplitudes of each of the harmonic components, and $\phi_{2,\delta}$, $\phi_{4,\delta}$ and $\phi_{6,\delta}$ their respective phase angles.

The load current is defined as follows

$$i_{l,\delta}(t) = \hat{i}_{l,\delta}\cos\left(\omega t + \phi_{l,\delta} + \frac{2\pi}{3}(1-\delta)\right),\ \forall\delta \in \{1,2,3\}, \tag{A.40}$$

with

$$i_{l,3}(t) = -i_{l,2}(t) - i_{l,1}(t). \tag{A.41}$$

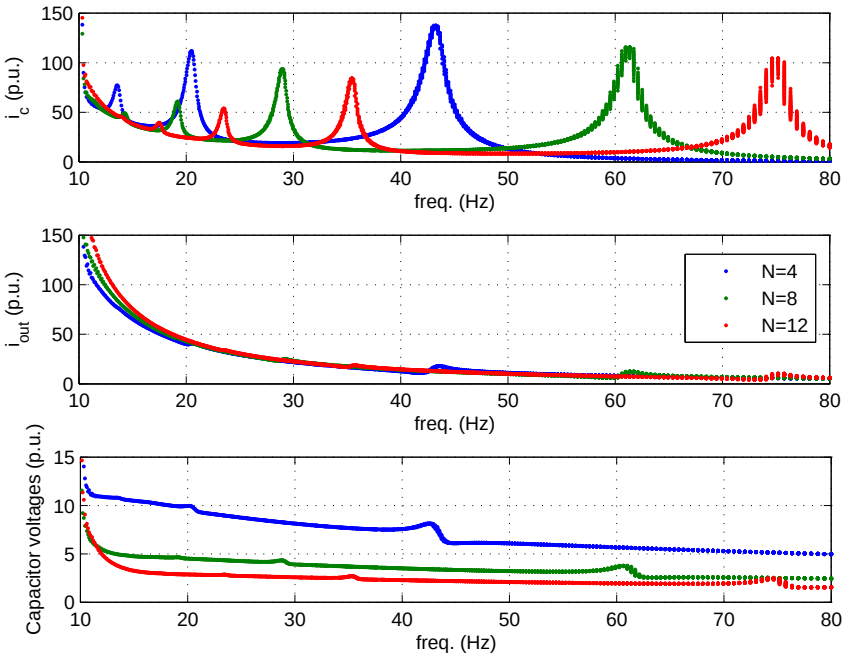

Figure A.4.: Amplitude of the MMC variables for different frequency values without quantization

Using the expression for the circulating current in eq. (A.39) and the expression for the load current in eq. (A.40), the values of the control functions μ^j as a function of the voltage of the modules can be obtained using eq. (A.33).

An additional equation is required since there are only five equations (derivatives of the currents) and six control functions μ^j. The new equation relates the voltage of the central node of the load with the currents in the circuit as follows

$$\begin{aligned} v_{N,0}(t) =& \frac{v_{dc}}{2} - \mu^{u,1}(t)v^{u,1}(t) - R\left(i_{c,1}(t) + \frac{i_{l,1}(t)}{2}\right) - L\frac{di_{c,1}(t)}{dt} - \\ & R_{l,1}i_{l,1}(t) - \frac{\zeta_1}{2}\frac{di_{l,1}(t)}{dt} - v_{ac,1}(t). \end{aligned} \tag{A.42}$$

Solving for μ^j using eqs. (A.33), (A.39), (A.40) and (A.42) yields

$$\begin{aligned} \mu^{u,1}(t) = -\frac{1}{2v^{u,1}(t)}\Bigg(&\zeta_1\frac{di_{l,1}(t)}{dt} + 2L\frac{di_{c,1}(t)}{dt} + R(i_{l,1}(t) + 2i_{c,1}(t)) + \\ & 2R_{l,1}i_{l,1}(t) + 2v_{ac,1}(t) - v_{dc} + 2v_{N,0}(t)\Bigg), \end{aligned} \tag{A.43}$$

$$\mu^{l,1}(t) = \frac{1}{2v^{l,1}(t)}\left(\zeta_1\frac{di_{l,1}(t)}{dt} - 2L\frac{di_{c,1}(t)}{dt} + R(i_{l,1}(t) - 2i_{c,1}(t)) + 2R_{l,1}i_{l,1}(t) + 2v_{ac,1}(t) + v_{dc} + 2v_{N,0}(t)\right), \tag{A.44}$$

$$\mu^{u,2}(t) = -\frac{1}{2v^{u,2}(t)}\left(\zeta_2\frac{di_{l,2}(t)}{dt} + 2L\frac{di_{c,2}(t)}{dt} + R(i_{l,2}(t) + 2i_{c,2}(t)) + 2R_{l,2}i_{l,2}(t) + 2v_{ac,2}(t) - v_{dc} + 2v_{N,0}(t)\right), \tag{A.45}$$

$$\mu^{l,2}(t) = \frac{1}{2v^{l,2}(t)}\left(\zeta_2\frac{di_{l,2}(t)}{dt} - 2L\frac{di_{c,2}(t)}{dt} + R(i_{l,2}(t) - 2i_{c,2}(t)) + 2R_{l,2}i_{l,2}(t) + 2v_{ac,2}(t) + v_{dc} + 2v_{N,0}(t)\right), \tag{A.46}$$

$$\mu^{u,3}(t) = \frac{1}{2v^{u,3}(t)}\left(\zeta_3\left(\frac{di_{l,1}(t)}{dt} + \frac{di_{l,2}(t)}{dt}\right) - 2L\frac{di_{c,3}(t)}{dt} + R(i_{l,1}(t) + i_{l,2}(t) - 2i_{c,3}(t)) + 2R_{l,3}\left(i_{l,1}(t) + i_{l,2}(t)\right) - 2v_{ac,3}(t) + v_{dc} - 2v_{N,0}(t)\right), \tag{A.47}$$

$$\mu^{l,3}(t) = -\frac{1}{2v^{u,3}(t)}\left(\zeta_3\left(\frac{di_{l,1}(t)}{dt} + \frac{di_{l,2}(t)}{dt}\right) + 2L\frac{di_{c,3}(t)}{dt} + R(i_{l,1}(t) + i_{l,2}(t) + 2i_{c,3}(t)) + 2R_{l,3}\left(i_{l,1}(t) + i_{l,2}(t)\right) - 2v_{ac,3}(t) - v_{dc} - 2v_{N,0}(t)\right). \tag{A.48}$$

Note that these solutions are continuous.

In order to obtain the value of $i_{0,\delta}$, it is necessary to analyze the energy transferred and received by each of the arms of the converter. The derivative of the energy stored on each arm can be computed as

$$\frac{dE^{u,\delta}(t)}{dt} = \frac{1}{CN}\left(i_{c,\delta}(t) + \frac{i_{l,\delta}(t)}{2}\right)\mu^{u,\delta}(t)v^{u,\delta}(t),\ \forall\delta \in \{1,2,3\}, \tag{A.49}$$

$$\frac{dE^{l,\delta}(t)}{dt} = \frac{1}{CN}\left(i_{c,\delta}(t) - \frac{i_{l,\delta}(t)}{2}\right)\mu^{l,\delta}(t)v^{l,\delta}(t),\ \forall\delta \in \{1,2,3\}. \tag{A.50}$$

In steady state, the average of the derivative of the total energy in each phase must be equal to zero. Using eqs. (A.39), (A.40) and (A.43) to (A.50), this value can be computed for all the phases of the converter as follows

$$\frac{\omega}{2\pi}\int_t^{t+\frac{2\pi}{\omega}}\left(\frac{dE^{u,\delta}(\tau)}{d\tau} + \frac{dE^{l,\delta}(\tau)}{d\tau}\right)d\tau = v_{dc}i_{0,\delta} - 2Ri_{0,\delta} - R\hat{i}^2_{2,\delta} - R\hat{i}^2_{4,\delta} - R\hat{i}^2_{6,\delta} - \frac{1}{4}R\hat{i}^2_{l,\delta} - \frac{1}{2}R_{l,\delta}\hat{i}^2_{l,\delta} = 0,\ \forall\delta \in \{1,2,3\}. \tag{A.51}$$

Solving for $i_{0,\delta}$ yields

$$i_{0,\delta} = \frac{v_{dc} - \sqrt{v_{dc}^2 - 8R\left(\frac{1}{2}R_{l,\delta}\hat{i}_{l,\delta}^2 + R\left(\hat{i}_{2,\delta}^2 + \hat{i}_{4,\delta}^2 + \hat{i}_{6,\delta}^2 + \frac{1}{4}\hat{i}_{l,\delta}^2\right)\right)}}{4R}. \tag{A.52}$$

Note that the value $i_{0,\delta}$ in each phase only depends on the circulating current components and the load current flowing through the same phase.

With the continuous analytical expressions obtained with the reduced order model, it is possible to analyze the MMC in more detail. A common problem that can be addressed is the minimization of the voltage ripple in the modules of the converter. In order to be able to reduce this variable optimally, it is necessary to obtain an explicit analytical expression of the voltage in terms of the rest of the variables.

The time domain solution of the voltage of the modules can be found by solving the differential equations in eq. (A.33). The differential equation for the voltage of the modules of the upper arms can be written as follows

$$\frac{dv^{u,\delta}(t)}{dt} = \frac{1}{CN}\left(i_{c,\delta}(t) + \frac{i_{l,\delta}(t)}{2}\right)\mu^{u,\delta}(t), \tag{A.53}$$

or multiplying $v^{u,\delta}(t)$ on both sides

$$v^{u,\delta}(t)\frac{dv^{u,\delta}(t)}{dt} = \frac{1}{CN}\left(i_{c,\delta}(t) + \frac{i_{l,\delta}(t)}{2}\right)\mu^{u,\delta}(t)v^{u,\delta}(t). \tag{A.54}$$

Note that, according to eqs. (A.43) to (A.45), the product $\mu^{u,\delta}(t)v^{u,\delta}(t)$ is independent of $v^{u,\delta}(t)$. Therefore, $v^{u,\delta}(t)$ can be computed as follows

$$\int v^{u,\delta}(t)\frac{dv^{u,\delta}(t)}{dt}dt = \int \frac{1}{CN}\left(i_{c,\delta}(t) + \frac{i_{l,\delta}(t)}{2}\right)\mu^{u,\delta}(t)v^{u,\delta}(t)dt, \tag{A.55a}$$

$$\frac{1}{2}(v^{u,\delta}(t))^2 = \int \frac{1}{CN}\left(i_{c,\delta}(t) + \frac{i_{l,\delta}(t)}{2}\right)\mu^{u,\delta}(t)v^{u,\delta}(t)dt + 2(\bar{v}^{\delta})^2, \tag{A.55b}$$

$$v^{u,\delta}(t) = \sqrt{\int \frac{2}{CN}\left(i_{c,\delta}(t) + \frac{i_{l,\delta}(t)}{2}\right)\mu^{u,\delta}(t)v^{u,\delta}(t)dt + (\bar{v}^{\delta})^2}, \tag{A.55c}$$

where

$$\bar{v}^{\delta} = \frac{v_{dc} - 2Ri_{0,\delta}}{N}. \tag{A.56}$$

An analogous procedure can be followed to find $v^{l,\delta}$. Note that the voltage in the modules $v^{u,\delta}$ and $v^{l,\delta}$ depends on the circulating current in eq. (A.39). Therefore, amplitudes of the different harmonics $\hat{i}_{2,\delta}$, $\hat{i}_{4,\delta}$ and $\hat{i}_{6,\delta}$ and their respective phase angles can be used to reduce the ripple of these voltages.

Table A.2 shows the numerical values of the parameters of the converter. Using these numerical values, the parameters of the circulating current in eq. (A.39) can be obtained. The expression in eq. (A.55c) is used for numerical optimization. The resulting values of amplitude and phase are shown also in table A.2.

Table A.2.: Parameter values of the 3-phase MMC (p.u.) at $\omega = 2\pi 50$ $\forall \delta \in \{1, 2, 3\}$

Variable	Value	Variable	Value	Variable	Value (rad.)
v_{dc}	2.19	$\hat{i}_{2,1}$	0.54	$\phi_{2,1}$	4.69
N	8 mod.	$\hat{i}_{4,1}$	0.17	$\phi_{4,1}$	1.51
ω	$2\pi 50$ rad.	$\hat{i}_{6,1}$	-0.06	$\phi_{6,1}$	0.98
R	0.004	$\hat{i}_{2,2}$	0.54	$\phi_{2,2}$	2.59
ωL	0.075	$\hat{i}_{4,2}$	0.17	$\phi_{4,2}$	3.6
$1/\omega C$	0.089	$\hat{i}_{6,2}$	-0.06	$\phi_{6,2}$	0.99
$\omega L_{l,\delta}$	0.15	$\hat{i}_{2,3}$	0.54	$\phi_{2,3}$	0.5
$R_{l,\delta}$	0.01	$\hat{i}_{4,3}$	0.17	$\phi_{4,3}$	-0.59
$\hat{i}_{l,\delta}$	1	$\hat{i}_{6,3}$	-0.05	$\phi_{6,3}$	0.87

This analysis yields the conclusion that including harmonics in the circulating current of order 6th or higher, produces no significant improvement in the reduction of the voltage ripple.

A.4. Conclusions

An extension of the reduced order model for 3-phase MMCs was presented and the implications of using continuous control signals were analyzed. With this model, the dimension of the state system can be reduced to 11 and the control signals to 6, independently of the number of modules used in the converter. As in the case of the single phase MMC, this model allows one to obtain analytical expressions that can be used to optimize parameters of the converter, such as the voltage ripple in the capacitors, and to obtain detailed references for control purposes. The reduced order model also gives the freedom of neglecting the quantization produced by the switching eliminating the discontinuities in the system. The implications of this were evaluated showing that, for some frequencies, the error produced by neglecting the quantization is significantly higher.

The simplified analysis presented in this section can be taken as a proof of concept of the capabilities of the method presented in chapters 2 and 3 for its applications to 3-phase MMCs. A more detailed analysis may be required, opening the door for future work.

B. Some matrix properties

In this appendix several useful matrix properties are compiled. For more information, see [Ber05]

Fact B.1. For $x \in \mathbb{R}^n$ and $A \in \mathbb{R}^{n\times n}$ the following inequality holds

$$\|Ax\| \leq \|A\|\|x\|$$

where $\|\cdot\|$ represents the Euclidean norm for vectors and the maximum singular value for matrices.

Fact B.2. Let $B \in \mathbb{R}^{n\times n}$, with B symmetric. Then B is positive definite (semidefinite) if and only if every leading principal sub-matrix is positive definite (semidefinite).[1]

Fact B.3. For $x \in \mathbb{R}^n$ and $A \in \mathbb{R}^{n\times n}$, with A symmetric, the following inequality holds

$$\|x\|^2\Lambda_{\min}(A) \leqslant x^TAx \leqslant \|x\|^2\Lambda_{\max}(A)$$

where $\Lambda_{\min}(\bullet)$ and $\Lambda_{\max}(\bullet)$ represent the minimum and maximum eigenvalue of the argument respectively, and $\|x\|^2 = x^Tx$.

Fact B.4. Let $A \in \mathbb{R}^{n\times n}$ be symmetric and $\beta, \alpha \in \mathbb{R}$. Then the following holds

$$I\alpha \prec A \prec I\beta$$

if and only if $\Lambda_{\max}(A) < \beta$ and $\Lambda_{\min}(A) > \alpha$

Fact B.5. Let $A \in \mathbb{R}^{n\times n}$ be symmetric. Then the following holds

$$\max(|\Lambda_{\min}(A)|, |\Lambda_{\max}(A)|) = \|A\|$$

where $\|A\|$ represents the norm of A defined as its maximum singular value.

Fact B.6. Let $A, B \in \mathbb{R}^{n\times n}$ be symmetric matrices with scalar entries $a_{i,j}, b_{i,j} \in \mathbb{R}$, $\forall i, j$ respectively. If $|a_{i,j}| \leq b_{i,j}$, $\forall i, j$, then

$$\|A\| \leq \|B\|$$

Fact B.7. Let us define matrix $\mathcal{A}$ as follows:

$$A \triangleq \begin{bmatrix} A_{1,1} & A_{1,2} \\ A_{1,2}^T & A_{2,2} \end{bmatrix}$$

[1] The leading principal sub-matrices are constructed by eliminating the last i rows and columns of B with $0 \leqslant i \leqslant n-1$.

where $A \in \mathbb{R}^{(n+m)\times(n+m)}$, $A_{1,1} \in \mathbb{R}^{n\times n}$, $A_{1,2} \in \mathbb{R}^{n\times m}$ and $A_{2,2} \in \mathbb{R}^{m\times m}$. Then $A \succ 0$ if and only if

$$A_{1,1} \succ 0$$

and

$$A_{2,2} - A_{1,2}^T A_{1,1}^{-1} A_{1,2} \succ 0$$

Fact B.8. Let $A, B \in \mathbb{R}^{n\times n}$ with A non-singular. Then $(A+B)^{-1}$ can be written as

$$(A+B)^{-1} = \sum_{i=0}^{\infty} (-1)^i A^{-1} (BA^{-1})^i.$$

provided that $\rho(BA^{-1}) < 1$, where $\rho(\cdot)$ refers to the spectral radius of the argument.

Bibliography

[AÄH+14] Antonios Antonopoulos, Lennart Ängquist, Lennart Harnefors, Kalle Ilves, and Hans-Peter Nee. Global asymptotic stability of modular multilevel converters. *IEEE Transactions on Industrial Electronics*, 61(2):603–612, 2014.

[AÄN09] A. Antonopoulos, Lennart Ängquist, and H-P Nee. On dynamics and voltage control of the modular multilevel converter. In *13th European Conference on Power Electronics and Applications, EPE*, 2009.

[AÄN13] Noman Ahmed, Lennart Ängquist, and Hans-Peter Nee. Continuous modeling of open-loop control based negative sequence current control of modular multilevel converters for HVDC transmission. In *Power Electronics and Applications (EPE), 2013 15th European Conference on*, pages 1–10. IEEE, 2013.

[AÄN+14] N. Ahmed, L. Ängquist, S. Norrga, A. Antonopoulos, L. Harnefors, and H.-P. Nee. A computationally efficient continuous model for the modular multilevel converter. *Emerging and Selected Topics in Power Electronics, IEEE Journal of*, 2(4):1139–1148, Dec 2014.

[AÄNN12] Noman Ahmed, Lennart Ängquist, Staffan Norrga, and Hans-Peter Nee. Validation of the continuous model of the modular multilevel converter with blocking/deblocking capability. In *AC and DC Power Transmission (ACDC 2012), 10th IET International Conference on*, pages 1–6. IET, 2012.

[ÄAS+11] Lennart Ängquist, Antonios Antonopoulos, Daniel Siemaszko, Kalle Ilves, Michail Vasiladiotis, and Hans-Peter Nee. Open-loop control of modular multilevel converters using estimation of stored energy. *IEEE transactions on industry applications*, 47(6):2516–2524, 2011.

[AD06] F. Albertini and D. D'Alessandro. Lagrangian formulation and geometric control of switching lc electrical networks. In *Proceedings of the 45th IEEE Conference on Decision and Control*, pages 5204–5209, Dec 2006.

[AG94] Zijad Aganovic and Zoran Gajic. The successive approximation procedure for finite-time optimal control of bilinear systems. *IEEE Transactions on Automatic Control*, 39(9):1932–1935, 1994.

[AI15] F. B. Ajaei and R. Iravani. Enhanced equivalent model of the modular multilevel converter. *IEEE Transactions on Power Delivery*, 30(2):666–673, April 2015.

[ALQ13] R. P. Aguilera, P. Lezana, and D. E. Quevedo. Finite-control-set model predictive control with improved steady-state performance. *IEEE Transactions on Industrial Informatics*, 9(2):658–667, May 2013.

[AMM14] S. Almer, S. Mariethoz, and M. Morari. Dynamic phasor model predictive control of switched mode power converters. *Control Systems Technology, IEEE Transactions on*, 2014. To be published.

[APE17] V. Arredondo, M. A. Perez, and J. R. Espinoza. Capacitor voltage ripple control based on decoupled power analysis in MMC. In *2017 11th IEEE International Conference on Compatibility, Power Electronics and Power Engineering (CPE-POWERENG)*, pages 544–549, April 2017.

[Aus87] Alfred Auslender. Numerical methods for nondifferentiable convex optimization. *Nonlinear Analysis and Optimization*, pages 102–126, 1987.

[AXF99] S. K. Agrawal, X. Xu, and N. Faiz. Optimization of bilinear systems using higher-order method. In *American Control Conference, 1999. Proceedings of the 1999*, volume 2, pages 905–909 vol.2, Jun 1999.

[Bai78] John Baillieul. Geometric methods for nonlinear optimal control problems. *Journal of optimization theory and applications*, 25(4):519–548, 1978.

[BB12] D. Bernardini and A. Bemporad. Stabilizing model predictive control of stochastic constrained linear systems. *Automatic Control, IEEE Transactions on*, 57(6):1468–1480, June 2012.

[BBM17] Francesco Borrelli, Alberto Bemporad, and Manfred Morari. *Predictive control for linear and hybrid systems*. Cambridge University Press, 2017.

[BCK03] Marko Bacic, Mark Cannon, and Basil Kouvaritakis. Constrained control of siso bilinear systems. *IEEE Transactions on Automatic Control*, 48(8):1443–1447, 2003.

[Ber79] DP Bertsekas. Convexification procedures and decomposition methods for nonconvex optimization problems. *Journal of Optimization Theory and Applications*, 29(2):169–197, 1979.

[Ber05] Dennis S Bernstein. *Matrix mathematics: Theory, facts, and formulas with application to linear systems theory*, volume 41. Princeton University Press Princeton, 2005.

[BFS15] Mario Berta, Omar Fawzi, and Volkher B Scholz. Quantum bilinear optimization. *arXiv preprint arXiv:1506.08810*, 2015.

[BKVH07] Stephen Boyd, Seung-Jean Kim, Lieven Vandenberghe, and Arash Hassibi. A tutorial on geometric programming. *Optimization and engineering*, 8(1):67–127, 2007.

[BLO05] James V Burke, Adrian S Lewis, and Michael L Overton. A robust gradient sampling algorithm for nonsmooth, nonconvex optimization. *SIAM Journal on Optimization*, 15(3):751–779, 2005.

[BMC+09] Andrea Giovanni Beccuti, Sébastien Mariéthoz, Sébastien Cliquennois, Shu Wang, and Manfred Morari. Explicit model predictive control of DC–DC switched-mode power supplies with extended Kalman filtering. *IEEE Transactions on Industrial Electronics*, 56(6):1864–1874, 2009.

[Bro72] Roger W Brockett. System theory on group manifolds and coset spaces. *SIAM Journal on control*, 10(2):265–284, 1972.

[Bro73] RW Brockett. Lie theory and control systems defined on spheres. *SIAM Journal on Applied Mathematics*, 25(2):213–225, 1973.

[Bro75] Roger W Brockett. On the reachable set for bilinear systems. In *Variable Structure Systems with Application to Economics and Biology*, pages 54–63. Springer, 1975.

[BS11] Michael Baake and Ulrike Schlägel. The peano-baker series. *Proceedings of the Steklov Institute of Mathematics*, 275(1):155–159, 2011.

[BSBG16] A. Beddard, C. Sheridan, M. Barnes, and T. Green. Improved accuracy average value models of modular multilevel converters. *IEEE Transactions on Power Delivery*, PP(99):1, 2016.

[BT89] Paul T Boggs and Jon W Tolle. A strategy for global convergence in a sequential quadratic programming algorithm. *SIAM journal on Numerical Analysis*, 26(3):600–623, 1989.

[BT95] Paul T Boggs and Jon W Tolle. Sequential quadratic programming. *Acta numerica*, 4:1–51, 1995.

[BT00] Paul T Boggs and Jon W Tolle. Sequential quadratic programming for large-scale nonlinear optimization. *Journal of Computational and Applied Mathematics*, 124(1):123–137, 2000.

[BV04] Stephen Boyd and Lieven Vandenberghe. *Convex optimization*. Cambridge university press, 2004.

[BV14] S. Barik and H. Vikalo. Sparsity-aware sphere decoding: Algorithms and complexity analysis. *Signal Processing, IEEE Transactions on*, 62(9):2212–2225, May 2014.

[BvdBV01] H. H. J. Bloemen, T. J. J. van den Boom, and H. B. Verbruggen. An optimization algorithm dedicated to a MPC problem for discrete time bilinear models. In *Proceedings of the 2001 American Control Conference. (Cat. No.01CH37148)*, volume 3, pages 2376–2381 vol.3, 2001.

[BvdBV04] HHJ Bloemen, TJJ van den Boom, and HB Verbruggen. Optimization algorithms for bilinear model–based predictive control problems. *AIChE journal*, 50(7):1453–1461, 2004.

[BVP+12] H. Borhan, A. Vahidi, A.M. Phillips, M.L. Kuang, I.V. Kolmanovsky, and S. Di Cairano. MPC-based energy management of a power-split hybrid electric vehicle. *Control Systems Technology, IEEE Transactions on*, 20(3):593–603, May 2012.

[BX09] Wei Bian and Xiaoping Xue. Subgradient-based neural networks for nonsmooth nonconvex optimization problems. *IEEE Transactions on Neural Networks*, 20(6):1024–1038, 2009.

[CA13] Eduardo F Camacho and Carlos Bordons Alba. *Model predictive control*. Springer Science & Business Media, 2013.

[Can04] Mark Cannon. Efficient nonlinear model predictive control algorithms. *Annual Reviews in Control*, 28(2):229–237, 2004.

[CB12] Eduardo F Camacho and Carlos A Bordons. *Model predictive control in the process industry*. Springer Science & Business Media, 2012.

[CMC+14] Patrizio Colaneri, Richard H Middleton, Zhiyong Chen, Danilo Caporale, and Franco Blanchini. Convexity of the cost functional in an optimal control problem for a class of positive switched systems. *Automatica*, 50(4):1227–1234, 2014.

[CMPR03] Hernán Cendra, Jerrold E Marsden, Sergey Pekarsky, and Tudor S Ratiu. Variational principles for lie–poisson and hamilton–poincaré equations. *Moscow Math. J*, 3(3):833–867, 2003.

[COY16] N. R. Chaudhuri, R. Oliveira, and A. Yazdani. Stability analysis of vector-controlled modular multilevel converters in linear time-periodic framework. *IEEE Transactions on Power Electronics*, 31(7):5255–5269, July 2016.

[CWR13] Shan Chai, Liuping Wang, and Eric Rogers. Model predictive control of a permanent magnet synchronous motor with experimental validation. *Control Engineering Practice*, 21(11):1584–1593, 2013.

[D'A10] Claudia D'Ambrosio. *Application-oriented mixed integer non-linear programming*. PhD thesis, Springer, 2010.

[DC14] Fujin Deng and Zhe Chen. A control method for voltage balancing in modular multilevel converters. *Power Electronics, IEEE Transactions on*, 29(1):66–76, 2014.

[DC15] Fujin Deng and Zhe Chen. Elimination of DC-link current ripple for modular multilevel converters with capacitor voltage-balancing pulse-shifted carrier PWM. *IEEE Transactions on Power Electronics*, 30(1):284–296, January 2015.

[DFMM15] Vahid Rasouli Disfani, Lingling Fan, Zhixin Miao, and Yan Ma. Fast model predictive control algorithms for fast-switching modular multilevel converters. *Electric Power Systems Research*, 129:105–113, 2015.

[DGvdM14] G. Darivianakis, T. Geyer, and W. van der Merwe. Model predictive current control of modular multilevel converters. In *Energy Conversion Congress and Exposition (ECCE), 2014 IEEE*, pages 5016–5023, Sept 2014.

[DIOP95] Francis J Doyle III, Babatunde A Ogunnaike, and Ronald K Pearson. Nonlinear model-based control using second-order volterra models. *Automatica*, 31(5):697–714, 1995.

[DLL15] Sixing Du, Jinjun Liu, and Teng Liu. Modulation and closed-loop-based DC capacitor voltage control for mmc with fundamental switching frequency. *IEEE Transactions on Power Electronics*, 30(1):327–338, January 2015.

[dOKM00] S.L. de Oliveira Kothare and M. Morari. Contractive model predictive control for constrained nonlinear systems. *Automatic Control, IEEE Transactions on*, 45(6):1053–1071, Jun 2000.

[DPK+13] R. Darus, J. Pou, G. Konstantinou, S. Ceballos, and V.G. Agelidis. Circulating current control and evaluation of carrier dispositions in modular multilevel converters. In *ECCE Asia Downunder (ECCE Asia), 2013 IEEE*, pages 332–338, June 2013.

[DQB+15] S. Debnath, Jiangchao Qin, B. Bahrani, M. Saeedifard, and P. Barbosa. Operation, control, and applications of the modular multilevel converter: A review. *IEEE Transactions on Power Electronics*, 30(1):37–53, January 2015.

[DQS15] Suman Debnath, Jiangchao Qin, and Maryam Saeedifard. Control and stability analysis of modular multilevel converter under low-frequency operation. *IEEE Transactions on Industrial Electronics*, 62(9):5329–5339, 2015.

[DS98] N. R Draper and H. Smith. *Applied Regression Analysis*. Wiley-Interscience, 1998.

[DS13] S. Debnath and M. Saeedifard. A new hybrid modular multilevel converter for grid connection of large wind turbines. *Sustainable Energy, IEEE Transactions on*, 4(4):1051–1064, 2013.

[DS16] S. Debnath and M. Saeedifard. Simulation-based gradient-descent optimization of modular multilevel converter controller parameters. *IEEE Transactions on Industrial Electronics*, 63(1):102–112, January 2016.

[DWYZ16] Apparao Dekka, Bin Wu, Venkata Yaramsu, and Navid R Zargari. Dual-stage model predictive control of modular multilevel converter. In *2016 IEEE International Conference on Industrial Technology (ICIT)*, pages 1073–1078. IEEE, 2016.

[DWYZ17] A. Dekka, B. Wu, V. Yaramasu, and N. R. Zargari. Model predictive control with common-mode voltage injection for modular multilevel converter. *IEEE Transactions on Power Electronics*, 32(3):1767–1778, March 2017.

[DWZC16] S. Du, B. Wu, N. Zargari, and Z. Cheng. A flying-capacitor modular multilevel converter (FC-MMC) for medium-voltage motor drive. *IEEE Transactions on Power Electronics*, PP(99):1, 2016.

[DWZF16] A. Dekka, B. Wu, N. R. Zargari, and R. L. Fuentes. Dynamic voltage balancing algorithm for modular multilevel converter: A unique solution. *IEEE Transactions on Power Electronics*, 31(2):952–963, February 2016.

[EDD11] Stefan P Engel and Rik W De Doncker. Control of the modular multilevel converter for minimized cell capacitance. In *Power Electronics and Applications (EPE 2011), Proceedings of the 2011-14th European Conference on*, pages 1–10. IEEE, 2011.

[Ekm05] Mats Ekman. *Modeling and control of bilinear systems: application to the activated sludge process*. PhD thesis, Acta Universitatis Upsaliensis, 2005.

[Ell09] David L Elliott. *Bilinear control systems: matrices in action*, volume 169. Springer Science & Business Media, 2009.

[EM01] Robert W. Erickson and Dragan Maksimovic. *Fundamentals of Power Electronics*. Kluwer Academic Publishers, 2 edition, 2001.

[Erl14] Istvan Erlich. CEP special issue on power system control. *Control Engineering Practice*, 30(0):91 – 92, 2014.

[FDG08] Adhemar B Fontes, Carlos ET Dorea, and Marcio R da S Garcia. An iterative algorithm for constrained MPC with stability of bilinear systems. In *Control and Automation, 2008 16th Mediterranean Conference on*, pages 1526–1531. IEEE, 2008.

[FTY04] M. F. L. Foo, Ai Hui Tan, and T. T. V. Yap. Optimisation of a static nonlinear compensator for bilinear systems. In *Instrumentation and Measurement Technology Conference, 2004. IMTC 04. Proceedings of the 21st IEEE*, volume 3, pages 2187–2192 Vol.3, May 2004.

[FZXX15] Shengfang Fan, Kai Zhang, Jian Xiong, and Yaosuo Xue. An improved control system for modular multilevel converters with new modulation strategy and voltage balancing control. *Power Electronics, IEEE Transactions on*, 30(1):358–371, Jan 2015.

[GDY+16] Z. Gong, P. Dai, X. Yuan, X. Wu, and G. Guo. Design and experimental evaluation of fast model predictive control for modular multilevel converters. *IEEE Transactions on Industrial Electronics*, 63(6):3845–3856, June 2016.

[Gey09] Tobias Geyer. Generalized model predictive direct torque control: Long prediction horizons and minimization of switching losses. In *Decision and Control, 2009 held jointly with the 2009 28th Chinese Control Conference. CDC/CCC 2009. Proceedings of the 48th IEEE Conference on*, pages 6799–6804. IEEE, 2009.

[Gey11] T. Geyer. A comparison of control and modulation schemes for medium-voltage drives: Emerging predictive control concepts versus PWM-based schemes. *Industry Applications, IEEE Transactions on*, 47(3):1380–1389, May 2011.

[GF08] CE Gounaris and CA Floudas. Convexity of products of univariate functions and convexification transformations for geometric programming. *Journal of Optimization Theory and Applications*, 138(3):407–427, 2008.

[GGJ11] U.N. Gnanarathna, A.M. Gole, and R.P. Jayasinghe. Efficient modeling of modular multilevel HVDC converters (mmc) on electromagnetic transient simulation programs. *IEEE Transactions on Power Delivery*, 26(1):316–324, 2011.

[GGS01] Graham C Goodwin, Stefan F Graebe, and Mario E Salgado. *Control system design*. 2001.

[GHW+14] G. Guo, X. Hu, J. Wen, X. You, M. Li, and X. Chu. The modulation and simulation of voltage source converter based on half bridge sub module. In *Proc. Int Power System Technology (POWERCON) Conf*, pages 2047–2055, October 2014.

[GJL+13] Congzhe Gao, Xinjian Jiang, Yongdong Li, Zhe Chen, and Jingyun Liu. A dc-link voltage self-balance method for a diode-clamped modular multilevel converter with minimum number of voltage sensors. *Power Electronics, IEEE Transactions on*, 28(5):2125–2139, 2013.

[GKR16] Philip E Gill, Vyacheslav Kungurtsev, and Daniel P Robinson. A stabilized SQP method: global convergence. *IMA Journal of Numerical Analysis*, page drw004, 2016.

[GPM89] Carlos E Garcia, David M Prett, and Manfred Morari. Model predictive control: theory and practicea survey. *Automatica*, 25(3):335–348, 1989.

[GPW15] S.M. Goetz, A.V. Peterchev, and T. Weyh. Modular multilevel converter with series and parallel module connectivity: Topology and control. *Power Electronics, IEEE Transactions on*, 30(1):203–215, Jan 2015.

[GQ14a] T. Geyer and D. Quevedo. Multistep finite control set model predictive control for power electronics - part 2: Analysis. *Power Electronics, IEEE Transactions on*, 2014. To be published.

[GQ14b] T. Geyer and D. E. Quevedo. Multistep finite control set model predictive control for power electronics. *IEEE Transactions on Power Electronics*, 29(12):6836–6846, December 2014.

[GU13] S. Gjerde and T.M. Undeland. Dynamic performance of the modular series connected converter in a 100 kvdc- transformerless offshore wind turbine. In *OCEANS - Bergen, 2013 MTS/IEEE*, pages 1–9, 2013.

[HA14] Matthew W Harris and Behçet Açıkmeşe. Lossless convexification of non-convex optimal control problems for state constrained linear systems. *Automatica*, 50(9):2304–2311, 2014.

[Han04] Deren Han. Global optimization with polynomials. *High Performance Computation for Engineered Systems (HPCES)*, 2004.

[HAN+13] Lennart Harnefors, Antonios Antonopoulos, Staffan Norrga, Lennart Ängquist, and Hans-Peter Nee. Dynamic analysis of modular multilevel converters. *IEEE Transactions on Industrial Electronics*, 60(7):2526–2537, 2013.

[HCVH17] Hassan Hijazi, Carleton Coffrin, and Pascal Van Hentenryck. Convex quadratic relaxations for mixed-integer nonlinear programs in power systems. *Mathematical Programming Computation*, 9(3):321–367, 2017.

[HL04] Didier Henrion and J-B Lasserre. Solving nonconvex optimization problems. *IEEE control systems*, 24(3):72–83, 2004.

[Hol16] Joachim Holtz. Advanced pwm and predictive controlan overview. *IEEE Transactions on Industrial Electronics*, 63(6):3837–3844, 2016.

[HS04] Camile WJ Hol and Carsten W Scherer. Sum of squares relaxations for polynomial semidefinite programming. In *Proc. Symp. on Mathematical Theory of Networks and Systems (MTNS), Leuven, Belgium*, 2004.

[HTM13] Shaojun Huang, Remus Teodorescu, and Laszlo Mathe. Analysis of communication based distributed control of MMC for HVDC. In *Power Electronics and Applications (EPE), 2013 15th European Conference on*, pages 1–10, 2013.

[HU89] J-B Hiriart-Urruty. From convex optimization to nonconvex optimization. necessary and sufficient conditions for global optimality. In *Nonsmooth optimization and related topics*, pages 219–239. Springer, 1989.

[HZM16] M. Huang, J. Zou, and X. Ma. An improved phase-shifted carrier modulation for modular multilevel converter to suppress the influence of fluctuation of capacitor voltage. *IEEE Transactions on Power Electronics*, 31(10):7404–7416, October 2016.

[HZM17] M. Huang, J. Zou, and X. Ma. Hybrid modular multilevel converter with redistributed power to reduce sub-module capacitor voltage fluctuation. *IEEE Transactions on Power Electronics*, 2017. Early acces.

[HZXF15] Liqun He, Kai Zhang, Jian Xiong, and Shengfang Fan. A repetitive control scheme for harmonic suppression of circulating current in modular multilevel converters. *IEEE Transactions on Power Electronics*, 30(1):471–481, January 2015.

[IAH+11] Kalle Ilves, Antonios Antonopoulos, Lennart Harnefors, Staffan Norrga, Lennart Ängquist, and H-P Nee. Capacitor voltage ripple shaping in modular multilevel converters allowing for operating region extension. In *IECON 2011-37th Annual Conference on IEEE Industrial Electronics Society*, pages 4403–4408. IEEE, 2011.

[IANN12a] K. Ilves, A. Antonopoulos, Staffan Norrga, and H-P Nee. A new modulation method for the modular multilevel converter allowing fundamental switching frequency. *Power Electronics, IEEE Transactions on*, 27(8):3482–3494, 2012.

[IANN12b] Kalle Ilves, Antonios Antonopoulos, Staffan Norrga, and Hans-Peter Nee. Steady-state analysis of interaction between harmonic components of arm and line quantities of modular multilevel converters. *IEEE transactions on power electronics*, 27(1):57–68, 2012.

[IHNN13] K. Ilves, L. Harnefors, S. Norrga, and H.-P. Nee. Predictive sorting algorithm for modular multilevel converters minimizing the spread in the submodule capacitor voltages. In *ECCE Asia Downunder (ECCE Asia), 2013 IEEE*, pages 325–331, 2013.

[IMKNZ00] Arieh Iserles, Hans Z Munthe-Kaas, Syvert P Nørsett, and Antonella Zanna. Lie-group methods. *Acta Numerica 2000*, 9:215–365, 2000.

[INHN14] K. Ilves, S. Norrga, L. Harnefors, and H.-P. Nee. On energy storage requirements in modular multilevel converters. *Power Electronics, IEEE Transactions on*, 29(1):77–88, Jan 2014.

[JJ16] A. Jamshidifar and D. Jovcic. Small-signal dynamic DQ model of modular multilevel converter for system studies. *IEEE Transactions on Power Delivery*, 31(1):191–199, February 2016.

[JJF15] D. Jovcic and A. Jamshidi Far. Phasor model of modular multilevel converter with circulating current suppression control. *IEEE Transactions on Power Delivery*, 30(4):1889–1897, August 2015.

[JMMG13] P. D. Judge, M. M. C. Merlin, P. D. Mitcheson, and T. C. Green. Power loss and thermal characterization of IGBT modules in the alternate arm converter. In *Proc. IEEE Energy Conversion Congress and Exposition*, pages 1725–1731, September 2013.

[Jur11] Velimir Jurdjevic. Optimal control on lie groups and integrable hamiltonian systems. *Regular and Chaotic Dynamics*, 16(5):514–535, 2011.

[KB11] Anthony Kelman and Francesco Borrelli. Bilinear model predictive control of a hvac system using sequential quadratic programming. *IFAC Proceedings Volumes*, 44(1):9869–9874, 2011.

[KCV+09] Samir Kouro, Patricio Cortés, René Vargas, Ulrich Ammann, and José Rodríguez. Model predictive controla simple and powerful method to control power converters. *IEEE Transactions on Industrial Electronics*, 56(6):1826–1838, 2009.

[KGM14] P. Karamanakos, T. Geyer, and S. Manias. Direct voltage control of DC-DC boost converters using enumeration-based model predictive control. *IEEE Transactions on Power Electronics*, 29(2):968–978, Feb 2014.

[KHL14] G. J. Kish, C. Holmes, and P. W. Lehn. Dynamic modeling of modular multilevel DC/DC converters for HVDC systems. In *IEEE 15th Workshop on Control and Modeling for Power Electronics (COMPEL)*, June 2014.

[KKGB15] J. Kolb, F. Kammerer, M. Gommeringer, and M. Braun. Cascaded control system of the modular multilevel converter for feeding variable-speed drives. *IEEE Transactions on Power Electronics*, 30(1):349–357, January 2015.

[KNM95] Mayuresh V Kothare, Vesna Nevistic, and Manfred Morari. Robust constrained model predictive control for nonlinear systems: a comparative study. In *Decision and Control, 1995., Proceedings of the 34th IEEE Conference on*, volume 3, pages 2884–2885. IEEE, 1995.

[KPC+16] G. Konstantinou, J. Pou, S. Ceballos, R. Picas, J. Zaragoza, and V. G. Agelidis. Control of circulating currents in modular multilevel converters through redundant voltage levels. *IEEE Transactions on Power Electronics*, PP(99):1, 2016.

[KPKL14] Seok-Kyoon Kim, Chang Reung Park, Jung-Su Kim, and Young I Lee. A stabilizing model predictive controller for voltage regulation of a DC/DC boost converter. *IEEE Transactions on Control Systems Technology*, 22(5):2016–2023, 2014.

[Kre75] Arthur J Krener. Bilinear and nonlinear realizations of input-output maps. *SIAM Journal on Control*, 13(4):827–834, 1975.

[Kre77] Arthur J Krener. The high order maximal principle and its application to singular extremals. *SIAM Journal on Control and Optimization*, 15(2):256–293, 1977.

[LCM16] J. Lyu, X. Cai, and M. Molinas. Frequency domain stability analysis of MMC-based HVDC for wind farm integration. *IEEE Journal of Emerging and Selected Topics in Power Electronics*, 4(1):141–151, March 2016.

[LGZ16] T. LI, A. M. Gole, and C. Zhao. Harmonic instability in MMC-HVDC converters resulting from internal dynamics. *IEEE Transactions on Power Delivery*, PP(99):1, 2016.

[LHWB06] M. Lazar, W. P M H Heemels, S. Weiland, and A. Bemporad. Stabilizing model predictive control of hybrid systems. *Automatic Control, IEEE Transactions on*, 51(11):1813–1818, Nov 2006.

[LJW16] Yalong Li, E. A. Jones, and Fei Wang. The impact of voltage-balancing control on switching frequency of the modular multilevel converter. *IEEE Transactions on Power Electronics*, 31(4):2829–2839, April 2016.

[LK94] N. E. Leonard and P. S. Krishnaprasad. Control of switched electrical networks using averaging on lie groups. In *Decision and Control, 1994., Proceedings of the 33rd IEEE Conference on*, volume 2, pages 1919–1924 vol.2, Dec 1994.

[LLH+17] Y. Lyu, C. Li, Y. H. Hsieh, F. C. Lee, Q. Li, and R. Xu. Capacitor voltage ripple reduction with state trajectory analysis for modular multilevel converter. In *2017 IEEE Applied Power Electronics Conference and Exposition (APEC)*, pages 1829–1836, March 2017.

[LM03] A. Lesnicar and R. Marquardt. An innovative modular multilevel converter topology suitable for a wide power range. In *Power Tech Conference Proceedings, 2003 IEEE Bologna*, volume 3, pages 1–6, June 2003.

[LPDP13] Andres Lopez, Diego Patino, Rafael Diez, and Gabriel Perilla. An equivalent continuous model for switched systems. *Systems & Control Letters*, 62(2):124–131, 2013.

[LQA+14] Andres Lopez, Daniel E Quevedo, Ricardo P Aguilera, Tobias Geyer, and Nikolaos Oikonomou. Reference design for predictive control of modular multilevel converters. In *Australian Control Conference (AUCC)*, 2014.

[LQA+15] Andres Lopez, Daniel E Quevedo, Ricardo P Aguilera, Tobias Geyer, and Nikolaos Oikonomou. Validation of a reduced order model for modular multilevel converters and analysis of circulating current. In *17th European Conference on Power Electronics and Applications (EPE'15 ECCE Europe)*, 2015.

[LQA+18a] A. Lopez, D. E. Quevedo, R. P. Aguilera, T. Geyer, and N. Oikonomou. Reference design for control of MMCs. *IEEE Journal of Emerging and Selected Topics in Power Electronics*, 2018. In Review.

[LQA+18b] A. M. Lopez, D. E. Quevedo, R. P. Aguilera, T. Geyer, and N. Oikonomou. Limitations and accuracy of a continuous reduced-order model for modular multilevel converters. *IEEE Transactions on Power Electronics*, 33(7):6292–6303, July 2018.

[LQAG18] A. Lopez, D. E. Quevedo, R. P. Aguilera, and T. Geyer. On the convexity of the optimization problem underlaying MPC for bilinear systems with applications to power converters. *Systems & Control Letters*, 2018. In Review.

[LSL+12] Chuang Liu, Pengwei Sun, Jih-Sheng Lai, Yanchao Ji, Mingyan Wang, Chien-Liang Chen, and Guowei Cai. Cascade dual-boost/buck active-front-end converter for intelligent universal transformer. *IEEE Transactions on Industrial Electronics*, 59(12):4671–4680, December 2012.

[LWCL16] Pu Liu, Yue Wang, Wulong Cong, and Wanjun Lei. Grouping-sorting-optimized model predictive control for modular multilevel converter with reduced computational load. *IEEE Transactions on Power Electronics*, 31(3):1896–1907, March 2016.

[LWY+15] Shaohua Li, Xiuli Wang, Zhiqing Yao, Tai Li, and Zhong Peng. Circulating current suppressing strategy for MMC-HVDC based on nonideal proportional resonant controllers under unbalanced grid conditions. *IEEE Transactions on Power Electronics*, 30(1):387–397, January 2015.

[LYLZ16] S. Lu, L. Yuan, K. Li, and Z. Zhao. An improved phase-shifted carrier modulation scheme for hybrid modular multilevel converter. *IEEE Transactions on Power Electronics*, PP(99):1, 2016.

[LZW+15] Binbin Li, Yi Zhang, Gaolin Wang, Wei Sun, Dianguo Xu, and Wei Wang. A modified modular multilevel converter with reduced capacitor voltage fluctuation. *IEEE Transactions on Industrial Electronics*, 62(10):6108–6119, October 2015.

[LZX+16a] B. Li, S. Zhou, D. Xu, S. Finney, and B. Williams. A hybrid modular multilevel converter for medium-voltage variable-speed motor drives. *IEEE Transactions on Power Electronics*, PP(99):1, 2016.

[LZX+16b] B. Li, S. Zhou, D. Xu, R. Yang, D. Xu, C. Buccella, and C. Cecati. An improved circulating current injection method for modular multilevel converters in variable-speed drives. *IEEE Transactions on Industrial Electronics*, 63(11):7215–7225, November 2016.

[Mar10] R. Marquardt. Modular multilevel converter: An universal concept for HVDC-networks and extended DC-bus-applications. In *Power Electronics Conference (IPEC), 2010 International*, pages 502–507, June 2010.

[May14] David Q Mayne. Model predictive control: Recent developments and future promise. *Automatica*, 50(12):2967–2986, 2014.

[MB15] P. M. Meshram and V. B. Borghate. A simplified nearest level control (NLC) voltage balancing method for modular multilevel converter (MMC). *IEEE Transactions on Power Electronics*, 30(1):450–462, January 2015.

[MC76] R. D. Middlebrook and S. Cuk. A general unified approach to modelling switching-converter power stages. In *1976 IEEE Power Electronics Specialists Conference*, pages 18–34, June 1976.

[MGP+15] Ji-Woo Moon, Jin-Su Gwon, Jung-Woo Park, Dae-Wook Kang, and Jang-Mok Kim. Model predictive control with a reduced number of considered states in a modular multilevel converter for HVDC system. *IEEE Transactions on Power Delivery*, 30(2):608–617, April 2015.

[MGRP10] M. Malinowski, K. Gopakumar, J. Rodriguez, and M.A. Perez. A survey on cascaded multilevel inverters. *Industrial Electronics, IEEE Transactions on*, 57(7):2197–2206, July 2010.

[MKK+06] Almir Mutapcic, Kwangmoo Koh, Seungjean Kim, Lieven Vandenberghe, and Stephen Boyd. Ggplab: a simple matlab toolbox for geometric programming. *web page and software: http://stanford. edu/boyd/ggplab*, 2006.

[ML99] Manfred Morari and Jay H Lee. Model predictive control: past, present and future. *Computers & Chemical Engineering*, 23(4):667–682, 1999.

[MLDD07] José Mare, Mircea Lazar, and José De Doná. Input to state stabilising nonlinear model predictive control based on QP. *IFAC Proceedings Volumes*, 40(12):222–227, 2007.

[MNW11] José Luis Morales, Jorge Nocedal, and Yuchen Wu. A sequential quadratic programming algorithm with an additional equality constrained phase. *IMA Journal of Numerical Analysis*, page drq037, 2011.

[Moe16] Nicholas Moehle. Value function approximation for direct control of switched power converters. *arXiv preprint arXiv:1601.05115*, 2016.

[MRRS00] David Q Mayne, James B Rawlings, Christopher V Rao, and Pierre OM Scokaert. Constrained model predictive control: Stability and optimality. *Automatica*, 36(6):789–814, 2000.

[MS13] Euripidis S Mistakidis and Georgios E Stavroulakis. *Nonconvex optimization in mechanics: algorithms, heuristics and engineering applications by the FEM*, volume 21. Springer Science & Business Media, 2013.

[MV15] M. Marchesoni and L. Vaccaro. Study of the mmc circulating current for optimal operation mode in HVDC applications. In *Power Electronics and Applications (EPE'15 ECCE-Europe), 2015 17th European Conference on*, pages 1–10, September 2015.

[NÄI+12a] S. Norrga, L. Ängquist, K. Ilves, L. Harnefors, and H. Nee. Frequency-domain modeling of modular multilevel converters. In *IECON 2012 - 38th Annual Conference on IEEE Industrial Electronics Society*, pages 4967–4972, Oct 2012.

[NÄI+12b] Staffan Norrga, Lennart Ängquist, K. Ilves, Lennart Harnefors, and H-P Nee. Decoupled steady-state model of the modular multilevel converter with half-bridge cells. In *Power Electronics, Machines and Drives (PEMD 2012), 6th IET International Conference on*, pages 1–6, March 2012.

[NAK11] E. Nobuyama, T. Aoyagi, and Y. Kami. Robust control synthesis of bilinear systems with nonlinear weights by sum of squares optimization. In *System Theory, Control, and Computing (ICSTCC), 2011 15th International Conference on*, pages 1–6, Oct 2011.

[Nes13] Yurii Nesterov. *Introductory lectures on convex optimization: A basic course*, volume 87. Springer Science & Business Media, 2013.

[NLDD15] A. Nami, Jiaqi Liang, F. Dijkhuizen, and G.D. Demetriades. Modular multilevel converters for HVDC applications: Review on converter cells and functionalities. *Power Electronics, IEEE Transactions on*, 30(1):18–36, Jan 2015.

[NNSU16] H. Nademi, L. E. Norum, Z. Soghomonian, and T. Undeland. Low frequency operation of modular multilevel matrix converter using optimization-oriented predictive control scheme. In *2016 IEEE 17th Workshop on Control and Modeling for Power Electronics (COMPEL)*, pages 1–6, June 2016.

[NW06] Jorge Nocedal and Stephen J Wright. *Sequential quadratic programming*. Springer, 2006.

[OQLEA11] C Olalla, I Queinnec, R Leyva, and A El Aroudi. Robust optimal control of bilinear dc–dc converters. *Control Engineering Practice*, 19(7):688–699, 2011.

[OSNA13] Joao Inacio Yutaka Ota, Yuji Shibano, Naoto Niimura, and Hirofumi Akagi. Current control of a phase-shifted-pwm statcom using the modular multilevel cascade converter based on single-star bridge-cells (mmcc-ssbc). In *Energy Conversion Congress and Exposition (ECCE), 2013 IEEE*, pages 420–427, 2013.

[Owe75] D. H. Owens. Descent algorithm for the optimisation of bilinear systems. *Electronics Letters*, 11(15):335–336, July 1975.

[PAV+13] Antonis Papachristodoulou, James Anderson, Giorgio Valmorbida, Stephen Prajna, Pete Seiler, and Pablo Parrilo. Sostools version 3.00 sum of squares optimization toolbox for matlab. *arXiv preprint arXiv:1310.4716*, 2013.

[PBR+15] M.A. Perez, S. Bernet, J. Rodriguez, S. Kouro, and R. Lizana. Circuit topologies, modeling, control schemes, and applications of modular multilevel converters. *Power Electronics, IEEE Transactions on*, 30(1):4–17, Jan 2015.

[PCG+14] Patrick Panciatici, MC Campi, S Garatti, SH Low, DK Molzahn, AX Sun, and Louised Wehenkel. Advanced optimization methods for power systems. In *Power Systems Computation Conference (PSCC), 2014*, pages 1–18. IEEE, 2014.

[PCK+15] J. Pou, S. Ceballos, G. Konstantinou, V.G. Agelidis, R. Picas, and J. Zaragoza. Circulating current injection methods based on instantaneous information for the modular multilevel converter. *IEEE Transactions on Industrial Electronics*, 62(2):777–788, 2015.

[PCP+15] R. Picas, S. Ceballos, J. Pou, J. Zaragoza, G. Konstantinou, and V. G. Agelidis. Closed-loop discontinuous modulation technique for capacitor voltage ripples and switching losses reduction in modular multilevel converters. *IEEE Transactions on Power Electronics*, 30(9):4714–4725, September 2015.

[PH02] Panos M Pardalos and Donald Hearn. Applied optimization. *Applications of Interval Computations*, 3, 2002.

[PHW99] Ray Pörn, Iiro Harjunkoski, and Tapio Westerlund. Convexification of different classes of non-convex MINLP problems. *Computers & chemical engineering*, 23(3):439–448, 1999.

[PLA+12] M.A. Perez, R. Lizana, C. Azocar, J. Rodriguez, and Bin Wu. Modular multilevel cascaded converter based on current source h-bridges cells. In *IECON 2012 - 38th Annual Conference on IEEE Industrial Electronics Society*, pages 3443–3448, 2012.

[PPC+13] R. Picas, J. Pou, S. Ceballos, J. Zaragoza, G. Konstantinou, and V.G. Agelidis. Optimal injection of harmonics in circulating currents of modular multilevel converters for capacitor voltage ripple minimization. In *ECCE Asia Downunder*, pages 318–324, June 2013.

[PRFK12] M.A. Pérez, J. Rodríguez, E.J. Fuentes, and F. Kammerer. Predictive control of AC-AC modular multilevel converters. *IEEE Transactions on Industrial Electronics*, 59(7):2832–2839, July 2012.

[PSD+12] J. Peralta, H. Saad, S. Dennetiere, J. Mahseredjian, and S. Nguefeu. Detailed and averaged models for a 401-level MMC –HVDC system. *IEEE Transactions on Power Delivery*, 27(3):1501–1508, July 2012.

[PTA94] P.N. Paraskevopoulos, A.S. Tsirikos, and K.G. Arvanitis. A new orthogonal series approach to state space analysis of bilinear systems. *Automatic Control, IEEE Transactions on*, 39(4):793–797, Apr 1994.

[PY10] Panos M Pardalos and Vitaliy A Yatsenko. *Optimization and Control of Bilinear Systems: Theory, Algorithms, and Applications*, volume 11. Springer Science & Business Media, 2010.

[QAG14] Daniel E Quevedo, Ricardo P Aguilera, and Tobias Geyer. Predictive control in power electronics and drives: Basic concepts, theory, and methods. In *Advanced and Intelligent Control in Power Electronics and Drives*, pages 181–226. Springer International Publishing, 2014.

[QAP+12] D.E. Quevedo, R.P. Aguilera, M.A. Pérez, P. Cortés, and R. Lizana. Model predictive control of an AFE rectifier with dynamic references. *Power Electronics, IEEE Transactions on*, 27(7):3128–3136, July 2012.

[QB00] S Joe Qin and Thomas A Badgwell. An overview of nonlinear model predictive control applications. *Nonlinear model predictive control*, pages 369–392, 2000.

[QB03] S Joe Qin and Thomas A Badgwell. A survey of industrial model predictive control technology. *Control engineering practice*, 11(7):733–764, 2003.

[QG04] D. E. Quevedo and G. C. Goodwin. Control of EMI from switch-mode power supplies via multi-step optimization. In *American Control Conference, 2004. Proceedings of the 2004*, volume 1, pages 390–395 vol.1, June 2004.

[QS12] Jiangchao Qin and M Saeedifard. Predictive control of a modular multilevel converter for a back-to-back HVDC system. *IEEE Transactions on Power Delivery*, 27(3):1538–1547, 2012.

[REFA06] T Raff, C Ebenbauer, R Findeisen, and F Allgöwer. Nonlinear model predictive control and sum of squares techniques. *Fast Motions in Biomechanics and Robotics*, pages 325–344, 2006.

[RF16] Shailajah Rajesvaran and Shaahin Filizadeh. Modeling modular multilevel converters using extended-frequency dynamic phasors. In *Power and Energy Society General Meeting (PESGM), 2016*, pages 1–5. IEEE, 2016.

[RGM15] B.S. Riar, T. Geyer, and U.K. Madawala. Model predictive direct current control of modular multilevel converters: Modeling, analysis, and experimental evaluation. *IEEE Transactions on Power Electronics*, 30(1):431–439, Jan 2015.

[Ric12] Stefan Richter. *Computational complexity certification of gradient methods for real-time model predictive control*. Diss., Eidgenössische Technische Hochschule ETH Zürich, Nr. 20718, 2012, 2012.

[RKE+13] Jose Rodriguez, Marian P Kazmierkowski, Jose R Espinoza, Pericle Zanchetta, Haitham Abu-Rub, Hector A Young, and Christian A Rojas. State of the art of finite control set model predictive control in power electronics. *IEEE Transactions on Industrial Informatics*, 9(2):1003–1016, 2013.

[Rob09] NIM Gould DP Robinson. A second derivative sqp method: local convergence. 2009.

[RPK+16] S. Rodrigues, A. Papadopoulos, E. Kontos, T. Todorcevic, and P. Bauer. Steady-state loss model of half-bridge modular multilevel converters. *IEEE Transactions on Industry Applications*, 52(3):2415–2425, May 2016.

[RRTP78] Jacques Richalet, A Rault, JL Testud, and J Papon. Model predictive heuristic control: Applications to industrial processes. *Automatica*, 14(5):413–428, 1978.

[RWB11] S. Rohner, J. Weber, and S. Bernet. Continuous model of modular multilevel converter with experimental verification. In *Energy Conversion Congress and Exposition (ECCE), 2011 IEEE*, pages 4021–4028, 2011.

[Sac09] Yu. L. Sachkov. Control theory on lie groups. *Journal of Mathematical Sciences*, 156(3):381–439, 2009.

[SF85] M. K. Sundareshan and R. S. Fundakowski. Periodic optimization of a class of bilinear systems with application to control of cell proliferation and cancer therapy. *IEEE Transactions on Systems, Man, and Cybernetics*, SMC-15(1):102–115, Jan 1985.

[SHA13] A. Saccon, J. Hauser, and A. P. Aguiar. Optimal control on lie groups: The projection operator approach. *IEEE Transactions on Automatic Control*, 58(9):2230–2245, Sept 2013.

[SHN+16] Kamran Sharifabadi, Lennart Harnefors, Hans-Peter Nee, Remus Teodorescu, and Staffan Norrga. *Design, Control and Application of Modular Multilevel Converters for HVDC Transmission Systems*. John Wiley & Sons, 2016.

[SKF17] S. Sau, S. Karmakar, and B. G. Fernandes. Reduction of capacitor ripple voltage and current in modular multilevel converter based variable speed drives. In *2017 IEEE 3rd International Future Energy Electronics Conference and ECCE Asia (IFEEC 2017 - ECCE Asia)*, pages 1451–1456, June 2017.

[SLL+13] Q. Song, W. Liu, X. Li, H. Rao, S. Xu, and L. Li. A steady-state analysis method for a modular multilevel converter. *IEEE Transactions on Power Electronics*, 28(8):3702–3713, August 2013.

[SLN+12] Gum Tae Son, Hee-Jin Lee, Tae Sik Nam, Yong-Ho Chung, Uk-Hwa Lee, Seung-Taek Baek, Kyeon Hur, and Jung-Wook Park. Design and control of a modular multilevel HVDC converter with redundant power modules for noninterruptible energy transfer. *Power Delivery, IEEE Transactions on*, 27(3):1611–1619, 2012.

[SPD+13] H. Saad, J. Peralta, S. Dennetiere, J. Mahseredjian, J. Jatskevich, J. A. Martinez, A. Davoudi, M. Saeedifard, V. Sood, X. Wang, J. Cano, and A. Mehrizi-Sani. Dynamic averaged and simplified models for mmc-based HVDC transmission systems. *IEEE Transactions on Power Delivery*, 28(3):1723–1730, July 2013.

[Spi13] Karlheinz Spindler. Optimal control on lie groups: Theory and applications. *WSEAS TRANSACTIONS on MATHEMATICS*, 12(5):531–542, May 2013.

[SSG11] D. Soto-Sanchez and T.C. Green. Control of a modular multilevel converter-based HVDC transmission system. In *Power Electronics and Applications (EPE 2011), Proceedings of the 2011-14th European Conference on*, pages 1–10, 2011.

[ST95] Hanif D Sherali and Cihan H Tuncbilek. A reformulation-convexification approach for solving nonconvex quadratic programming problems. *Journal of Global Optimization*, 7(1):1–31, 1995.

[TAA+16] C. D. Townsend, R. Aguilera, P. Acuna, G. Konstantinou, J. Pou, G. Mirzaeva, and G. C. Goodwin. Capacitance minimization in modular multilevel converters: Using model predictive control to inject optimal circulating currents and zero-sequence voltage. In *2016 IEEE 2nd Annual Southern Power Electronics Conference (SPEC)*, Dec 2016.

[TGLC17] B. Tai, C. Gao, X. Liu, and Z. Chen. A novel flexible capacitor voltage control strategy for variable-speed drives with modular multilevel converters. *IEEE Transactions on Power Electronics*, 32(1):128–141, January 2017.

[TMG17] D Townsend, G Mirzaeva, and GC Goodwin. Capacitance minimization in modular multilevel converters: A reliable and computationally efficient algorithm to identify optimal circulating currents and zero-sequence voltages. In *Power Electronics and Drive Systems (PEDS), 2017 IEEE 12th International Conference on*, pages 98–104. IEEE, 2017.

[Top03a] MV Topunov. The convexity of the reachable set for a bilinear controllable system. *Journal of applied mathematics and mechanics*, 67(5):665–670, 2003.

[Top03b] MV Topunov. The reachable set of a quasi-commutative bilinear system: Its convexity. *Automation and Remote Control*, 64(8):1241–1249, 2003.

[TS02] Mohit Tawarmalani and Nikolaos V Sahinidis. *Convexification and global optimization in continuous and mixed-integer nonlinear programming: theory, algorithms, software, and applications*, volume 65. Springer Science & Business Media, 2002.

[TSC14] R. Trinchero, I.S. Stievano, and F.G. Canavero. Steady-state analysis of switching power converters via augmented time-invariant equivalents. *Power Electronics, IEEE Transactions on*, 29(11):5657–5661, Nov 2014.

[TZWE16] N.-T. Trinh, M. Zeller, K. Wuerflinger, and I. Erlich. Generic model of MMC-VSC-HVDC for interaction study with AC power system. *IEEE Transactions on Power Systems*, 31(1):27–34, January 2016.

[VBSH15] Mohsen Vatani, Behrooz Bahrani, Maryam Saeedifard, and Morten Hovd. Indirect finite control set model predictive control of modular multilevel converters. *IEEE Transactions on Smart Grid*, 6(3):1520–1529, 2015.

[VCR14] M. Vasiladiotis, N. Cherix, and A. Rufer. Accurate capacitor voltage ripple estimation and current control considerations for grid-connected modular multilevel converters. *IEEE Transactions on Power Electronics*, 29(9):4568–4579, Sept 2014.

[vdM13] W. van der Merwe. The output-current THD vs capacitor voltage ripple trade-off in the 2-cell single phase M2LC. In *EEE International Conference Industrial Technology (ICIT)*, pages 638–643, Feb 2013.

[VHS15] M. Vatani, M. Hovd, and M. Saeedifard. Control of the modular multilevel converter based on a discrete-time bilinear model using the sum of squares decomposition method. *IEEE Transactions on Power Delivery*, 30(5):2179–2188, October 2015.

[VLF+14] Sergio Vazquez, Jose I Leon, Leopoldo G Franquelo, Jose Rodriguez, Hector A Young, Abraham Marquez, and Pericle Zanchetta. Model predictive control: A review of its applications in power electronics. *IEEE Industrial Electronics Magazine*, 8(1):16–31, 2014.

[Wan09] Liuping Wang. *Model predictive control system design and implementation using MATLAB®*. Springer, 2009.

[WHMB18] Jun Wang, Xu Han, Hao Ma, and Zhihong Bai. Analysis and injection control of circulating current for modular multilevel converters. *IEEE Transactions on Industrial Electronics*, 2018.

[WKS10] Manfred Winkelnkemper, Arthur Korn, and Peter Steimer. A modular direct converter for transformerless rail interties. In *Industrial Electronics (ISIE), 2010 IEEE International Symposium on*, pages 562–567. IEEE, 2010.

[WP16] D. Wu and L. Peng. Analysis and suppressing method for the output voltage harmonics of modular multilevel converter. *IEEE Transactions on Power Electronics*, 31(7):4755–4765, July 2016.

[WQS+15] Liyao Wu, Jiangchao Qin, M. Saeedifard, O. Wasynczuk, and K. Shenai. Efficiency evaluation of the modular multilevel converter based on si and SiC switching devices for medium/high-voltage applications. *IEEE Transactions on Electron Devices*, 62(2):286–293, February 2015.

[XGZ15] J. Xu, A. M. Gole, and C. Zhao. The use of averaged-value model of modular multilevel converter in DC grid. *IEEE Transactions on Power Delivery*, 30(2):519–528, April 2015.

[Xu97] ZK Xu. Local saddle points and convexification for nonconvex optimization problems. *Journal of Optimization Theory and Applications*, 94(3):739–746, 1997.

[XZZ16] Jianzhong Xu, Penghao Zhao, and Chengyong Zhao. Reliability analysis and redundancy configuration of MMC with hybrid submodule topologies. *IEEE Transactions on Power Electronics*, 31(4):2720–2729, April 2016.

[Yak92] VA Yakubovich. Nonconvex optimization problem: The infinite-horizon linear-quadratic control problem with quadratic constraints. *Systems & Control Letters*, 19(1):13–22, 1992.

[YDLH16] H. Yang, Y. Dong, W. LI, and X. HE. Average-value model of modular multilevel converters considering capacitor voltage ripple. *IEEE Transactions on Power Delivery*, PP(99):1, 2016.

[YLL11] Hua Yang, Ning Li, and Shaoyuan Li. A data-driven bilinear predictive controller design based on subspace method. *Asian Journal of Control*, 13(2):345–349, 2011.

[YLL+17] L. Yang, Y. Li, Z. Li, P. Wang, S. Xu, and R. Gou. Loss optimization of MMC by second-order harmonic circulating current injection. *IEEE Transactions on Power Electronics*, 2017. Early acces.

[ZAL+12] Y. Zhang, G.P. Adam, T.C. Lim, S.J. Finney, and B.W. Williams. Analysis of modular multilevel converter capacitor voltage balancing based on phase voltage redundant states. *Power Electronics, IET*, 5(6):726–738, 2012.

[Zha11] Fuzhen Zhang. *Matrix theory: basic results and techniques*. Springer Science & Business Media, 2011.

[ZLJ16] F. Zhang, W. Li, and G. Jos. A voltage-level-based model predictive control of modular multilevel converter. *IEEE Transactions on Industrial Electronics*, 63(8):5301–5312, Aug 2016.

[ZZ15] Jianpo Zhang and Chengyong Zhao. The research of sm topology with DC fault tolerance in MMC-HVDC. *IEEE Transactions on Power Delivery*, 30(3):1561–1568, June 2015.

List of Figures

List of Tables